

Glass Defects Originating from Glass Melt/Fused Cast AZS Refractory Interaction

PROEFSCHRIFT

ter verkrijging van de graad van doctor aan de
Technische Universiteit Eindhoven, op gezag van
de Rector Magnificus, prof. dr. J.H. van Lint,
voor een commissie aangewezen door het College
van Dekanen in het openbaar te verdedigen op
woensdag 8 juni 1994 om 16.00 uur

door

Franciscus Arnoldus Gerardus van Dijk
geboren te Leende

Dit proefschrift is goedgekeurd door de promotoren:
prof.dr.ir. H. de Waal
en
prof.dr. F.J.J. van Loo

Table of contents.

Summary.	1
1. Introduction.	4
1.1. Problem definition.	4
1.2. Objective.	4
1.3. Structure of the study.	4
1.4. Industrial glass melting process.	5
1.5. Description of problem.	9
2. Glass defect generating mechanisms at glass/fused cast AZS.	14
2.1. Literature review.	14
2.1.1. Mechanisms of bubble generation from refractory linings.	14
2.1.2. Mechanisms of knot generation.	16
2.1.3. Discussion.	18
2.2. Validation of an electrochemical mechanism.	20
2.2.1 Introduction.	20
2.2.2. Description of the electrochemical mechanism.	21
2.2.3. Electrochemical measurements.	24
2.2.3.1. Rate-determining step of the internal reaction.	30
2.2.3.2. Shift of the location of oxygen formation.	36
2.2.4. Discussion and conclusions.	46
3. Cation diffusion into fused cast AZS.	55
3.1. Introduction.	55
3.2. Experimental procedures.	56
3.2.1. Profiles of concentration of the cations in the glass melt and the glassy phase of the AZS.	58
3.2.1.1. Measurement method.	58
3.2.1.2. Results of measured concentration	

profiles.	60
3.2.1.3. Summary of the measured concentration profiles in AZS.	70
3.2.1.4. Discussion of measured concentration profiles in the AZS.	73
3.2.2. Change in glass melt composition by diffusion into AZS.	77
3.2.2.1. Introduction.	77
3.2.2.2. Measurement method.	78
3.2.2.3. Results of glass analysis after refractory interaction and determination of e.e.h. values.	82
3.2.2.4. Discussion.	96
4. Effect of glass composition and temperature on glass defect potential originating from refractory.	104
4.1. Introduction.	104
4.2. Results of measured cation diffusion.	105
4.3. Practical application of the cation diffusion rules by a glass furnace model.	111
4.4. Discussion.	116
5. Bubble formation during the laboratory-scale tests.	123
5.1. Introduction.	123
5.2. Experimental method.	123
5.3. Test results.	124
5.4. Discussion.	130
6. Knot formation mechanism and characterization.	135
6.1. Introduction.	135
6.2. Knots in TV-screen glass products.	136
6.3. Dissolution of knots.	141
6.4. Concentration profiles of AZS-to-glass interface.	148
6.5. Chemical composition of the interface glass melt/fused cast AZS.	152

6.6. Examples of knots in industrial TV-screen glass production and their sources.	157
Annex 1.	161
Annex 2.	162
Annex 3.	171
Annex 4.	174
Annex 5.	174
Annex 6.	177

SUMMARY

The interaction of glass melts and refractories in industrial glass melting tanks has a large impact on the resulting glass quality. The mostly applied type of refractory in the glass industry, in direct contact with the glass melt, is fused cast AZS (Alumina Zirconia Silicate). Due to the interaction of the glass melt with fused cast AZS refractory, different kinds of inhomogeneities like stones, knots and bubbles can be generated. The objective of this study is to find, for fused cast AZS in contact with a glass melt, the mechanism of knot and bubble formation and the parameters that influence this mechanism. The ultimate objective is a (semi) quantitative model for glass defect prediction from fused cast AZS in contact with TV screen glass melts to be able to choose conditions of lowest glass defect formation rates.

Most of the bubbles arising at temperature levels above 1400°C are initially oxygen bubbles, originating from an electrochemical mechanism, acting in the refractory in contact with molten glass. When molten glass is brought into contact with fused cast AZS, the diffusion of cations from the glass melt into the AZS transports a positive charge into the AZS interior. The diffusion of the cations is caused by the lower partial Gibbs energy of the glass melt cations in the high Al_2O_3 containing glassy phase of the AZS refractory. The positive charge due to the cation diffusion is balanced by electrons moving from the glass melt/AZS interface into the AZS interior, resulting in an oxidation of the oxide ions of the melt at the AZS/glass melt interface. The electrons reduce the polyvalent ionic impurities (mainly iron) of the fused cast AZS. The rate of oxygen gas formation at the refractory/glass melt interface, as a result of the redox reaction, is determined by the diffusion rate of cations of the glass melt into the glassy phase (binding phase) of the fused-cast AZS.

The bubbles from this source arise, as mentioned, in the interface layer between fused-cast AZS and the glass melt. The

interface consists of a vitreous layer of products resulting from reactions between fused-cast AZS and glass melt, with ZrO_2 -nodules at the refractory end. A bubble generated in this interface area forces its way through this layer into the glass melt, sometimes squeezing part of this Al_2O_3 rich layer into the bulk of the melt. The high Al_2O_3 -content of the vitreous section of the interface gives these "particles" such a high surface tension that they become spherical knots in the glass melt. All this implies that one single mechanism accounts for the formation of both bubbles and knots at the interface glass melt/fused cast AZS.

The rate determining element of this process, the cation diffusion, has been measured for the oxides essential for a present-day TV-screen glass composition (Li_2O , Na_2O , K_2O , BaO , SrO , CaO and MgO). The effect of Li_2O on the oxygen bubble formation is very high, including not only its own contribution but also causing other oxides to have a larger effect than the effect of the same oxides for a glass without Li_2O . By far the highest effect of the other oxides, apart from Li_2O , is that of K_2O , particularly in the range around $1350^\circ C$ (bottom temperature of the melting tank). The formation rate of oxygen bubbles per mole per cent of the oxides under examination is in decreasing tendency: Li_2O , K_2O , Na_2O , BaO/SrO , CaO and MgO .

The diffusion rates of the cations of these oxides in the AZS and, consequently, the bubble formation potentials effected by the composition of the glass and the temperature, have been computed using a model for a simplified version of an industrial melting furnace with assumed realistic glass melt/fused cast AZS contact temperatures. The differences in the glass defect potential of the interaction between fused-cast AZS and different glass melts computed by this method, agrees with the amounts of bubbles and knots found in industrial produced TV glasses. Laboratory-scale tests show a rise in number, in oxygen content and in diameter of the generated bubbles, at increasing temperatures (from 1350 to $1500^\circ C$).

The chemical composition of the core of the knots, originating

from the interface between glass melt and fused-cast AZS remains stable during dissolution in the bulk glass melt until just before complete dissolution. This chemical composition provides us with a method to derive the temperature of their origin, since the chemical composition of the interface depends mainly on the chemical composition and the temperature of the glass melt.

1. Introduction.

1.1. Problem definition.

The interaction of glass melt and refractories in the industrial glass melting tanks has a large impact on the glass quality. Due to the interaction of the glass melt with refractory materials, different kinds of inhomogeneities like stones, knots, cords and bubbles are generated. It is estimated that, depending on the specific product and required glass quality, up to 10 % of the industrial glass production in continuously operating furnaces is rejected due to these kinds of defect sources (Lit. 1).

1.2. Objective.

The objective of this study is to find for the most applied type of refractory, fused cast AZS, the mechanism of knot and bubble formation and the parameters that influence this mechanism. The ultimate object is a (semi) quantitative model for glass reject prediction from fused cast AZS (alumina-zirconia-silica) in contact with TV screen glass melts, to be able to choose conditions of lowest defect rates.

1.3. The structure of the study.

A short description of the glass melting process and glass reject problem is given in this chapter.

A literature review on the generation of glass defects is given in chapter 2. This chapter also describes the measurements and results to validate the mechanism for bubble and knot formation during the interaction of fused cast AZS with a glass melt. The diffusion of cations, into the fused cast AZS, appears to be the rate determining step in the formation of bubbles and knots.

Often, in this study, fused cast AZS will be simply referred to as AZS.

In chapter 3, the experiments and results on the diffusion of the

most important cations of a TV screen glass will be presented. Although the cations are diffusing into the AZS, the name of the oxide of the cation is used to express the amount or rate of diffusion. The name of the oxide is used because the analytical measurement of the glass composition is also in oxides. With the results of the experimental work described in chapter 3, a simple model has been prepared which is presented in chapter 4. With this model it is possible to estimate the effect of the glass composition on the glass reject due to the interaction of the glass melt with fused cast AZS.

In chapter 5 the behaviour and nature of bubbles in the melt, arising in laboratory scale tests, due to interaction of glass melt and fused cast AZS, are described.

In chapter 6 the mechanism for knot formation, their chemical composition and dissolution kinetics are presented. A completely new method to find the source of knots is also presented in this chapter.

With this new method the temperature of the origin of the knots in the furnace can be determined after the chemical composition of the knot has been analyzed.

1.4. Industrial glass melting processes.

The industrial production of glass from raw material batch is generally a continuous process with a high degree of automatization.

There are many different kinds of glass products. The main glass products are:

- container glass
- flat glass
- domestic glass (tableware)
- insulation glass fiber products
- crystal glass
- textile and reinforcement fibers.
- glass for electronic applications.

Further there is a wide range of special glass compositions like:

- borosilicate glass

- opal glass
- potassium glass
- glass ceramics.

All these glasses have a different chemical composition with SiO_2 as main glass forming component.

The glass output of continuous glass melting furnaces varies from 5 tons/day, up to 800 tons/day. The melting area of such furnaces varies from a few m^2 , up to 300 m^2 .

In most cases, fossil fuels are the energy suppliers. In some cases electric boosting or all electric heating is applied. When fossil fuels are used, the hot flue gases are used to preheat the combustion air (except when pure oxygen is used instead of air). For small production units (<100 tons/day), in most cases a metallic recuperator is used, for larger units a more energy efficient regenerative system is generally applied.

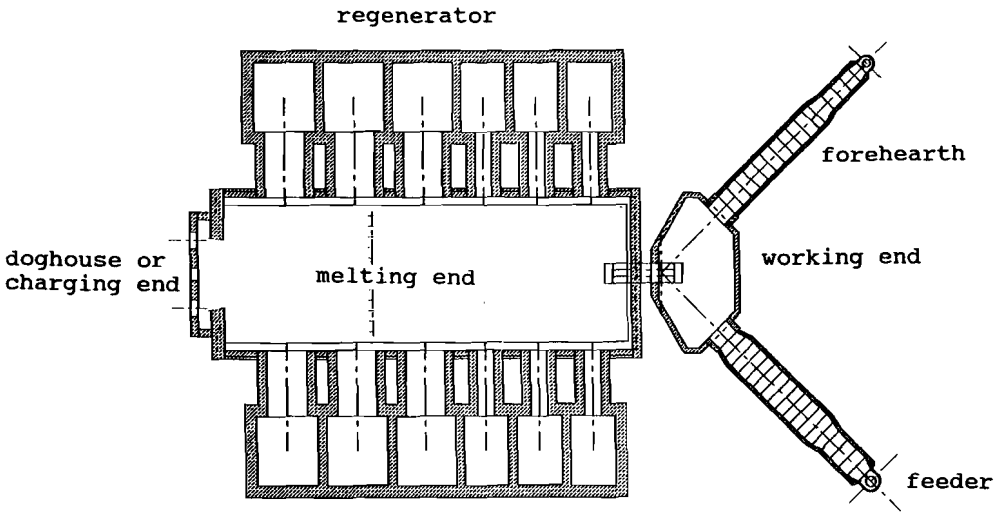
Often the furnace consists of a melting end, a working end and one or more forehearth and feeders. For the glass melting tank, nowadays, fused cast refractory materials are used. The melting end is kept on a temperature of 1400 till 1620 °C, depending on the glass composition, throughput and required glass quality. A well mixed batch of raw materials combined with cullet (from rejected glass or recycling waste glass) is continuously charged to the melting end. The batch floats on the glass melt and is heated by the radiation of the furnace crown and the flames from above and the transfer of heat from the hot glass melt from underneath.

During the heating process of the batch, a lot of chemical reactions take place: starting with solid state reactions between particles of the raw materials, which form low melting eutectic phases. The batch particles like sand or feldspar dissolve in these reactive melts, by diffusion processes. Because part of the raw materials are added as carbonates and often water is used in the batch making process, the melting of the batch is accompanied by dissociation reactions which lead to the formation of gases like carbon dioxide and water vapour. The largest part of these gases and the air entrapped between the batch particles are

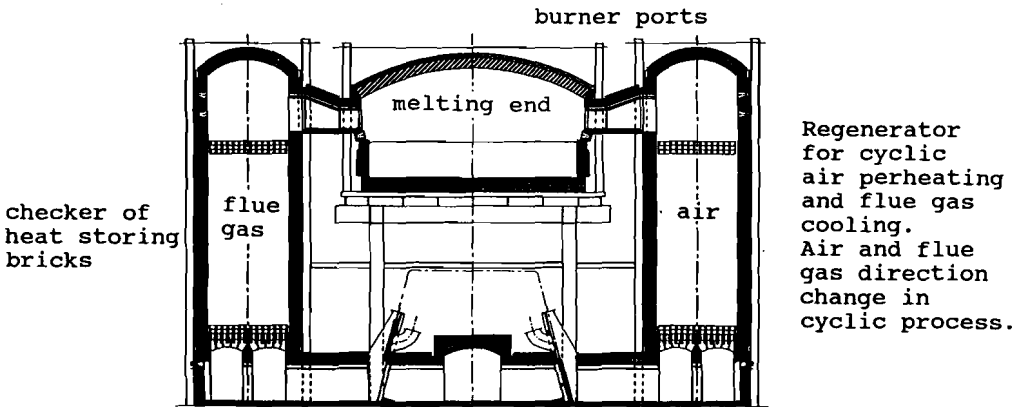
released from the batch before it is completely melted. Although a small part will be trapped in the glass melt. A fining agent is used (mostly sulfate, antimone (V) oxide or arsenic (V) oxide) to remove these gas inclusions (bubbles) by blowing them up at a certain temperature level, thereby increasing their rising (buoyancy driven) velocity in the moderately viscous melt. The complete dissolution of all solid particles and the homogenisation of the glass are other main processes which have to take place in the melting end. The quality of the glass product is strongly dependent on the conditions during this melting process. For the quality of the glass, the main parameters are: process stability, melting end temperature, temperature distribution, mean residence time, residence time distribution, batch composition, redox state, quality of the refractory materials and the aging of the complete furnace system. In most furnaces, the glass leaves the melting end through the throat, after a mean residence time of 25 to 60 hours for most of the industrial processes, into the so called working end. In the working end the glass is cooled down and conditioned (to obtain a melt with an uniform temperature) before the melt flows to the forehearth(s). There the melt will be cooled down and conditioned to the temperature related to the viscosity needed for the forming process of the required shape and weight. In the forehearth, often stirrers are located to increase the chemical and the temperature homogeneity. In the feeder the glass melt output is controlled with the aid of a plunger (sometimes in combination with a tube) and the glass melt output flows through a hole at the end of this feeder. This glass is cut in a constant interval of time. The portions of glass made in this way are called gobs. These gobs are made with a narrow weight and size range, necessary for exact article shape and dimensions.

The lay out of a typical, so called regenerative cross fired, industrial furnace is illustrated by figure 1.1. The glass quality achieved with such a process is mostly sufficient for articles with relatively modest quality requirements.

figure 1.1 Cross fired regenerative container or T.V. glass furnace.



horizontal cross section



vertical cross section

For more general information about glass, glass melting, furnaces and glass defects the standard literature of Scholze (Lit. 2), Trier (Lit. 3), Noelle (Lit. 4) and Jebesen-Marwedel and Brueckner (Lit. 5) is recommended.

1.5. Description of the problem.

In many areas of glass manufacturing production losses due to glass defects such as bubbles, stones and knots are very high.

- Bubbles or blisters are gaseous inclusions in the glass.
- Stones are solid unmolten or recrystallized material inclusions in the glass.
- Knots are vitreous particles of a deviating chemical composition compared to the bulk and consequently, a different index of refraction, which brings about a local lens effect. The vitreous particle may contain inclosed crystals like recrystallized zirconia, nepheline or leucite.

An example, for high production losses due to these glass defects, is the colour television screen industry, where manufacturers are rejecting screens because of the presence of extremely small bubbles, stones or knots. For the production of screens for computer monitors, spherical bubbles with a volumetric diameter of 0.35 mm are rejected. For the production of normal consumer TV screens products with spherical bubbles larger than 0.40 mm in small screens or 0.6 mm for some areas of the larger TV screens will be rejected.

All visible knots and stones will lead to rejection.

These rigid customer requirements, for the TV screen production leads to losses due to such glass defects of 5 to 25 %, depending on the size of the screens. For the production in one glass furnace with a capacity of approximately 180 tons/day, 1% rejection means a loss of US \$500,000 on an annual basis. Most manufacturers have several of these kinds of melting tanks for the production of TV screens. This means that the number of glass defects has a large influence on the profitability for all TV

screen manufacturers but also for other manufacturers of high quality glass like float glass for automotive windshields and mirrors, reinforcement fibers etc.

There are a large number of possible sources of glass defects. For stones the following are the most common (Lit. 6):

- pollution of raw materials.
- pollution of cullet.
- refractory - clay-type refractory.
 - sintered AZS and zircon or cements.
 - fused cast AZS.

For knots, the fused cast AZS is the most common source.

For bubbles the following sources are common (lit. 7):

- the primary melting of raw materials.
- incomplete fining process.
- reactions of the melt with refractories and metals.
- reboil (The nucleation and growth of bubbles in previously bubble free glass, by overheating or sudden changes in redox state).
- lapping-in bubbles, by moving parts (e.g. stirrers, plunger, tube or gobber) in the feeder.
- bubbles, originating from organic particles.

For the exact determination of the origin of glass defects 1) the appearance, 2) generally the shape, 3) the location in the article, 4) the mineralogical and 5) chemical analysis of the defect has to be available. Further, it is essential to be well acquainted with the refractories installed, furnace conditions, fluctuations in furnace conditions, furnace settings, stirrer settings and gob making. In such cases, often the origin(s) of the glass defects can be found.

During production of glass for products which require a high glass quality, the reject originating from refractory is considerable: causing approximately 50% of all the glass defects. In the start up period of a furnace, with extremely high glass rejects (Lit. 8), practically all the products which are rejected show defects originating from refractory/melt interactions. Therefore this study will deal with the glass defects generated

at the glass melt/fused cast AZS interface. Fused cast AZS (see table 1.1) is chosen because it is by far the most applied fused cast material for the melters in the glass industry today.

Table 1.1

Fused cast AZS.

	fused cast AZS 32/33	fused cast AZS 41
Chemical composition in weight %.		
ZrO ₂	32-33	40-41
Al ₂ O ₃	50-51	45-46
SiO ₂	15-16	12-13
Na ₂ O	1	1
CaO, Fe ₂ O ₃ , TiO ₂ , MgO	0,2	0,3
Crystallographical composition in weight %.		
Zirconia (Baddeleyite)	32,0	41,0
Corundum	47,0	42,0
Glass phase	21,0	17,0

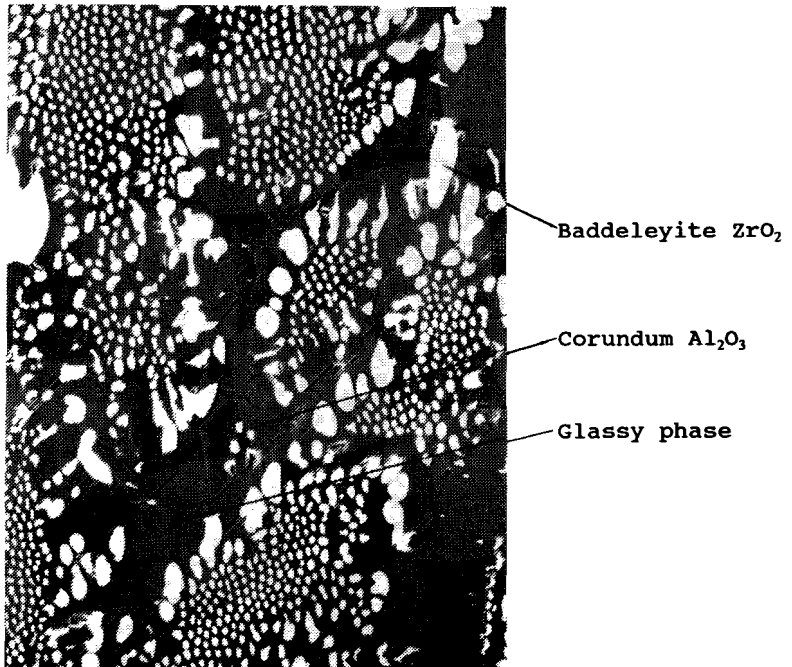
The glassy phase of AZS refractory, consists of about 70 weight% SiO₂, 4 weight% Na₂O, 22 weight% Al₂O₃, 3 weight% ZrO₂ (Lit. 1), 0.3 weight% Fe₂O₃ and 0.3 weight% TiO₂ (Lit. 9).

The fused cast AZS is produced by melting the raw materials in an electric arc furnace at about 2200-2400 °C. The main raw materials

are about 50% recycling of fused cast AZS from direct reject blocks or over cast and the primary raw materials: zirconium silica, zirconia, alumina and soda ash. The melt is treated with oxygen to oxidize zirconium oxy-carbo-nitride or other reduced constituents, produced by the reaction with the graphite electrodes during melting. The molten material is then cast into molds to, or very near to, the final shape of the block desired (lit. 8). The molds are mostly made from a special kind of sand. The mold with the fused cast ceramic is cooled down very slowly in order to anneal (free of thermal stresses) the fused cast product. The produced fused cast AZS contains baddeleyite (ZrO_2) and corundum (Al_2O_3) crystals which are kept together by a glassy phase. The material is not very homogeneous. Crystal size, chemical composition of the glassy phase and porosity differ locally in one block.

Figure 1.2

Typical example of the microstructure of fused cast AZS (32/33), magnification 500 X.



Literature references chapter 1.

- [1] R.G.C. Beerkens, A.J. Faber;
Refractories in contact with molten glass;
TNO Industrial Research TPD-GL-RPT-93-091.
 - [2] H. Scholze;
Glas, Natur, Struktur und Eigenschaften;
Springer-Verlag 1977.
 - [3] W. Trier;
Glasschmelzöfen, Konstruktion und Betriebsverhalten;
Springer-Verlag 1984.
 - [4] G. Noelle;
Technik der Glasherstellung;
Verlag Harri Deutsch 1979.
 - [5] H. Jebesen-Marwedel, R. Brueckner;
Glastechnische Fabrikationsfehler;
Springer-Verlag 1980.
 - [6] G. Duvierre, A. Krings, E. Sertain;
Defects and their origin in glass;
Glasteknisk Tidskrift 45 (1990) p. 63-70.
 - [7] E.L. Swarts;
Gases in glass;
Ceram. Eng. Sci. Proc. 7 (1986) p. 390-403.
 - [8] A.D. Davis, L.L. Cureton;
Start-up and surface blistering of fused-cast refractories;
Ceram. Eng. Sci. Proc. 8 (1987) p. 276-284.
 - [9] M. Dunkl;
Studies on the glassy and reaction phases given off by fused
cast AZS blocks and their effects on the glass quality;
Glastech. Ber. 62 (1989) p. 389-395.
-

2. Glass defect generating mechanisms at glass/fused cast AZS.

2.1. Literature review.

2.1.1. Mechanisms of bubble generation from refractory linings.

Refractory porosity.

Fused cast AZS bodies have a detectable porosity. Pristine fused cast AZS material has no open porosity but there are some closed voids and pores which arise from the manufacturing process. These pores are filled with gases. The amount of pores in the material is strongly dependent on the applied production process. The gases in these pores have an air like composition, with nitrogen and oxygen as main components (Lit. 1) and some carbon dioxide (Lit 2).

When the refractory is in contact with glass, the refractory material will react with the glass melt and will slowly dissolve in this melt: the closed pores will be opened and then release their gas content, forming bubbles.

Impurities in the refractory.

Impurities, which can oxidize, are for example elemental carbon originating from graphite electrodes of the fusion casting operation, sulfur or zirconium carbide originating from raw materials of the AZS. The dissociation/oxidation of nitrides/oxy-nitrides, produced by reactions with the graphite electrodes during melting of the AZS, could give nitrogen gas. At first, during the heating of the fused cast AZS at temperatures higher than 1400 °C, these oxidation reactions, involving the formation of nitrogen, carbon dioxide, carbon mono-oxide (Lit. 1 & 3) and/or sulfur dioxide (Lit. 4) are a cause of bubble formation. When fused cast AZS is cooled down and heated up again, generally O₂ bubbles are formed. Generally, at temperature levels higher than 1400 °C these O₂ bubbles are formed every time when the temperature is increased. (Lit. 1 & 3). As the material is cyclically cooled down and heated up again, at every heating up period, new oxygen bubbles are generated from the AZS in glass

melt contact but also in the absence of glass melt contact. In the cooling down period, oxygen is resorbed again, this can be caused by the redox reactions of polyvalent ions (as impurities) in the refractory material. The oxygen is resorbed by the polyvalent ions because generally the redox reaction of a polyvalent ion shifts to the oxidized side when the temperature is decreased. The fused cast AZS contains as impurities (<0,3 weight%) the oxides of polyvalent ions like iron ($\text{Fe}^{2+}/\text{Fe}^{3+}$) and titanium ($\text{Ti}^{2+}, \text{Ti}^{4+}$). For example: $4 \text{Fe}^{2+} + \text{O}_2 \rightarrow 4 \text{Fe}^{3+} + 2 \text{O}^{2-}$

Electrochemical reactions.

When a refractory (conductive for electrons, oxide ions and cations) is brought into contact with a glass melt, an electrical potential (emf) is generated between the refractory and the glass melt because generally no thermodynamic equilibrium exists between these materials.

The Gibbs energy changes, for redox reactions occurring in an electrochemical cell may be expressed in the form of an electromotive force. The electromotive force of the cell, or difference in electrical potential between two electrodes, depends on the equilibrium constant of the chemical redox reactions that may take place in the cell, and the activities of reactants and products. Then the Gibbs energy change is equal to the electrical work at constant temperature and pressure. The electrical work is equal to the product of the voltage and the quantity of electricity (expressed in coulombs). The quantity of electrical charge corresponding to the molar quantities indicated in the balance chemical equation is nF , where n is the number of electrons transferred per molecule and F is the constant of Faraday. If this quantity of electrical charge is transported through a potential difference of E volts, the amount of work required is given by nFE . Since this electrical change does not involve pressure-volume work and is carried out isothermally the change in Gibbs energy, for a reversible process, is given by (Lit. 16).

$$\Delta G = - nFE$$

A relation between the electromotive force (emf) generated between glass melt/refractory interior and the formation of oxygen bubbles was found by Bossard and Begley (Lit. 5). They also showed a positive correlation between the electromotive force and the sodium oxide concentration difference between the glass melt and the refractory.

A similar influence of cations in the melt on the electromotive force, between the refractory and the glass melt, was found by Leger, Boffe and Plumet (Lit. 6).

For zircon, (zirconia silicate ZS) Baucke and Roeth reported (Lit. 7) oxygen bubble generation at the interface refractory/glass and they proposed a mechanism in which the O^{2-} from the glass is oxidized to O_2 and iron(III) and titanium(IV) in the refractory is reduced. The electrical charge is transported simultaneously by e^- and alkali⁺ species. According Baucke and Roeth, the reaction rate or O_2 formation at the interface refractory/glass melt in this mechanism is controlled mainly by the diffusion of alkali ions into the refractory material. The diffusion of cations is probably caused by the difference in partial Gibbs energy between the glass melt and the refractory of the cations. This oxygen bubble forming mechanism will be explained more extensively in this chapter.

2.1.2 Mechanisms of knot generation.

The generation of a (alumina rich) knot is due to one or more forces, which drive the fused cast AZS glass phase towards the refractory surface (above glass melt surface) and into the bulk of the glass melt.

The following forces may be distinguished:

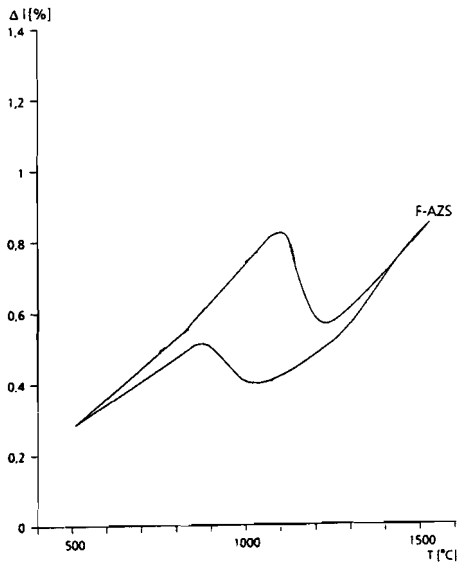
Gravity.

For relatively low viscosities of the glassy phase of the AZS nearest to the refractory hot-face, glassy phase could vacate the refractory and be replaced by the glass melt via capillary action (Lit 6).

Zirconia transformation and hysteresis.

Displacement of the fused cast AZS glassy phase could be caused by the thermal expansion of zirconia. Between 900 and 1200 °C a irregularity in the thermal expansion appears by the reversible phase transition from monoclinic to tetragonal ZrO_2 (Lit. 8). This alteration of crystal form, reverses the step-sided expansion curve and may cause shrinkage (see figure 2.1). By this expansion and shrinkage, a pumping action could occur, expelling glassy phase from the AZS material (Lit. 4).

figure 2.1 Thermal expansion of fused cast AZS 32/33.



Gas formation.

The gas forming mechanisms are described in section 2.1.1.

In the literature (e.g. 1, 3, 9 and 10), the gas formation in the refractory and at the interface refractory/glass is found to be the most important cause of pushing out liquid or glassy phases (exudation) from the fused cast AZS interior.

The concentration profiles of cations in the interface region of the glass melt/fused cast AZS (see chapter 6 of this study) show an increasing amount of Al_2O_3 in the interface, going from glass melt to fused cast AZS. A rise of Al_2O_3 content in glass melts, increases the viscosity of the glass melts dramatically. In chapter 3 and 6 it is also shown that shear stress (owing to forced convection) has hardly an effect on the concentration profile of the interface glass melt/fused cast AZS. Convection will only remove, as a ream, the part of the boundary layer at the glass melt side, with a relatively low Al_2O_3 content and therefore low viscosity. The increased removal of the boundary layer at the glass melt side due to convection, accelerates the corrosion of the refractory and deteriorates the homogeneity of the melt. The knots found in practice generally have a high Al_2O_3 content, as will be shown in chapter 6, therefore a force from within the refractory has to push out parts of the transition layer between molten glass and refractory.

This implies that mainly the bubble forming mechanism in the refractory interior is responsible for the presence, of bubbles and knots in the glass, originating from fused cast AZS.

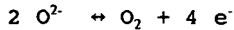
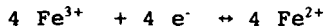
2.1.3. Discussion.

The bubble forming mechanism appears to be the key for the glass defects (bubbles, stones and knots) originating from fused cast AZS. This bubble formation can be caused by more than one mechanism. Investigators (Lit. 1, 3, 11), performing experiments using fused cast AZS materials which have been heated up more than once to a temperature higher than 1400 °C, reported the generation of oxygen bubbles, except during the first heating period when bubbles of other compositions were found. The bubbles generated during the first heating period were mainly produced by the oxidation of impurities in the fused cast AZS.

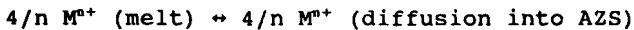
From the mechanisms for the bubble formation process mentioned in 2.1.1., only the redox reactions of iron and titanium and the electrochemical reactions lead to the generation of oxygen

bubbles.

In the test without glass contact of Dunkl (Lit. 3, 11), the exudation at 1550 °C of the glassy AZS phase stopped after 80 hours as the AZS has been heated up for the first time. At the first heating period the exudation of the glassy phase is caused by bubble formation due to the oxidation of the impurities. According to Dunkl, no bubble formation and further changes of redox states of polyvalent ions take place after 80 hours of isothermal treatment. A further indication which proves that the change in valence of the polyvalent ions by redox reactions takes place in a limited time, is the short dwell time (2 hours), at constant temperature, used in the experiments with heating cycles. This is confirmed by Ratto (Lit. 12) using temperature cycles from 1350 to 1550 °C and reverse. A few hours, after reaching the maximum temperature the exudation of glassy phase stopped. However, in experiments done by Meden and Van der Pas (Lit. 13) in fused cast AZS crucibles filled with molten glass, fresh oxygen bubbles were still found after a isothermal treatment of 500 hours at 1400 and 1500 °C. This means that the proposed mechanism for oxygen formation (Lit. 1, 3) by the redox shift of the polyvalent ion impurities in the fused cast AZS cannot be the only reason for the oxygen formation, certainly not in situations where the temperature has been constant for a long period of time. Reactions of iron in AZS at high temperatures:



The existence of electrochemical reactions, for which the reaction rates are controlled by the diffusion of cations of the glass melt into the refractory material, would give a much better explanation for the long duration of the oxygen bubble formation at the glass melt/AZS interface at constant temperature levels.



The diffusion of cations from the glass melt into the AZS transports a positive charge in the AZS. The positive charge is balanced by electrons moving simultaneously from the glass melt/AZS interface into the AZS interior. The electrons shift the $\text{Fe}^{3+}/\text{Fe}^{2+}$ ratio and O_2 is formed by the reaction, $2 \text{O}^{2-} \rightarrow \text{O}_2 + 4 \text{e}^-$ (at the glass melt/refractory interface) as long as there is cation diffusion.

Baucke and Roeth (Lit. 7) reported the above described mechanism for the interaction of zirconia silicate refractory with molten glass.

2.2. Validation of an electrochemical mechanism.

2.2.1 Introduction.

The mechanism suggested by Baucke and Roeth (Lit. 7) for the formation of oxygen bubbles for glass melts in contact with zirconia silicate will be verified in this study, using fused cast AZS in direct molten glass contact.

A glass melt which is brought into contact with fused cast AZS is not in a chemical equilibrium with the refractory material. The partial Gibbs free energy of glass melt components like sodium, potassium, barium and strontium are lower in the high Al_2O_3 containing glassy phase of the AZS material. Therefore these elements will diffuse from the molten glass, in the form of cations, into the AZS material.

The electroneutrality in the AZS material, can (theoretically) be maintained: a) by the diffusion of O^{2-} into the AZS material, b) by the diffusion of Al^{3+} and/or Zr^{4+} from the AZS material in the glass melt or c) by the diffusion of electrons from the glass melt into the fused cast AZS. A requirement for the last mentioned transport is the presence of polyvalent ions in the AZS, which can react with the electrons.

At high temperatures, the glass melt and the fused cast AZS are electrically conductive and AZS contains, as impurities,

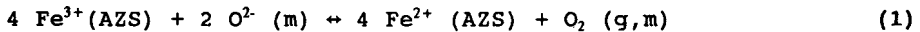
polyvalent ions like iron and titanium.

Therefore, the charge balancing of the cation diffusion by the electrons is possible. The charge balancing electrons are withdrawn from the oxygen ions in the glass melt which causes the formation of O₂ particularly at the interface glass melt/refractory.

In this chapter the proposed hypotheses of electrochemical reactions, as the major cause for the formation of O₂ bubbles, is validated experimentally using electrochemical methods.

2.2.2. Description of the electrochemical mechanism.

In 1988, Baucke and Roeth (Lit. 7) suggested a mechanism for the formation of oxygen bubbles at the interface of the glass melt and ZS (zirconia silicate). Here, it will be illustrated that a similar mechanism, in an adapted form also applies for the case of fused cast AZS, implying a redox reaction between an oxidic melt and fused cast AZS. This AZS contains as impurities a minor amount of polyvalent ions (such as iron) in their higher valence states (Fe³⁺), which is frozen in, during the formation of the AZS blocks. When the temperature is high enough and if a second redox system is present, the polyvalent ion can be reduced:



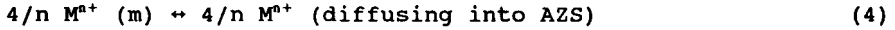
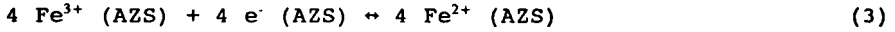
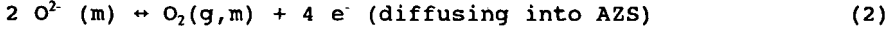
in which (m) stands for melt and (g,m) for the gaseous state or physically dissolved gas in the melt.

According to Frischat (Lit. 17) the bond strength of oxygen ions in the glass structure is so large that they may be regarded as stable for processes like diffusion of alkali ions.

Therefore, polyvalent ion/oxygen reaction can take place in the refractory interior, only if the conductivity of the electrons (generated by oxidation of the oxygen ions at the surface) in the refractory is high enough in order to migrate to the locations of the higher-valence ions in the AZS interior.

The negative charge migration into the AZS is kept in balance

(which is a constraint to keep electro neutrality conditions) by the migration of cations from the melt into the refractory.

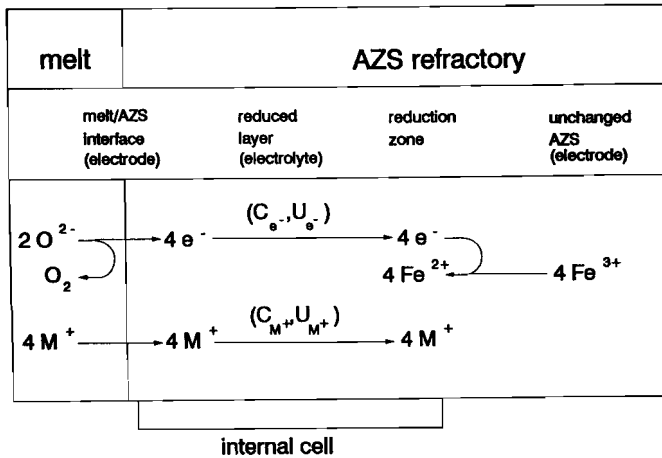


This means the AZS should also be capable of conducting cations M. $\text{M} = \text{K}^+, \text{Na}^+, \text{Li}^+$, for example.

Figure 2.2.1 shows the reaction scheme.

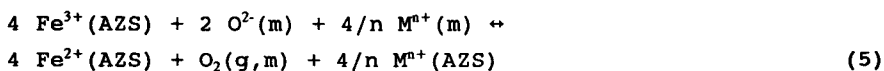
figure 2.2.1

Outline of the hypothesis on the formation of O_2 bubbles. [7]



The oxygen ions release electrons near the AZS surface which are consumed in the 'reduction zone' between the reduced system and the still oxidized internal redox system. The reaction front keeps moving deeper and deeper from the glass melt into the refractory interior. Through the intermediary 'reduced layer' electrons and

cations of identical current densities are simultaneously transported, on account of the electro-neutrality condition. The layer between glass melt/AZS interface and the redox reaction front in the AZS forms an internal galvanic cell with the interface between melt and refractory as negative electrode (anode). For this anode the oxygen ion reservoir is the melt. The unchanged AZS is the positive electrode (cathode). The reduced layer is acting as a cation-conducting solid electrolyte (a 'salt-bridge' for the cation and a 'wire' for the electron conductivity). The overall cell reaction, in this case, is the summation of reactions (2), (3) and (4) involves reactions and diffusion.



The electromotive force (emf) of the internal cell is expressed by equation (6):

$$E_{\text{AZS/m}} = E_{\text{AZS/m}}^0 + \frac{RT}{F} \ln \frac{(a_{\text{Fe}^{3+}}(\text{AZS}) \cdot a_{\text{O}^{2-}}^{1/2}(\text{m}) \cdot a_{\text{M}^{n+}}^{1/n}(\text{m}))}{(a_{\text{Fe}^{2+}}(\text{AZS}) \cdot f_{\text{O}_2(\text{g,m})}^{1/4} \cdot a_{\text{M}^{n+}}^{1/n}(\text{AZS}))} \quad (6)$$

in which a = activity of the ions in question, $f_{\text{O}_2(\text{g,m})}$ = oxygen fugacity at the interface glass melt/AZS, R = gas constant, F = Faraday's constant and $E_{\text{AZS/m}}^0$ = the standard emf for this system at the temperature T in question. Most tests in this study have been performed under isothermal conditions.

The internal cell resistance is determined, according to Baucke and Roeth in Zircon (ZrSiO_4), by the concentration $C_{\text{M}^{n+}}$ and the mobility $U_{\text{M}^{n+}}$ or the diffusion coefficient of the cations in the solid electrolyte, the 'reduced layer'.

It is impossible to measure the emf of the internal cell either directly because the melt/AZS electrode is a fictitious one, or indirectly because the electron migration through the solid substance represents an inherent, internal short-circuiting of the

cell.

The cell voltage can be measured indirectly only if the internal cell is integrated in an experimental cell arrangement in which electrodes are incorporated:

$$E_c(t) = E(t=0) - \Delta E(t) - (i_i \cdot R_i)(t) \quad (7)$$

in which $-(i_i \cdot R_i)$ is symbolizing the decrease of the measured external cell voltage by the internal current and internal resistance of the solid electrolyte.

The $-\Delta E(t)$ describes the change in Gibbs energy difference between the glass melt anode and the external AZS cathode, by the diffusion of the cations of the glass melt in the AZS, changing the chemical composition of the glass melt and eventually also the chemical composition at the external AZS cathode, thus changing the ΔG between AZS and the glass melt during the exposure time. The cell reaction is irreversible owing to the diffusion of cations and electrons from the AZS surface into the reducing zone. With a given Gibbs energy of the cell reaction (5)

$$\Delta G_{AZS/m} = - 4 F E_{AZS/m} \quad (8)$$

the rate of the redox reactions in the AZS appears to be proportional to the increase in thickness (ds/dt) of the reduced layer (Lit. 7). In the next part of the chapter, experimental support will be given for the thesis that the diffusion of the cations determines the reaction rates.

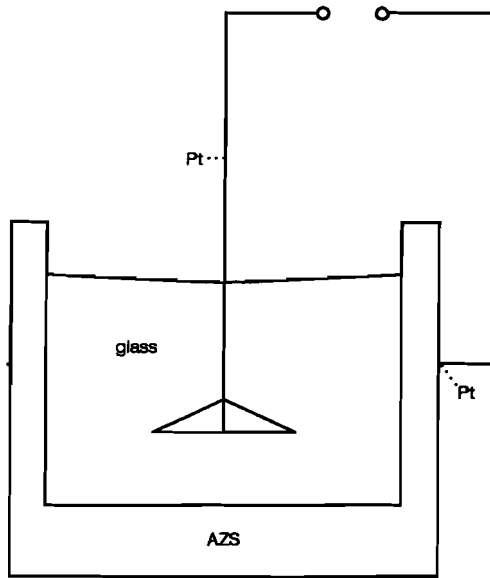
2.2.3. Electrochemical measurements.

In order to validate the proposed mechanisms, the internal cell has been examined using the equipment given by figure 2.2.2, which comprises an AZS (ER 1681) crucible with a platinum wire (diameter 1 mm) surrounding it as a ring. In the glass melt (about 360 g of the so called 354-glass or 395 glass or lithium glass, see annex 1 for the chemical composition) a platinum probe, with a surface

area of about 800 or 20 mm² has been positioned. The electrochemical cell consists of a platinum electrode, the glass melt, the internal cell with a time-dependent reduced layer thickness $s(t)$ in the AZS, the unaffected AZS having a thickness $(d-s(t))$ and a second platinum electrode.

figure 2.2.2

Test set up.



The increase in the thickness of the reacted (reduced) zone, may result in a change in the resistance of the internal cell.

$$R_{M+}(t) = s(t)/AFC_{M+}U_{M+} \quad (9)$$

in which A stands for the cell surface area.

The electrical resistance of the internal short-circuiting of the

internal cell is expressed by

$$R_e(t) = s(t)/AFC_e U_e \quad (10)$$

in which C_e is the concentration and U_e the mobility of the free electrons in the reduced layer.

The resistance for electron transport of the unaffected refractory is expressed as:

$$R'_e(t) = (d-s(t))/AFC'_e U'_e \quad (11)$$

in which, C'_e is the concentration and U'_e the mobility of the free electrons in the original AZS.

In the case of short-circuiting the external cell or applying an external voltage (see figure 2.2.3), the following argumentation for the electrical resistances in this practical arrangement can be made: The surface of the glass melt/AZS contact is very large compared to the surface of the glass/platinum or the platinum/AZS electrodes, so the current densities in the refractory will be very low compared to those at the platinum electrode contacts. Therefore the polarization resistance to the migration of cations, $R_{\phi, M}^+$, and of electrons $R_{\phi, e}$ across the melt-to-AZS interface is presumably negligible at high temperatures and low external current densities.

The electrical resistance of the melt: R_m , is nearly constant at a given temperature. Probably, the small increases in the concentration of corrosion products in the glass melt, originating from the AZS and the small decreases of cations due to the diffusion into the AZS, hardly effects the value of R_m .

The mechanism for oxygen bubble formation suggested by Baucke and Roeth has been experimentally tested for zirconium silicate refractory by these authors.

In the here presented study, electrochemical measurements are performed, in order to test experimentally whether this mechanism is also valid for the interaction of fused cast AZS (Electrofused

Cast Alumina Zirconia Silica) and molten glasses.

The electrochemical measurements applied in this study have been:

1. Measurement of the external cell voltage, E_c .

These measurements are carried out to illustrate that indeed an external cell voltage exists and that this external cell voltage becomes gradually lower by the diffusion of cations in the fused cast AZS. When the external cell voltage drops due to the diffusion of cations in the fused cast AZS it is important to know if the chemical composition of the glass melt has an influence on this drop. When this is the case the rate of the reaction and electron transfer (8) is determined by the diffusion rate of the cations which also determines the formation of oxygen bubbles in the case that the proposed mechanism is valid.

2. Cell short-circuiting.

If the proposed electrochemical mechanism is valid, it must be possible to shift a part of the oxidation away from the glass melt/AZS surface. In a short-circuiting test set-up a part of the oxidation at the glass melt/AZS should be shifted to the platinum electrode surface in the glass melt. If this experiment is positive, part of the required electrons necessary for the redox reactions in the AZS interior are transported through the external circuit. In that case the mechanism responsible for the oxygen bubble formation is of an electrochemical nature.

Probably, the short circuiting of the cell only shifts a relatively small part of the oxygen bubble formation from the AZS glass melt surface to the platinum-to-melt electrode surface. Therefore a third measurement method has been applied.

3. Electrolysis by external applied voltage U , with the outer surface of the AZS crucible as the negative electron donating pole and a positive pole in the glass melt.

In this way a larger part of the oxygen bubble formation at the interface AZS/glass melt can be forced to shift to the platinum-to-melt electrode surface and the generated electrons are transferred via the external circuit to the outer crucible

wall. At conditions in which a sufficient part of the oxygen bubble formation is shifted, the possibility of suppression of the bubble formation at the molten glass/AZS interface can be proven. This can be done by counting the number of bubbles formed at the interface AZS/glass melt. The possibility of suppression of the oxygen bubble formation by a counter current proves the existence of the proposed electrochemical mechanism. Further points of interest are the influence of the applied external voltage on the diffusion rate of the cations into the refractory and on the electric current.

These three tests are used to prove the validity of the proposed mechanism for the interaction of fused cast AZS with a glass melt. In that case the diffusion of the cations of the glass melt into the fused cast AZS should determine the rate of oxygen (bubble) formation. Then, quantification of the diffusion of the cations gives a possibility to predict the tendency of oxygen formation at the interface fused cast AZS/glass melt.

As shown in the illustration of figure 2.2.3, in this experimental study the cell has been subjected to:

1. measurement of external cell voltage, E_c ;
2. short-circuiting of AZS with a platinum electrode;
3. electrolysis by external voltage U , with the AZS crucible outerwall as the negative pole.

In accordance with the law of electro-neutrality the summation of the current densities in the AZS have to be always zero:

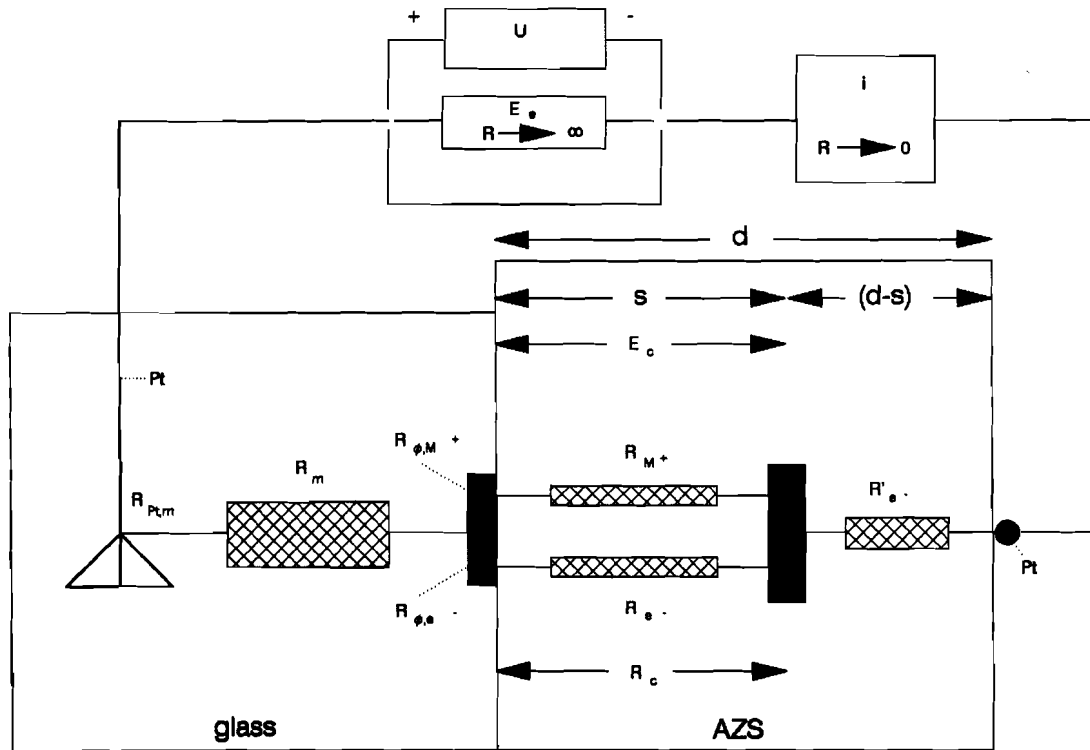
$$\sum_{i=0}^{AZS} i = 0 \quad (12)$$

in other words:

$$\sum_{i=0}^{AZS} i_M^{a+} + i_c + i'_c = 0 \quad (13)$$

figure 2.2.3

Electrochemical cell in detail.



in which

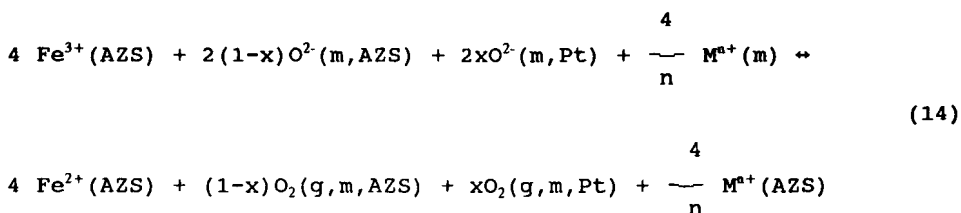
i_M^{a+} = current density by cations

i_e = current density of electrons in internal cell

i'_e = current density of electrons in unaffected AZS

2.2.3.1. Rate-determining step of the internal reaction

The complete cell reaction is the summation of the cathodic electrode reaction in the AZS interior, the cation migration in the AZS and two competing (if short circuited) anodic electrode reactions: a) oxygen formation at the AZS surface and b) (if short circuiting the external loop) at the platinum electrode in the glass melt.



in which $\text{O}^2(\text{m,AZS})$, $\text{O}^2(\text{m,Pt})$, $\text{O}_2(\text{g,m,AZS})$ and $\text{O}_2(\text{g,m,Pt})$ stand for oxide and oxygen in the melt at the AZS surface (m,AZS) and at the platinum electrode (m,Pt), and x for the fraction of oxygen formation at the platinum electrode. The melt is not completely homogeneous, for instance at the interface fused cast AZS/ glass melt, the chemical composition, due to corrosion products, is somewhat different from the bulk composition. This inhomogeneity of the melt is probably not essential for this (qualitative) study, as long as the electric current densities are not too high. Therefore the melt will be treated in the electrochemical measurements as a homogeneous melt.

The emf for equation (14) in a homogeneous melt with the assumption:

$$a_{O^{2-}(m,AZS)} = a_{O^{2-}(m,Pt)} = a_{O^{2-}(m)} \text{ is}$$

$$E_{AZS/m/Pt} = E_{AZS/m/Pt}^0 + (RT/F) \ln \frac{a_{Fe^{3+}(AZS)} \cdot a_{O^{2-}(m)}^{1/2} \cdot a_{M^{n+}(m)}^{1/n}}{a_{Fe^{2+}(AZS)} \cdot f_{O_2^{(1-x)/4}(g,m,AZS)} \cdot f_{O_2^{x/4}(g,m,Pt)} \cdot a_{M^{n+}(AZS)}^{1/n}} \quad (15)$$

in which $E_{AZS,m,Pt}^0$ is the standard potential for any value of x . The emf cannot be measured for all values of x , due to the short-circuiting of the internal cell.

The driving force of reaction (14) depends on x , if the partial pressure of oxygen at the platinum electrode differs from the oxygen fugacity in the melt. If they are identical, the emf, $E_{AZS,m,Pt}$, is independent of x and the emf of $E_{AZS,Pt}$ (15) with $x=1$ will be identical with the value for the internal cell, $E_{AZS,m}$, with $x=0$ (6).

The resulting external cell voltage which can be measured, is

$$\begin{aligned} E_c(t) &= E_{AZS/Pt}(t=0) - \Delta E(t) - (i_i \cdot R_i)(t) \\ &= E_{AZS/m}(t=0) - \Delta E(t) - (i_i \cdot R_i)(t) \end{aligned} \quad (16)$$

and its time-dependence

$$\frac{dE_c}{dt} = -d(\Delta E + i_i \cdot R_i)/dt \quad (17)$$

provides details on the time-dependency of the effect of the 'internal iR drop' of the internal cell, and the change in the Gibbs free energy between the glass melt and the AZS outer crucible wall.

The migration of cations (4) may change the measured emf value during this process, whatever the value of x will be.

Measurement of the external cell voltage.

The objectives of these experiments are:

- To illustrate that there is in the course of time a change in the externally measured cell voltage, between the glass melt and the AZS, due to the diffusion of cations of the melt into the AZS (change in ΔE) and the change in internal $i_p R_i(t)$ by a change in the size of the reduced layer.
- To determine if the change in this external cell voltage depends on the chemical composition of the molten glass.

At $t=0$ the measured external cell voltage depends on the 'internal iR drop' and the $E_{AZS/m/Pt}$. The $E_{AZS/m/Pt}$ (15) is a function of the standard Gibbs energy and for instance the O^{2-} activity, both are dependent on the glass composition.

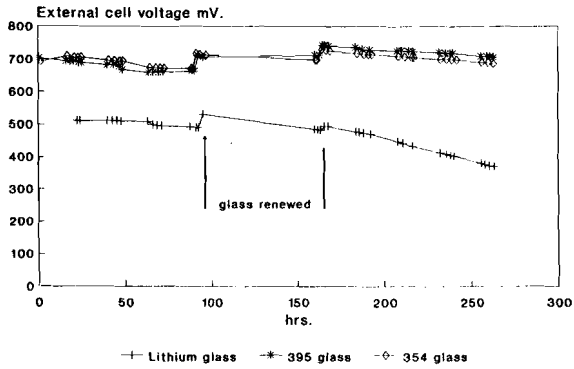
In the case of the measurement of the external cell voltage the R_i is equal to the summation of R_{M+} and R_c . The electrical current in the internal cell is i_i .

The test set-up of figures 2.2.2 and 2.2.3 has been applied and the external cell voltage between the platinum electrode in the glass melt and the platinum ring at the outside of the crucible was measured. The AZS 32 (ER 1681) crucible was filled with cullet and heated up with 175 °C/h up till the test temperature. As soon as the required temperature has been reached, the test starts. After 90 and 160 hours, the glass melt has been renewed with a fresh glass melt of the same composition. During the glass renewal the crucible has been taken out of the test furnace and the glass has been poured out. In the meantime fresh glass is taken out of an other furnace with the same temperature as the test furnace. The AZS test crucible is immediately refilled by the freshly molten glass and placed in the furnace again. The duration of the glass renewal procedure is about 1 minute. The glass melt has been renewed to decrease the effect of the change in glass melt composition (due to diffusion of cations and AZS corrosion products) on the measurement of the external cell voltage. Figure 2.2.4 shows the in this study measured time dependent

figure 2.2.4 Measurements of the external cell voltage of three different glass types at different temperatures as a function of time.

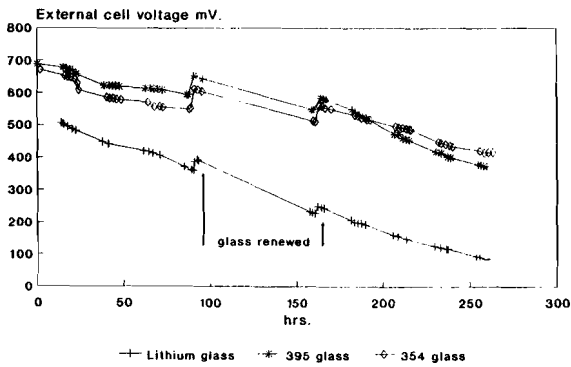
1350 C

figure 2.2.4.a



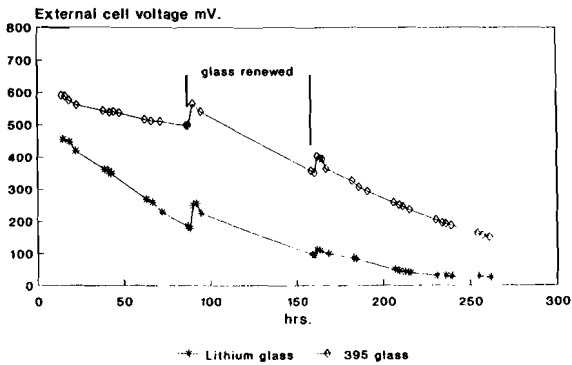
1425 C

figure 2.2.4.b



1500 C

figure 2.2.4.c



external voltages of three different glass types at different temperatures.

The graphs show for 354 and/or 395 glass (see annex 1 for the glass composition) a drop in the E_c in the course of time for the three test temperatures. At higher temperatures the measured drop in E_c is larger. After 90 hours the glass is renewed and the measured E_c increases almost to the starting values in the tests at 1425 and 1500 °C and even at a higher value than the starting E_c value in the test at 1350 °C.

The new glass has the original composition without losses of cations which have been diffused into the AZS and also without the corrosion products of the AZS in it. This means that the Gibbs energy difference between the glass melt and AZS increases again due to the renewal of the glass melt. Thus the driving force of the cation diffusion is increased by the renewal of the glass melt and therefore the internal current of the internal cell will increase, with a internal cell resistance practically equal just before and after the glass renewal.

Experiments with 354 and 395 glasses at 1350 °C.

In the experiments with 354 and 395 glass at 1350 °C the E_c just after glass renewal at 90 hours is even larger than the starting value. The E_c measured after the glass renewal at 160 hours, is larger than the E_c after 90 hours (see figure 2.2.4.a). This implies that, in the time between glass renewal, the change in Gibbs energy of the total practical cell ΔE is larger than the change in $i_i R_i$ of the internal cell. The $i_i R_i$ of the internal cell is probably decreasing during the experiments of 354 and 395 glass at 1350 °C, although the R_i is increasing due to the increase of the size of the reduced layer. Therefore, if the proposed mechanism is valid, the decrease in the i_i seems to be relatively larger than the increase of the R_i . The overall effect is a small decrease of the $i_i R_i$ during the experiment at this temperature and these glasses. This would explain the larger E_c values after each glass melt renewal at 90 and 160 hours.

Experiments with 354 and 395 glasses at 1425 and 1500 °C. In the experiments with the same glasses (354 and 395 glass) at 1425 and 1500 °C there is a decrease in time for the measured external cell voltage. Also the values at 90 and 160 hours, just after glass renewal, are decreasing in the test duration (see figure 2.2.4.b and 2.2.4.c). This implies that either the internal $i_p R_i$ of the internal cell in the duration of the experiment is increasing or the chemical composition of the AZS, due to the diffusion of the cation of the molten glass into the AZS, which leads to composition changes even at the outer surface of the AZS at the platinum ring electrode. This brings a reduction of the Gibbs energy difference in the system and therefore in the measured E_c . The increase of the $i_p R_i$ value of the internal cell in the duration of the experiment is contradictory to the observations at 1350 °C with these glasses. The decrease of the measured E_c , at 1425 and 1500 °C in the experiments with 354 and 395 glass, is probably not caused by an increase in $i_p R_i$. This decrease of the E_c is probably caused by the decrease of the concentration of cations in the glass melt by diffusion into the AZS on one hand and the increase of the concentration of the diffused cation in the AZS till the platinum electrode at the outside on the other hand. The change in E_c due to the decrease of cations in the glass melt is illustrated by the increase of the E_c just after the renewal of the glass in figure 2.2.4. The only small decrease in E_c after glass renewal at 90 hours compared to the starting value of the E_c and the larger drop of the E_c after the glass renewal at 160 hours compared with the starting value of the E_c agrees very well with the measured change in chemical composition of the AZS material at the outside of the crucible at the platinum electrode. This will be presented in chapter 3.

Experiments with lithium glass.

For the lithium glass (see annex 1) the same argumentation can be applied, with the remark that the mobility and the penetration depth of the cation(s) has to be much larger as in the other glasses to explain the measured E_c values. Indeed, the larger

mobility and penetration rate of the cations of the lithium glass into the AZS will be demonstrated in chapter 3 and 4 of this study.

The time dependency of the measured E_c and the strong influence of temperature and the glass melt composition, means that the rate of the internal reaction (5) probably depends on the velocity of diffusion of the cations from the melt into the AZS refractory. The resistance of the (internal) short-circuiting of the internal cell R_c (10) can therefore not be decisive, otherwise the glass melt composition would not have such a large influence on the E_c . Indicating that probably,

$$R_{M+} > R_c \text{ or } (C_M^{n+} \cdot U_M^{n+}) < (C_c^- \cdot U_c^-)$$

2.2.3.2. Shift of the location of oxygen formation.

Cell short-circuiting.

The objectives of these experiments are:

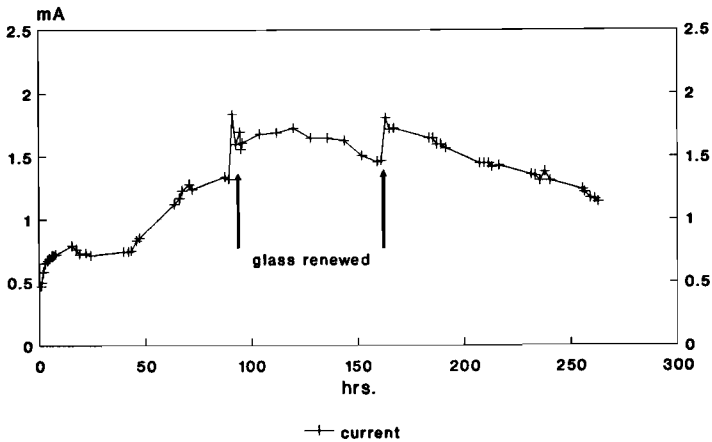
- To determine whether by short-circuiting, in the test set-up of figures 2.2.2 and 2.2.3, a part of the oxidation of the oxide ions can be shifted from the AZS surface to the platinum-to-melt surface.
- The measurement of the electric (external) current, in order to obtain an estimation of the resistance ratio for electron transfer between the non reduced part and the reduced part of the AZS.

Besides the short-circuiting of the cell, the test circumstances were the same as in the previous tests described in 2.2.3.1. In a circuit in which a platinum electrode in the melt, is short-circuited with the AZS, oxygen bubbles are formed at the surface of this electrode. This means that part of the oxidation of oxide ions has shifted from the AZS surface to the platinum-to-melt interface (14) with $0 < x < 1$. Besides, electrons migrate from the platinum electrode to the reduction zone under the AZS surface, via the external circuit and the non reduced part of the

refractory. The electric current measured on a short-circuited cell shows to be sensible for small differences in circumstances, figure 2.2.5 gives a good example of the tendency and order of magnitude of the measured current.

figure 2.2.5 Measured external current of a short-circuiting cell.
Test with AZS 32 (ER 1681).

Short-circuiting cell 354 glass, 1425 C



The steep rises in electric current during the two tests, one after 90 and one after 161 hours, are due to the renewal of the glass, which suddenly increases the Gibbs free energy between glass melt and AZS again. This is because the new glass has the original composition without loss of cation, which has been diffused into the AZS. The new glass also does not contain corrosion products of the AZS.

The low initial current, at $t=0$ till $t=50$ hours, in the test is probably caused by the poor electrical contact between the

platinum outer ring and the initially "dry" AZS. After the test temperature is reached, the AZS starts to expel glassy phase and the electrical contact between the surface of the AZS and the platinum ring improves. After about 50 until 90 hours the measured electric external current increases. In the middle of the duration of the experiment, $t=90$ till $t=161$ hours, the measured electric current is more or less stable. At the end of the test, $t=161$ till $t=260$ hours, the measured electric current is decreasing. To explain the measured current in figure 2.2.5, two time dependent effects have to be considered, the thickness of the reduced layer and the driving force.

On the time scale, the thickness of the reduced layer increases at the expense of the original (non reduced) refractory layer thickness. Figure 2.2.4.b gives the external voltage of a not short circuiting cell, at 1425 °C using 354 glass. The external cell voltage (as a measure for the driving force) initially is about 700 mV and finally, after 260 hours, around 400 mV. The increase of external current between 50 and 90 hours of the test duration is probably caused by the increase of the reduced layer and therefore the decrease of the non reduced layer. In the middle part of the experiment the possible increase of measured external current due to the increase of the reduced layer has been compensated by the decrease of driving force. In the last part of the test duration the decrease of driving force is larger than the possible increase of external current due to the decreasing layer thickness of the non reduced refractory.

Electrolysis by external voltage U , at the outer surface of the AZS crucible.

The objectives of these experiments are:

- To investigate the possibility of suppressing bubble formation on the interface glass melt/AZS.
- To examine the influence of the external voltage on the diffusion of the cations.

- To determine the relation of external voltage on the electric current.

Test set-up

The set-up is the same as for the previous tests (see figures 2.2.2 and 2.2.3). The only difference in this test is the implementation of a fixed voltage between the platinum ring surrounding the AZS crucible (negative pole) and the platinum probe in the glass.

For the electrical network see figure 2.2.3.

Test conditions:

applied voltage	0; 1; 2.5; 5 or 39.5 V
test period	48 hours (one 72-hour test)
temperature	1425°C
glass type	354 glass
probe area	800 and 20 mm ²
crucible diameter	inside: 70 mm; outside: 89 mm
material	AZS 32 (ER 1681)

The parameters that have been analyzed or measured, are the electric current, the cation diffusion (concentration profiles) in the glassy phase of the AZS after the exposure time and the bubble formation at the AZS-to-glass interface.

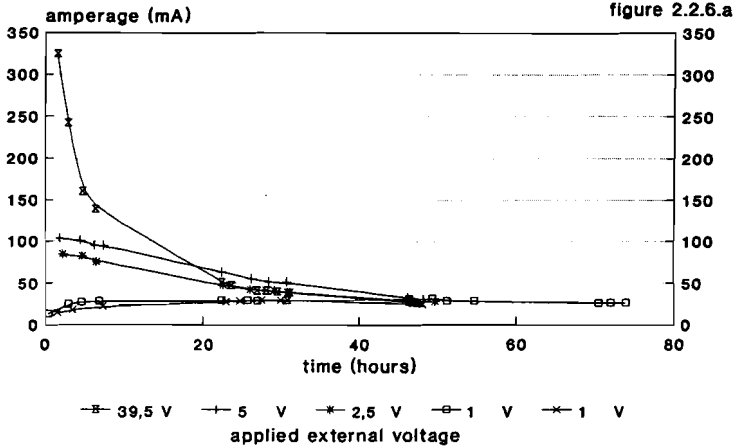
A) Electric current.

The measured current running through the cell varied (see figure 2.2.6.a). At 39.5, 5 and 2.5 V the measured amperage drops at first; at 1 V it increases slightly at first. After about 48 hours the electric current is virtually identical for the four differences in potential, and remains stable for extended periods (figure 2.2.6 b).

The current density depends on the probe area. The steady-state amperage with the 800 mm² probe was about 28 mA and that of the 20 mm² probe about 12 mA (see figure 2.2.6 a and 2.2.6 c). This indicates that the electrical resistance at the interface platinum-glass is relatively large.

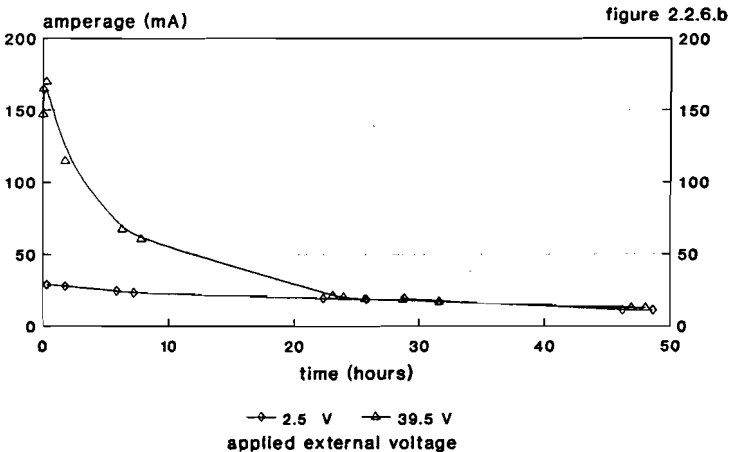
figure 2.2.6 Measurement of the current through the external circuit, applying different external voltage's.

Electrolysis current amperage on time scale



1425 C, 354 glass
800 mm² electrode area

Electrolysis current amperage on time scale



1425 C, 354 glass
20 mm² electrode area

B) Diffusion of cations into the glassy phase of the AZS.

To study the effect of the voltage on the diffusion processes, special attention has been paid to the concentration profiles of Na_2O , K_2O , BaO and Al_2O_3 in the AZS after an experiment. Annex 2, table 1 gives the measured values.

The method which has been applied for the determination of the concentration profiles will be given in the next chapter.

For the present tests, the concentration profiles in the glassy phase in the AZS have been determined as closely as possible to the platinum ring position surrounding the outer part of the crucible (measuring concentration profiles at the same vertical positions). The value of the applied external voltage, appears to have hardly any systematic effect on the concentration profiles of K_2O and BaO . See figure 2.2.7, 2.2.8 and annex 2, table 1 for the measurements using a 20 mm^2 glass melt electrode area.

However, the effect of the external voltage on the profile of Na_2O at the outside of the crucible is considerable for 354 glass. The tests with an external negative potential between the AZS electrode and glass electrode showed a strong accumulation in Na_2O concentration deep in the AZS at the position close to the platinum ring surrounding the outer part of the crucible. See figure 2.2.9.

The difference in potential (extra negative charge at the crucible electrode) has brought about additional diffusion of sodium from the glass melt into the glassy phase of the AZS towards the negative pole at the outer surface of the crucible. This accumulated additional Na^+ diffusion increased for higher potentials. The Al_2O_3 concentration in the glassy phase of the AZS increases along with the Na_2O concentration. See figure 2.2.10. This is probably due to the increase in solubility of Al_2O_3 (from corundum) in the glassy phases with an increased Na_2O concentration.

The mobility of cations in glass depends on the ion radius and ion charge. The fact that the sodium ion has the highest velocity could, therefore, be accounted for, from the combination of the

figure 2.2.7 and 2.2.8 Concentration profiles of K_2O and BaO after applying different external voltages.

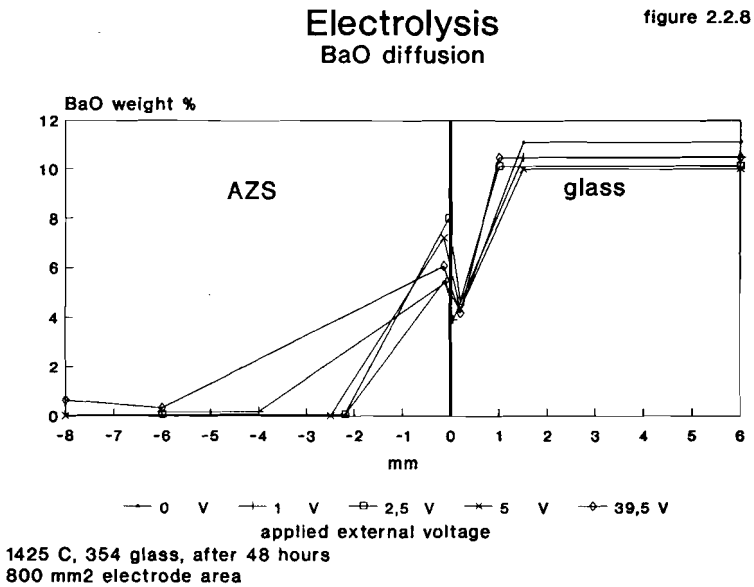
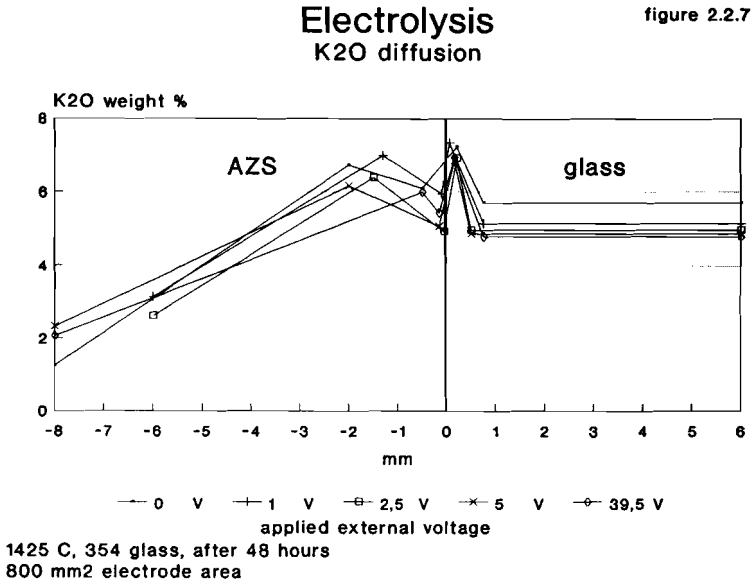
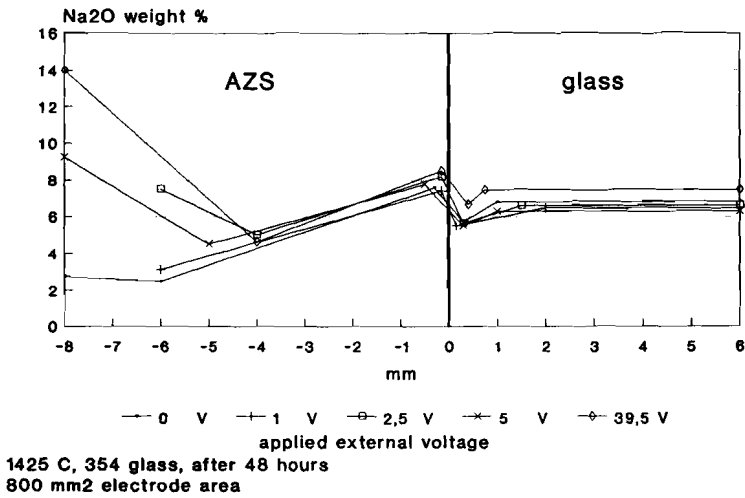


figure 2.2.9 and 2.2.10 Concentration profiles of Na_2O and Al_2O_3 after applying different external voltages.

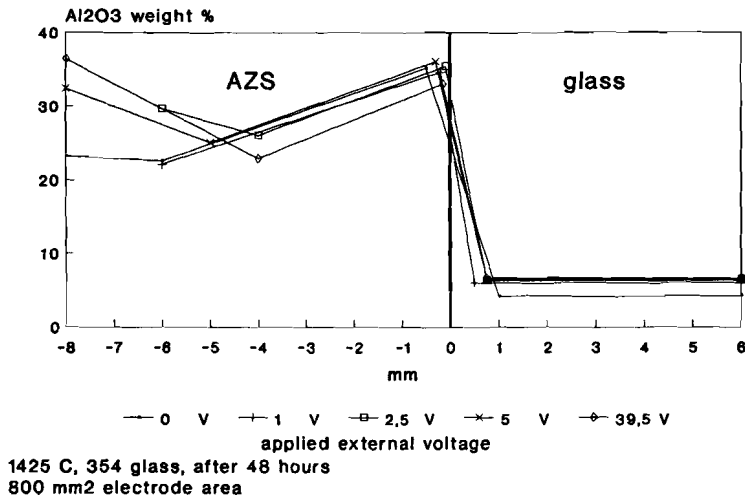
Electrolysis Na₂O diffusion

figure 2.2.9



Electrolysis Al₂O₃ diffusion

figure 2.2.10



ion radius (Na^+ 0.97; K^+ 1.33; and Ba^{2+} 1.34 Å) and the ion charge. The double charge of an ion reduces the mobility of the ion dramatically compared to an univalent ion of the same radius (Lit. 18). The effect which the electrical field of an ion has on the fundamental relations in oxide systems are described by A. Dietzel (Lit. 19). The effect of the electric potential on the velocity of diffusion of Na^+ , which is far stronger than in the case of the other cations, has been determined on earlier occasions. Doremus (Lit. 15) has determined the mobilities of alkali cations in vitreous silica under the influence of an electric potential at lower temperatures (max. 380°C). The mobility of Na^+ was a factor of 1000 higher than that of K^+ . That of Li^+ (ion radius 0.68 Å), however, was far lower (about a factor of 10) than that of Na^+ . The latter fact, therefore, is not in agreement with the assumption that small ion radius, show a higher mobility under the influence of an electric potential. If Doremus's estimate of the relative mobility of the various cations also applies to the system and temperature of these investigations, the mobilities of the other cations are too low for the determination of the difference in concentration profiles of these cations between the presence and the absence of an external potential using this coarse test method. Also the platinum ring with a wire diameter of 1 mm surrounding the outer crucible surface is not an optimum condition for a quantitative measurement, because the increase of the Na_2O concentration was half cylindrical around this very local platinum-AZS contact. Theoretically, a platinum AZS ribbon along the total height at the outer wall would be a large improvement for more quantitative tests, but it is practically impossible to establish a good electrical contact between the total ribbon surface and the crucible wall during the experiment.

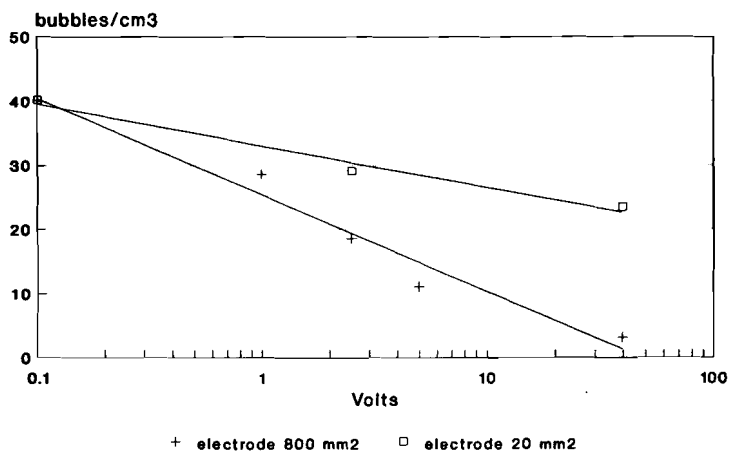
C) Bubble formation at AZS/glass melt interface.

The application of an external voltage (negative pole at the outer wall) shows a reduction in the number of bubbles generated in the

Electrolysis

number of bubbles from AZS

figure 2.2.11



1425 C, 354 glass, after 48 hours

AZS/glass melt interface.

An increase in potential results in a drop in the number of bubbles, counted after 48 hours, at this interface. See figure 2.2.11. There is a linear relationship between the number of bubbles and the logarithmic value of the voltage. Although the external current, after 48 hours, is independent of the external voltage in this test set-up, the external current depends on the used electrode in the glass melt. Figure 2.2.11 also shows the smaller drop in the amount of bubbles at the AZS interface at the end of the tests using the 20 mm² electrode compared to the 800 mm² electrode. The measured quantitative relationship probably depends on the applied test set-up, specially the used electrodes in the glass melt and at the AZS crucible outer wall. If an external voltage with a positive pole at the outer wall of the crucible would be applied, according to the theory, the number of bubbles generated at the interface glass melt/AZS would be increased. The

internal reduction rate however would be reduced. In the case of a positive pole at the outer wall of AZS crucible, at a high external voltage, the cation migration can even change in the direction from the glassy phase of the AZS into the glass melt.

2.2.4 Discussion and conclusions.

External cell voltage:

In this study it has been measured and shown that the rate of the decrease of the external cell voltage, and therefore a change in Gibbs energy (8), during a test depends on the chemical composition of the attacking glass melt.

This implies that the rate of the internal reaction probably depends on the penetration of the different cations (depending on the glass composition) in the glassy phase of the AZS.

Cell short-circuiting:

In a short circuited external cell, some oxygen bubble formation on the platinum electrode in the glass melt has been observed which means that a part of the oxidation of oxide ions has shifted from the AZS/glass melt interface to the platinum-to-glass melt surface.

Electrolysis by external voltage:

With an external voltage, with the AZS crucible outer surface as a negative pole, it is possible to reduce the amount of oxygen bubbles generated in the AZS-to-glass melt interface.

These measurements and observations also confirm the proposed mechanism.

In an industrial process it will be difficult to apply an external voltage for bubble reduction because then, at the positive pole (in the melt) oxygen bubbles will be formed. The outside of the AZS is relatively cold with a high electrical resistance at these low temperatures. Sodium cations accumulate in the AZS which increases the corrosion and affects the mechanical properties of the AZS material.

In the electrolysis by an external voltage, with the AZS outer surface as negative pole, the following phenomena have been examined:

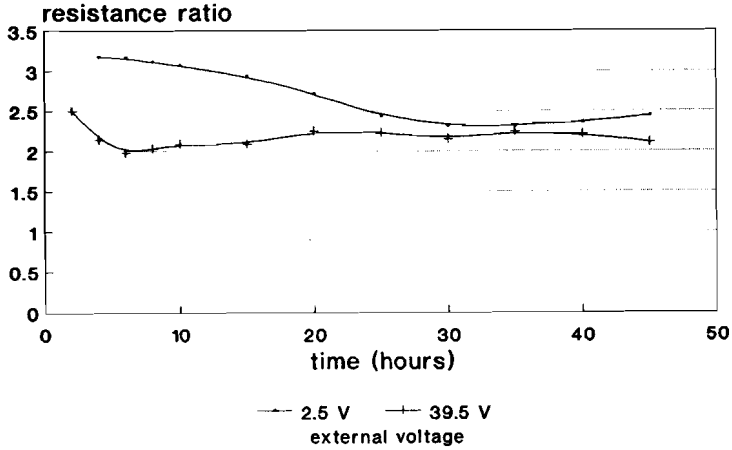
1. The electrode area for the electrode in the melt as well as probably (not investigated) also for the platinum wire at the AZS surface affects the external measured current at a specific voltage.
2. After some time, at different externally applied voltages, the external current tends to the same steady-state level, only dependent on the electrode area.
3. The number of bubbles at the AZS/glass melt interface, after 48 hours, depends on the applied external voltage.
4. The initial current density of an electrode surface depends on the applied voltage.
5. The diffusion rate of Na^+ increases markedly with an increase in voltage. This increase, like the increase in external current, is remarkably higher for the 800 mm² glass melt electrode than for the 20 mm² one.
6. At a specific voltage level, the glass melt electrode area also affects the bubble suppression.

These six items justify the conclusion that the resistance of the external cell with the measured current densities depends on time and the area of the platinum electrodes.

The ratio of the applied fixed external voltage and the measured external current values (V_{external}/i'_c) gives the resistance of the test set-up. In other words the sum of the resistances of the platinum wires, platinum electrode to glass melt, glass melt itself, glass melt to AZS, AZS to platinum ring, the non reduced AZS and the reduced AZS. During electrolysis the resistance of the reduced layer, according to Baucke and Roeth (Lit. 7), can formally be treated as, $(R_{M+} \cdot R_c / (R_{M+} + R_c))$.

The so calculated resistances are for instance dependent on time, external voltage and surface area of the platinum glass melt electrode. In figure 2.2.12 the ratio of the calculated total resistances is given as a function of time for the two used

Ratio of total resistance between the glass electrodes of 20 and 800 mm², when external voltage is applied. figure 2.2.12



platinum electrodes (resistance ratio(t) = $\{(V_{\text{external}}/i'_{e.})_{20 \text{ mm}^2} / (V_{\text{external}}/i'_{e.})_{800 \text{ mm}^2}\} (t)$ at two different externally applied voltages (2.5 and 39.5 V).

The ratio between the measured resistance, for the case of the 20 mm² electrode divided by the case of the 800 mm² electrode, is more or less constant in time, which implies that the main resistance, from the beginning, lies here at the interface platinum electrode/glass melt where oxygen bubbles are formed. The decrease of the electric current during the experiments when an external voltage is applied, means an increase of the electric resistance in time mainly at the interface platinum electrode/glass melt. An increase of resistance of a platinum electrode in a glass melt is a well known phenomenon. Normally this is due to a electrical double layer which establishes itself very fast (milliseconds) (Lit. 14). In this study it takes up to two days in order to obtain a constant current level and thus a constant resistance. Such a time

scale, points in the direction of a diffusion limited process. The behaviour of equal electrical current for different potentials resembles that of a complete concentration polarization (Lit. 14). At the platinum electrode in the glass melt oxygen bubbles are formed, and are released from the glass melt. It is possible that the transport (diffusion) of O^{2-} ions in the glass melt to the platinum electrode is the cause for the increase of the resistance and the 'steady state' level of the total resistance of the measured electrical loop after about 48 hours. In other words, the increase of the resistance possibly could be caused by the formation of a O^{2-} diffusion layer.

A larger surface of the platinum glass melt electrode and the already mentioned platinum cylinder instead of the platinum wire at the outer surface of the AZS crucible would improve the quantitative accuracy of the measurements.

The external voltage level affects the bubble suppression at the interface glass melt/AZS (see figure 2.2.11). The higher the external voltage with the negative pole at the outer wall of the crucible the lower the number of bubbles generated at the interface glass melt/AZS. A low number of bubbles at the interface glass melt/AZS means that the amount of electrons i_e formed by oxidation of O^{2-} to O_2 is decreased at the interface glass melt/AZS. This is to be expected because the electrons (i_e) from the glass melt/AZS interface now have to move in the direction of the negative pole of the implied external voltage.

The electric current due to the migration of cations is equal to the summation of the current of electrons in the internal cell and the non reduced AZS.

$$i_M^{n+} = -(i_e + i'_e)$$

The ultimate externally measured amperage (i'_e) in the final test phase (after 48 hours) is the same at the various different external voltages. This means that after 48 hours, at a higher voltage with less bubble formation (less i_e) at the interface glass melt/AZS, the cation diffusion into the AZS has to be

smaller.

The statement that at a higher externally applied voltage, after 48 hours, the amount of cation diffusion into the AZS becomes smaller as the current is equal for all tests with the same electrode, looks strange at first. Above it has been explained that the main part of the electrical resistance, is at and close to the interface platinum electrode/glass melt. The potential drop across the AZS in the tests caused by the externally applied voltage, after 48 hours, is not so dominant anymore. Under these conditions the differences in the chemical partial Gibbs energy of the cations in the glass melt and the glassy phase of the AZS become important again as driving force, for the diffusion rate of cations (i_M^{n+}). In figure 2.2.9 it is shown that the tests with a high externally applied voltage lead to a high concentration of sodium oxide in the glassy phase of the AZS.

This high concentration of sodium oxide in the glassy phase of the AZS is accumulated in the first 24 hours of the test duration, when the measured external current has been large compared with the tests with no or small externally applied voltages. Therefore, after 48 hours, the rate of cation diffusion in the tests with high externally applied voltage has decreased considerably and is smaller than in the tests with low externally applied voltages. The decrease in rate of cation diffusion is caused by the decrease in difference of Gibbs energy between the AZS and the molten glass.

In this study, the objective has been the validation of the proposed mechanism for fused cast AZS in contact with molten glass. A more detailed study with different glass compositions (e.g. sodium free glass) of the effects of external electric potential on the cation diffusion and suppression of bubble formation at the interface glass melt/AZS could increase the insight of the mechanism. Also the hypothesis of the formation of a diffusion layer for O^{2-} at the platinum electrode in the glass melt as the main electrical resistance if a external voltage is applied, needs more intensive study.

Nevertheless, the objective of the validation of the mechanism in

which the diffusion of cations into the glassy phase of the fused cast AZS is controlling the formation of oxygen bubbles at the interface glass melt/fused cast AZS has been met.

Literature references chapter 2.

- [1] F.W. Kraemer;
Analysis of gases evolved by AZS refractories and by refractory/glass melt reactions. Techniques and results. Contribution to the bubble forming mechanism of AZS material.
Glastech. Ber. 65 (1992) p. 93-98.
- [2] E.L. Swarts;
Bubble generation at glass/refractory interfaces. A review of fundamental mechanisms and practical considerations.
Glastech. Ber. 65 (1992) p. 87-92.
- [3] M. Dunkl;
Studies on the glassy and reaction phases given off by fused cast AZS blocks and their effects on glass quality.
Glastech. Ber. 62 (1989) p. 389-395.
- [4] D. Walrod;
A study of the driving force behind AZS glass phase exudation.
Ceram. Eng. Sci. Proc. 10 (1989) p. 338-347.
- [5] A.G. Bossard, E.R. Begley;
Refractory blistering in glass.
Symposium on defects in glass. An. Meet. ICG.
Tokyo 1966 p. 69-81.
- [6] L. Leger, M. Boffe, E. Plumet;
Electrochemical phenomenon at the glass-refractory material interface.
Glass Technology 1 (1960) p 174-179.
- [7] F.G.K. Baucke, G. Roeth;
Electrochemical mechanism of the oxygen bubble formation at the interface between oxidic melts and zirconium silicate refractories.
Glastech. Ber. 61 (1988) p. 109-118.
- [8] W. Trier;
Glassmelzofen, Konstruktion und Betriebsverhalten.
Springer Verlag 1984 p. 64
ISBN 3-540-12494-2

- [9] H. Meyer, H. Poehnitzsch;
Ueber die Ursache des Glasaustritts und der Blasenbildung an
schmelzgegossenen Steinen bei hohen Temperaturen.
Glastech. Ber. **38** (1965) p. 393-397.
- [10] O. Schmid;
Ueber die Glasphase in schmelzflussig gegossenen
Aluminiumoxyd-Zirkonoxysteinen.
Glastech. Ber. **38** (1965) p 200-206.
- [11] M. Dunkl;
Investigation of the liberation of glassy phase from fused
cast AZS materials.
Glastech. Ber. **63K** (1990) p. 370-380.
- [12] P. Ratto;
What can we expect from fused cast refractories.
Glass machinery 1991 p. 62-64.
- [13] G. Meden, T. van der Pas;
Invloed van het uitstoken van ZAC 1681 op de mate van
belvorming.
OC 81/350.
- [14] A.J. Bard, L.R. Faulkner;
Electrochemical methods; Fundaments and applications.
John Wiley & Sons, New York 1980.
- [15] R.H. Doremus;
Electrical conductivity and electrolysis of alkali ions in
silica glass.
Phys. and chem. of glasses, **10** (1969), p. 28-33.
- [16] F. Daniels, R.A. Alberty;
Physical chemistry, Chapter 7.
John Wiley & Sons. New York 1966.
- [17] G.H. Frischat;
Ionic diffusion in oxide glasses.
Trans Tech S.A.
- [18] H.H. Blau;
Fourth Int. Congr. on Glass, Paper VI 6.
Paris, 1956.

[19] A. Dietzel;

Die Kationenfeldstärken und ihre Beziehungen zu
Entglasungsvorgängen, zur Verbindungsbildung und zu den
Schmelzpunkten von Silicaten.

Z. für Elektrochem. **48** (1942) p. 9-23.

3. Cation diffusion into fused cast AZS.

3.1 Introduction.

When a glass melt is brought into contact with AZS, due to a difference in chemical potential, a transport process of cations will take place, to come to chemical equilibrium. Simultaneously with the transport of positive load, due to the transport of cations in the AZS, electrons are transported to the reduction front in the interior of the AZS and redox reactions take place at the refractory/glass melt interface (oxygen formation) and at the reduction front in the interior of the AZS (reduction of polyvalent electrons). The combined transport process of cations and electrons determines the oxygen bubble formation at the refractory/glass melt interface. The underlying mechanism has been described in chapter 2 and this is the main mechanism responsible for the formation of bubbles and knots at the interface of fused cast AZS and molten glass in industrial operation.

In this chapter the experiments with fused cast AZS 32/33 (ER 1681) crucibles and different glasses are described. In the first part of the chapter the concentration profiles of sodium, potassium, barium and strontium in the melt at the interface with AZS and the glassy phase of the AZS are shown. The chemical composition of the interface glass melt/fused cast AZS should correspond with the original chemical composition of knots and will be used in chapter 6 'Knot formation mechanism and characterization' for the identification of knots. The concentration profiles in the glassy phase of the AZS give information about the penetration depth of the cations. This is important for the second part of this chapter. In the second part of this chapter the 'total or overall' diffusion rate of cations is derived. For a straightforward determination of the diffusivity the penetration depth of the cations should not have the tendency to exceed the crucible wall thickness. The overall diffusion rate of a cation in a crucible experiment is determined by measuring the change in chemical composition of the glass melt as a function

of time. Here, the rate of diffusion will be expressed in so called electron equivalent per hour (e.e.h.) which is the positive charge transported by the cation in the fused cast AZS, determined in a standard test set-up. The e.e.h. is the result of a combination of effects like AZS surface area, mobility of the cation, difference in partial Gibbs energy of the cation in the melt and in the glassy phase of the AZS and the time the AZS has been exposed to the glass melt.

The e.e.h. is therefore only a relative value for the diffusion rate. In chapter 4, a model will be presented which determines the influence of the temperature and chemical composition of the glass melt on the formation of glass defects from the fused cast AZS using the measured e.e.h. values.

3.2 Experimental procedures.

Test data:

- crucible ER 1681 (Fused cast AZS)
inner diameter 70.5 mm
outer diameter 89.0 mm
height 75 mm
depth 52-55 mm
weight about 950 g
- glass types 395 glass: table 3.1
354 glass: table 3.1
lithium glass: table 3.1
- glass quantity about 360 g (cullet)
- temperatures 1350; 1425; 1500°C
- electrical heated furnace (Naber)
- test periods: a) 100 hours, including at the end a
temperature alternation (last nine
hours): four times a cycle of one hour
at standard temperature +25°C and one
hour at standard temperature -25°C,
followed by one hour at standard

- temperature (described as: "100 hrs. alt. temp." in figures).
- b) 100 hours with forced convection in melt, at a rotation speed of $w=0.2$ and 2.0 cycles min^{-1} . Using a rod shaped stirrer with diameter of 21 mm, stirrer height 13.5 mm above crucible bottom. (described as: "100 hrs. $w=0.2$ " or "100 hrs. $w=2.0$ " in figures).
 - c) 260 hours:glass renewal after about 90 and after 160 hours
 - d) 600 hours:glass renewal after about 90, 163, 258, 331, 426 and 499 hours.

Note: The experiments with temperature alternation and forced convection (increased corrosion) have been executed to determine the influence of these parameters on the bubble formation (see chapter 5).

Neither the temperature alternation nor the application of shear stress (owing to forced convection) had any appreciable effect on either the diffusion profile or the concentration profile in the AZS. This implies that these tests are indicative of the reproducibility of the measuring method. This also implies that the diffusion in the glass melt is not the rate determining step of the electrochemical process but the diffusion of the cations in the glassy phase in the fused cast AZS.

The cation diffusion rate has been determined:

- A. by analysis of the profiles of the concentration of the cations in the glass and the glassy phase in the AZS.
- B. by analysis of the composition of the glass which was renewed during the 260 and 600 hour tests.

3.2.1. Profiles of the concentration of the cations in the glass melt and the glassy phase of the AZS.

3.2.1.1 Measurement method.

The crucible has been filled with cullet and has been heated, with a rate of 175 °C/h, up to the test temperature. The test time starts as the test temperature has been reached.

After completion of the experimental melting time, the crucible has been taken out of the furnace and cooled during 5 minutes at room temperature. The crucible has been subsequently put into an annealing furnace at 520 °C and cooled down slowly overnight. The cracks in the glass were filled with 'Canada Balsam', of which the volatile part has been evaporated at 130 °C. From the crucible a slice has been cut of about 10 mm thickness. A sample with a diameter of 20 mm has been drilled from this slice, with the interface AZS-glass in the middle of the sample. The sample was polished for measurements using a scanning electron microscope (SEM) and energy dispersive X-ray analysis (EDX) system.

The SEM is a Philips 505 and the EDX, an Edax PV9900.

Every spot measurement (very localised EDX measurement) was done under identical conditions:

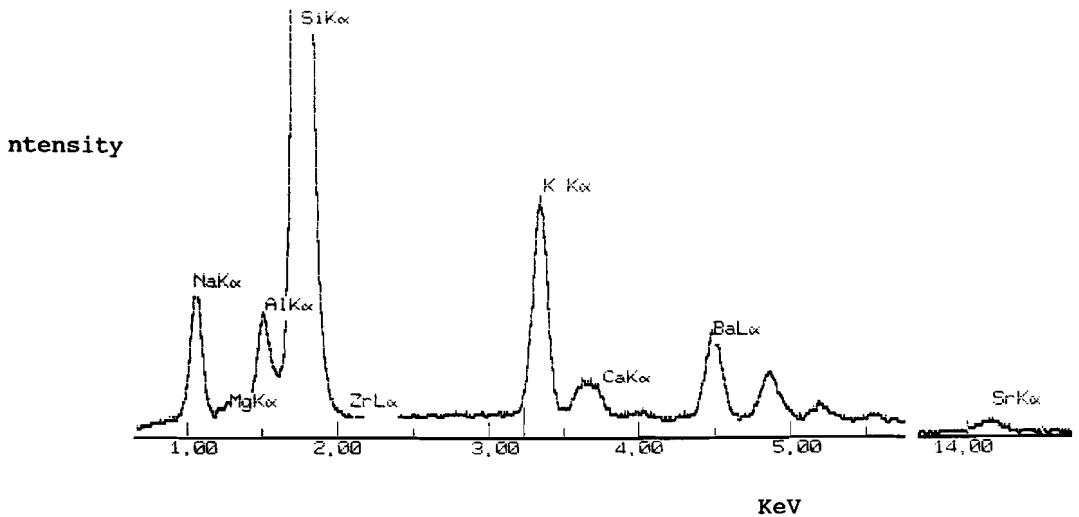
time	: 100 live (real measurement time) seconds
magnification	: 5200 x
selected area	: 6.3 x 4.6 micrometer per spot measurement
current	: 0.70 nA
voltage	: 25 kV
sample position:	eucentric (34.5 mm)

The fluorescence peaks in the measurements of the intensities can be seen in figure 3.2.1.

The measured intensity is calculated compared to a standard sample using background correction. The local concentration of the different elements is calculated as oxides in weight% and has been normalised to 100%.

The chemical composition of the glass and of the glassy phase of the AZS matrix has been measured. The dividing line (zero in the

figure 3.2.1 Fluorescence peaks in the EDX measurements of the intensities.



figures) between glass and AZS is formed by the last ZrO_2 nodules. The measurements started at a distance of 6000 micrometer from this dividing line in the glass. By definition, a negative distance means, the distance from the dividing line and measured spot in the glassy phase of the AZS. The standard procedure was always two spot measurements on 6000, 4000, 2000, 1500, 1000, 750, 500, 400, 300, 200, 150, 100, 50, 0, -50, -100, -150, -200, -300, -500, -1000, -2000, -4000, -6000 micrometers. In this way the spot measurements started at the glass side (positive value) going to the glassy phase (negative value) of the fused cast AZS. Close to the interface glass/AZS, the number of spot measurements were increased.

3.2.1.2 Results of measured concentration profiles.

The concentration profiles of the most important cations, which can be measured with EDX in the glasses from annex 1, are Na_2O , K_2O , BaO and SrO . Here the measured concentration profiles of these oxides will be presented in detail.

Na_2O

The general shape of the concentration profile of Na_2O from the glass side into the fused cast AZS, (in the figures from right to left) is a slight concentration decrease, just before the first ZrO_2 nodules are reached and then even an increase to a maximum concentration higher than in the used glasses.

Table 2 in annex 2 shows the measured values. An example of the reproducibility is presented in figure 3.2.2. An example for the effects of the progress of the concentration profile during the exposure time is presented in figure 3.2.3. The penetration depth of the diffusion into the AZS shows the expected strong increase with the duration of the test period.

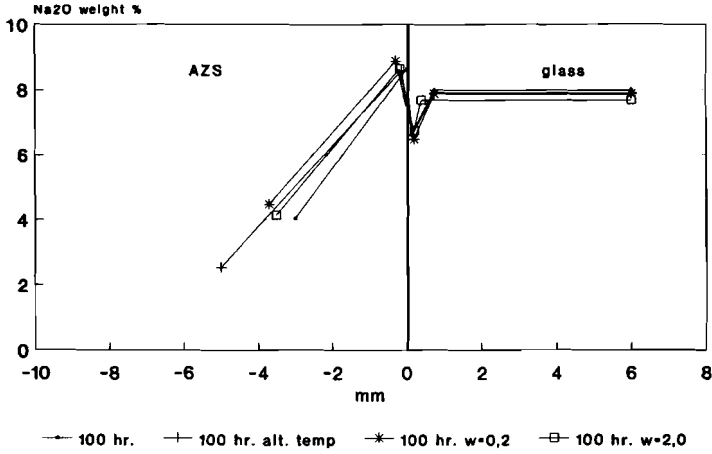
The maximum Na_2O concentration in the AZS generally increases slightly in the course of time. Owing to the increase in diffusion depth going with longer periods the location of the maximum concentration is shifted ever deeper into the AZS.

The effect of the temperature is presented in figure 3.2.4. At 1350°C (the lowest test temperature) the maximum concentration is generally highest and the penetration depth obviously smallest. The effect of the different glass types is very obvious, for instance given by figure 3.2.5. An increase in the concentration of Na_2O in the molten glass yields an increase in concentration of Na_2O in the glassy phase of the AZS. The sodium from the lithium containing glass has an exceptionally large diffusion depth compared to 354 glass and 395 glass.

The crucible wall was about 9 mm thick. At 1350°C , after only 100 hours the penetration depth of Na_2O was markedly less than this 9 mm.

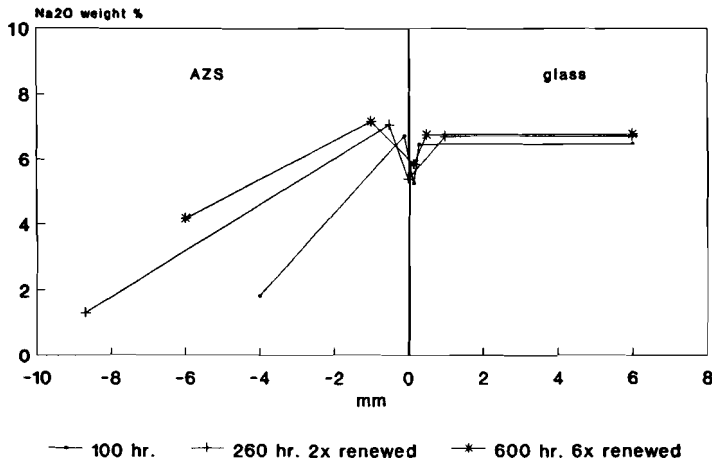
Na₂O diffusion in AZS
354 glass, 1350 C

figure 3.2.2



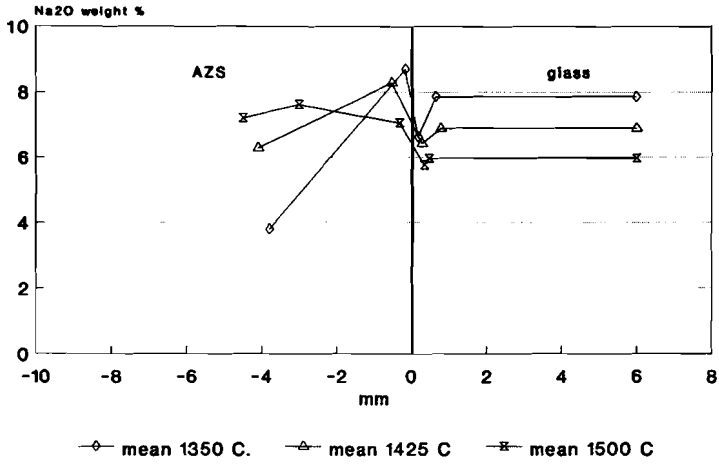
Na₂O diffusion in AZS
395 glass, 1350 C

figure 3.2.3



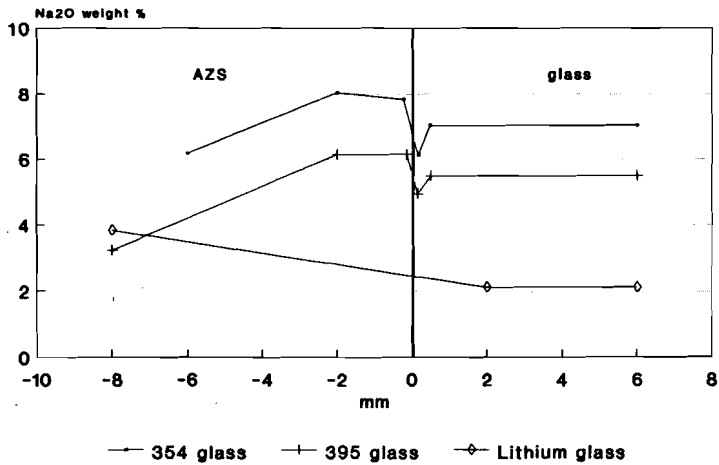
Na₂O diffusion in AZS
354 glass, 100 hr.

figure 3.2.4



Na₂O diffusion in AZS
1425 C, 260 hr.

figure 3.2.5



2x renewed

K₂O

The general shape of the concentration profile of K₂O, going from the glass into the fused cast AZS, shows an increase just before the first ZrO₂ nodules are reached. The maximum of the first peak (going from the melt into the AZS) is close to the position where the first ZrO₂ nodules occur. After this first maximum, the K₂O concentration decreases with about the same angle to a minimum and increases again to a new maximum.

Table 3 in annex 2 shows the measured values. An example of the reproducibility is presented in figure 3.2.6. An example for the K₂O concentration profile during the progress of time is presented in figure 3.2.7.

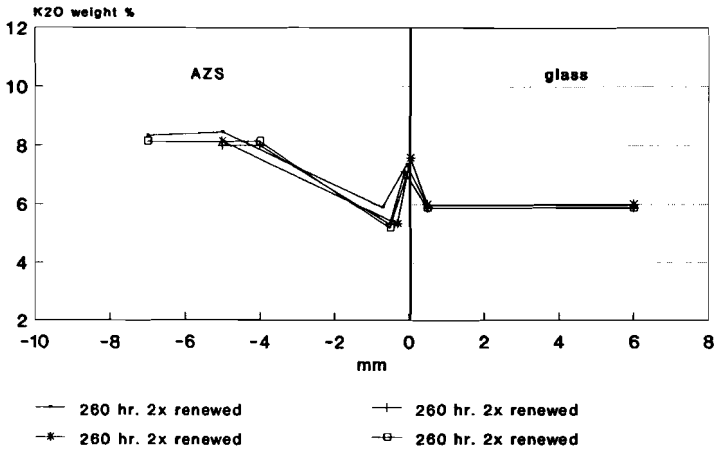
As with Na₂O, the penetration depth into the AZS shows the expected strong increase with the duration of the test period. The maximum K₂O concentration in the AZS increases as the test lasts longer. Owing to the increase in the penetration depth, after longer periods, the location of the maximum K₂O concentration is shifted ever deeper into the AZS.

The effect of the temperature is shown for example in figure 3.2.8. At a low temperature the maximum concentration is generally highest and the penetration depth smallest (the effect of the temperature on the penetration depths is obvious in the measurements after 260 hrs, see table 3 annex 2). In the glass-to-AZS interface the K₂O concentration goes up as the temperature goes down.

The effect of the use of different glass types is very obvious, for example demonstrated by figure 3.2.9. An increase in concentration of K₂O in the glass yields an increase in concentration in the glassy phase of the AZS. The K₂O from the lithium containing glass has an exceptionally large penetration depth compared to 354 glass and 395 glass. The crucible wall was about 9 mm thick. At 1350°C and after only 100 hours, the penetration depth of K₂O was markedly less than this 9 mm for all cases.

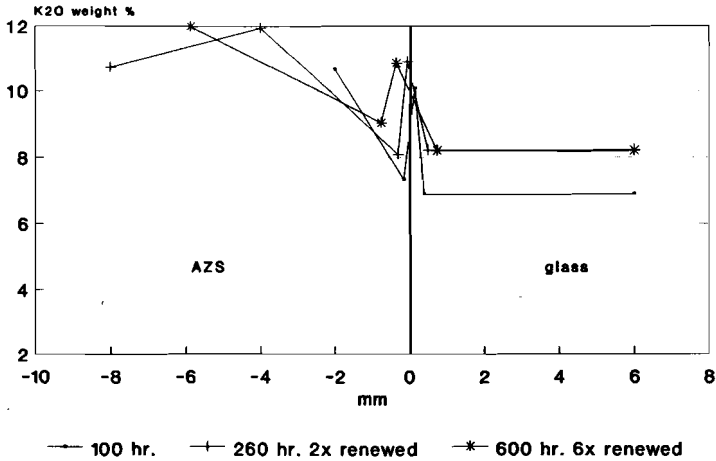
K2O diffusion in AZS
354 glass, 1425 C

figure 3.2.6



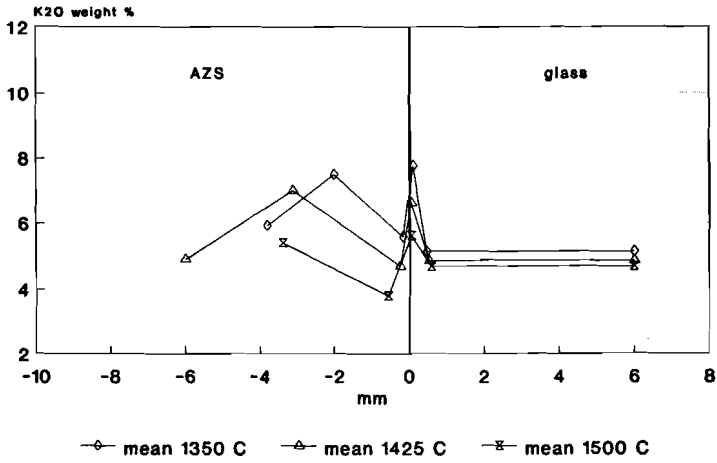
K2O diffusion in AZS
395 glass, 1425 C

figure 3.2.7



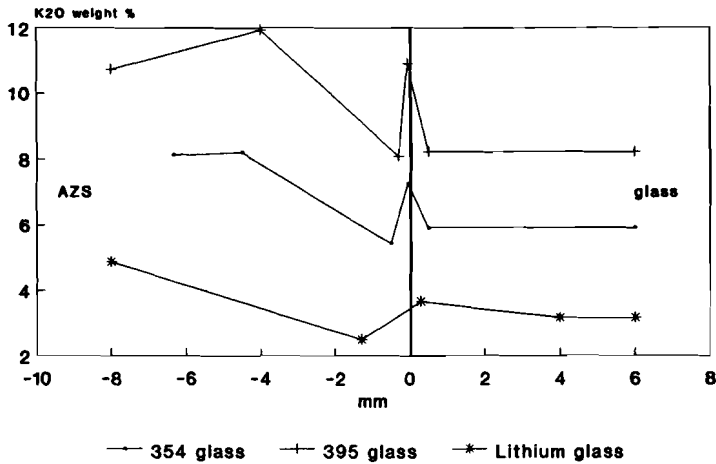
K2O diffusion in AZS
354 glass, 100 hr.

figure 3.2.8



K2O diffusion in AZS
1425 C, 260 hr.

figure 3.2.9



2x renewed

BaO

The general shape of the concentration profile of BaO going from the glass side into the fused cast AZS, shows a decrease starting before the first ZrO₂ nodules of the AZS are found. The minimum lies close to the first ZrO₂ nodules. From that point on the BaO content increases to a maximum, and then drops relatively steep in the direction of the AZS interior.

Table 4 in annex 2 shows the measured values. An example of the reproducibility is presented in figure 3.2.10. An example of the effects of the progress of time is presented in figure 3.2.11. The penetration depth into the AZS increases along with the increase in the test duration. The maximum BaO concentration in the AZS remains unchanged (within the measuring inaccuracy limits).

The effect of the temperature is shown for example in figure 3.2.12. Both BaO concentration and the penetration depth into the AZS go down as the temperature decreases.

The effect of the use of different glass types is very obvious, illustrated by figure 3.2.13. An increase in the BaO concentration in the molten glass (lithium free glass), yields an increase in the concentration in the AZS (difference between 354 glass and 395 glass).

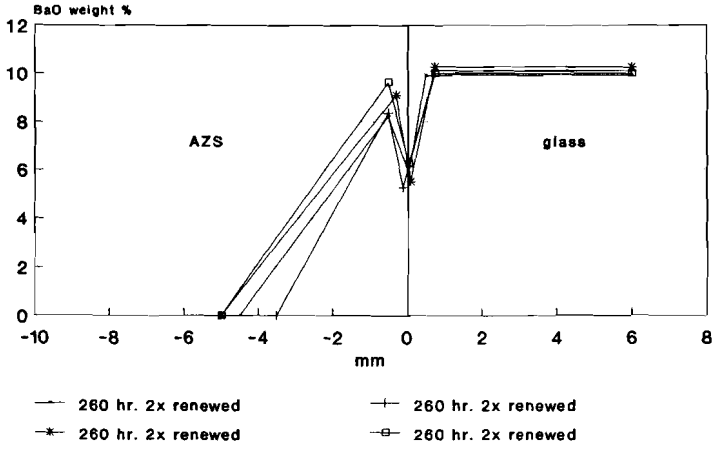
At 1350 °C (figure 3.2.14) and slightly less pronounced, at 1425°C (figure 3.2.13) the BaO concentration in the case of lithium glass, is higher in the glassy phase of the AZS compared to 395 glass with almost the same amount of BaO.

Again, the penetration depth of BaO from the lithium containing glass is exceptionally large compared to the situations measured for the 354 glass and 395 glass.

Only during the test with lithium glass after 260 hours at 1500°C, the penetration depth of BaO has the tendency to exceed the crucible wall thickness of 9 mm (annex 2, table 4).

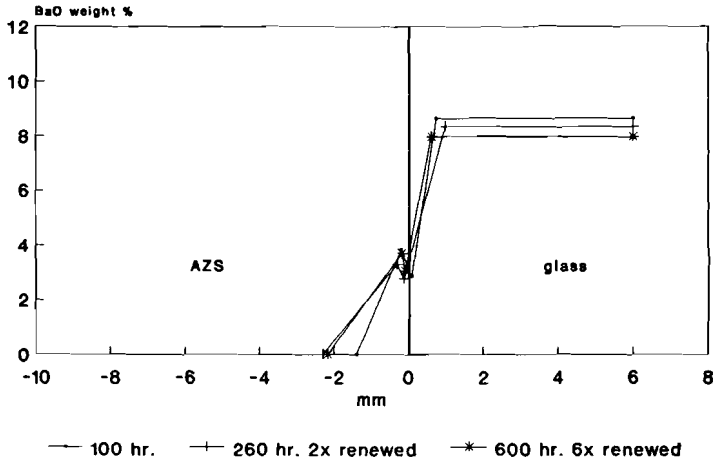
BaO diffusion in AZS
354 glass, 1425 C

figure 3.2.10



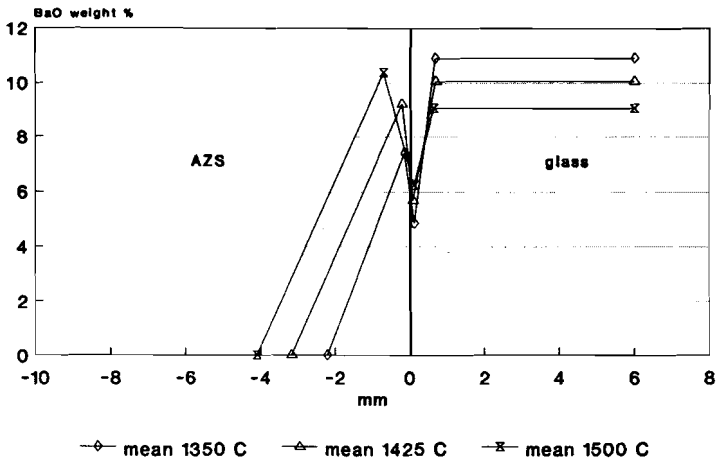
BaO diffusion in AZS
395 glass, 1350 C

figure 3.2.11



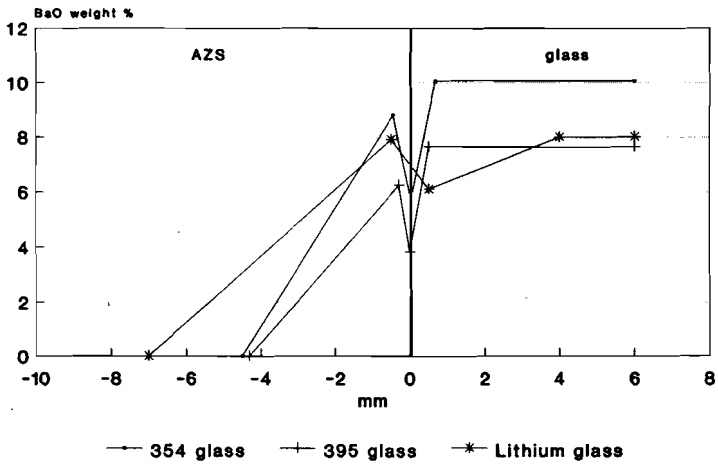
BaO diffusion in AZS
354 glass, 100 hr.

figure 3.2.12



BaO diffusion in AZS
1425 C, 260 hr.

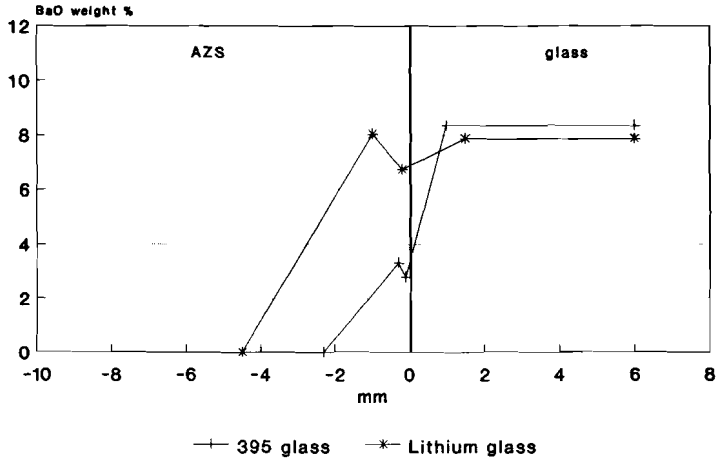
figure 3.2.13



2x renewed

BaO diffusion in AZS
1350 C, 260 hr.

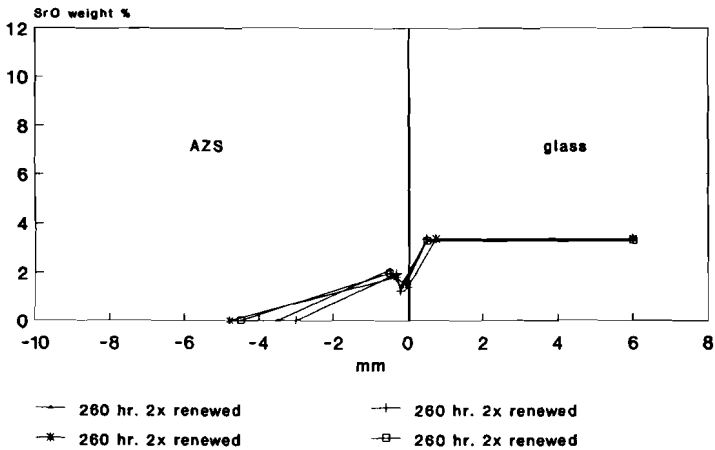
figure 3.2.14



2x renewed

SrO diffusion in AZS
354 glass, 1425 C

figure 3.2.15



SrO

The general shape of the concentration profiles of SrO is the same as the shape of the concentration profiles of BaO.

Table 5 in annex 2 shows the measured values. The reproducibility is illustrated in figure 3.2.15. An example of time dependency of the SrO concentration profile is presented in figure 3.2.16.

The penetration depth into the AZS increases with the increase in the test duration. The maximum SrO concentration in the AZS remains unchanged (within the inaccuracy of the measurements) with the increase in the test duration. The effect of the temperature has been shown by figure 3.2.17. Both SrO concentration and the penetration depth into the AZS decrease as the temperature decreases.

The effect of the use of different glass types is also very obvious and presented in figure 3.2.18. Generally, an increase in the concentration in the molten glass, yields an increase in the concentration in the AZS (shown by the difference between 354 glass and 395 glass).

At 1350°C (figure 3.2.19) and at a smaller degree at 1425°C (figure 3.2.18), the SrO concentration of the lithium containing glass in the glassy phase of the AZS is higher compared to 395 glass with only a slightly higher amount of SrO.

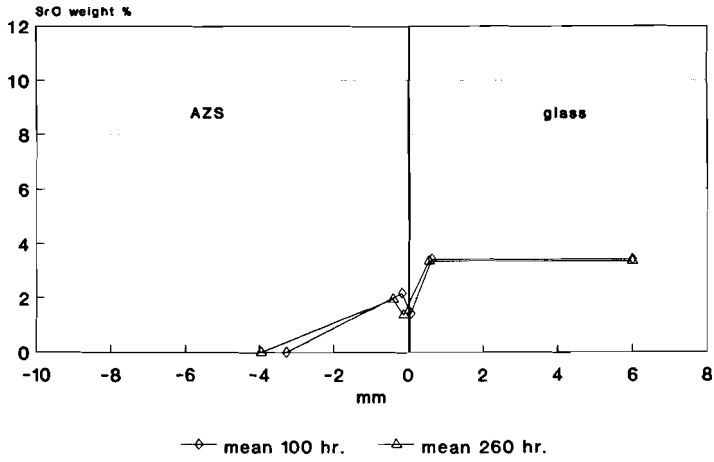
Again, the penetration depth of SrO from the lithium glass is exceptionally large compared to that of 354 glass and 395 glass. Only during the test with lithium glass, after 260 hours at 1500°C, the penetration depth of SrO could be much more than 9 mm if a refractory thickness above this value had been used (annex 2, table 5).

3.2.1.3 Summary of the measured concentration profiles in AZS.

- For the systems presented here, the penetration depth increases when the temperature increases and/or the test period is extended.

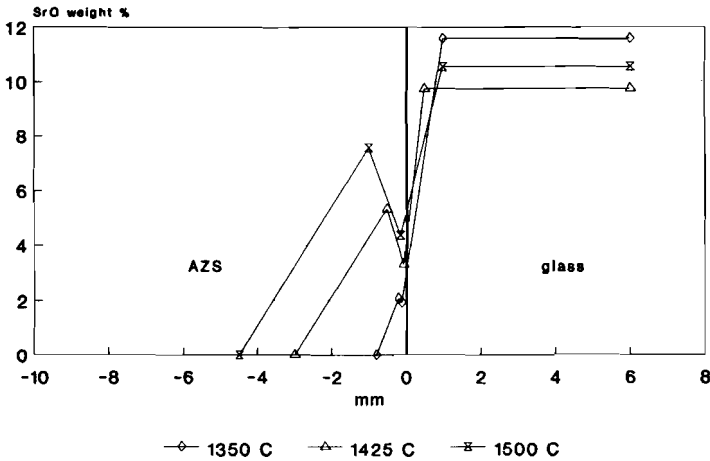
SrO diffusion in AZS
354 glass, 1425 C

figure 3.2.16



SrO diffusion in AZS
395 glass, 260 hr.

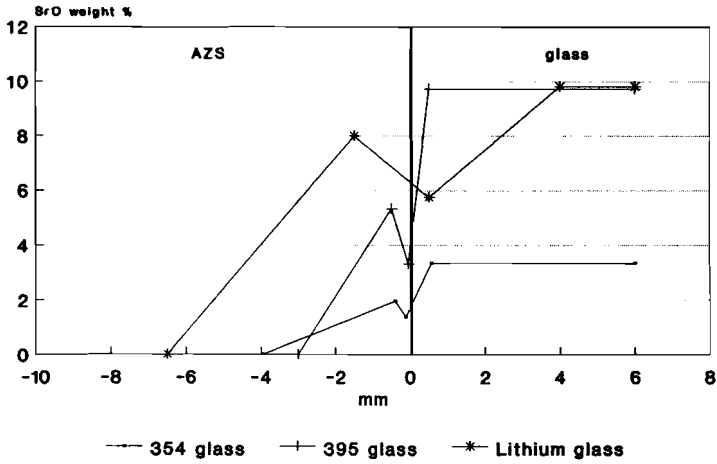
figure 3.2.17



2x renewed

SrO diffusion in AZS
1425 C, 260 hr.

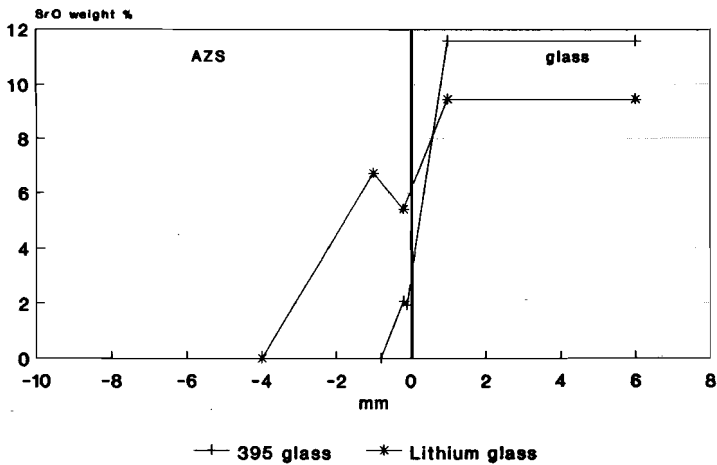
figure 3.2.18



2x renewed

SrO diffusion in AZS
1350 C, 260 hr.

figure 3.2.19



2x renewed

- The penetration depths of sodium and potassium far exceed those of barium and strontium.
- The maximum concentration of potassium and to a less degree that of sodium decreases when the temperature rises (in the range from 1350 to 1500°C) and increases when the test periods are extended.
- The maximum concentrations of barium and strontium increase when the temperature increases, but they remain unchanged (after 100 hours) when the test periods are extended.
- The penetration depth of Na, K, Ba, Sr from the lithium glass into the AZS, invariably far exceeds those from the 354 glass and 395 glass.
- The concentrations of BaO and SrO in the glassy phase of the AZS, in the experiments with lithium containing glass, are higher compared to lithium free glass with the same BaO and SrO concentration. Since the concentrations of Na₂O and K₂O in the lithium glass were far lower than in the used lithium free glasses, it is difficult to make the similar statement for sodium or potassium only on the basis of the sodium and potassium concentration profiles measured here.
Later in this chapter and in chapter 4 it will be shown that a similar concentration increase of sodium and potassium in the glassy phase of the AZS under the influence of lithium in the glass melt is very likely.
- The concentration profiles of the measured oxides, due to cation diffusion, do not follow the direct route from the concentrations of the glass composition to the composition of the glassy phase of the refractory (occurrence of up-hill diffusion).

3.2.1.4 Discussion of measured concentration profiles in the AZS.

One potential explanation for the difference in the behaviour of the lithium glass, with respect to penetration depths and diffusion rates, is the presence of a large amount of lithium oxide. The lithium ion diffuses in the AZS, which results in a

strong reduction in viscosity of the glassy phase of the AZS and a consequent increase in cation mobility. Although no data are available on the influence of lithium on the viscosity for the chemical composition range of the glassy phase of AZS, it is possible to give an estimate by making use of data for TV screen glass. For instance, the influence on the viscosity per weight % of Li_2O is approximately 3 respectively 6 times larger than that of Na_2O and K_2O .

An other interesting phenomenon is the presence of up-hill diffusion in the measured concentration profiles for all four presented cations (sodium, potassium, barium and strontium). In the case of potassium oxide, even two peak maximums in one concentration profile occur (figure 3.2.8). Up-hill diffusion occurs because in fact, not the gradient in the concentration profile but the gradient in the chemical potential respectively the activities of the diffusing cations determine the direction of the diffusion.

If the chemical potential of the oxides of sodium, potassium, barium and strontium is lower in the AZS glassy phase, for instance because of the high Al_2O_3 content compared to the glass melt, the system will try to shift into the direction of the lowest Gibbs energy. The cations will therefore diffuse into the glassy phase of the refractory until at last the activities are equal.

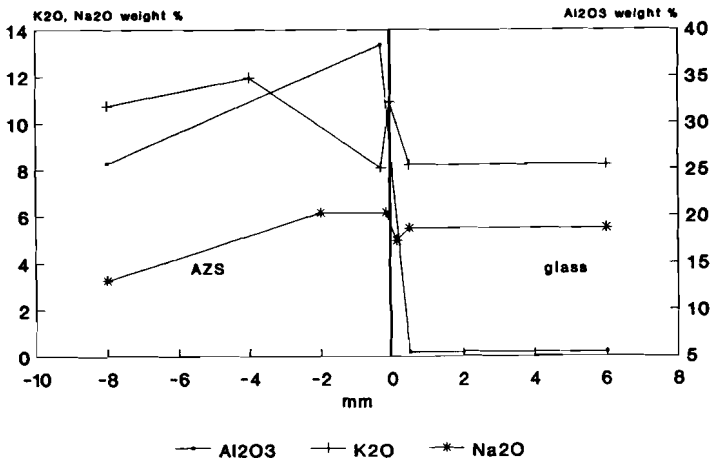
If the chemical composition of the glass, respectively the glassy phase of the fused cast AZS in the transition layer is studied, one sees that the chemical composition does not follow the direct route from the glass composition to the composition of the glassy phase of the original fused cast AZS. Dietzel (Lit. 1) explains this behaviour, by assuming that the glassy phase tries to adopt a structure that resembles that of a (thermodynamic relatively stable) crystal in the neighbourhood of the concentration route. The crystal structure distinguishes itself by its large thermodynamic stability and low Gibbs energy. Examples are: crystal formation of sodium nepheline ($\text{Na}_2\text{O} \cdot \text{Al}_2\text{O}_3 \cdot 2\text{SiO}_2$), leucite ($\text{K}_2\text{O} \cdot \text{Al}_2\text{O}_3 \cdot 4\text{SiO}_2$) or kaliophelite/kalsilite ($\text{K}_2\text{O} \cdot \text{Al}_2\text{O}_3 \cdot 2\text{SiO}_2$).

A indication of the thermodynamic stability of these crystals is their high melting point. The melting point of nepheline is 1526 °C, of leucite is 1686 °C and of kaliophelite/kalsilite is 1750 °C. Figure 3.2.20 shows a maximum in the K_2O content in the glassy phase, at the interface glass melt/AZS, which corresponds with about 25 weight% Al_2O_3 . The Al_2O_3 weight% of leucite is 23.4%. The second maximum concentration of K_2O deeper in the AZS meets a Al_2O_3 content of 32 weight%. The Al_2O_3 weight% of kaliophelite/kalsilite is 32.2 weight%. The "unusual" behaviour of the K_2O concentration profile at the interface and deeper in the AZS might therefore be explained by attempts to adopt the concentration of the thermodynamically stable leucite and kaliophelite/kalsilite compositions.

The position of the flat maximum of the Na_2O concentration and the concentration Al_2O_3 of 35 to 38 weight%, agrees very well with the concentration of Al_2O_3 in nepheline (35.9 weight%).

Concentration profiles
395 glass, 1425 C, 260 hr.

figure 3.2.20



crucible has been renewed several times during one test. The reason for the frequent renewal of the molten glass has been, to maintain the glass composition close to the original glass melt composition. In this way, the driving force for the diffusion of the cations in the AZS, the difference of the chemical potential of the cations between the molten glass and the AZS has been close to a practical situation.

The glass has been renewed by pouring glass out of the crucible and refilling it by freshly molten glass. The glass that has been poured out of the fused cast AZS crucible will be referred to as renewed glass. This glass has been cooled down to room temperature and has been analyzed by a method (XRF) described in section 3.2.2.2.

In the experiments of 260 hours duration, the refreshments of glass melts take place after about 90 and 160 hours. In the experiments of 600 hours, the refreshments of the glass melt take place after about 90, 163, 258, 331, 426 and 499 hours. The chemical composition of the glass has been measured before and after it has been in contact with the fused cast AZS of the crucible. The difference in chemical composition can be caused by evaporation, corrosion products of the crucible refractory and the diffusion of cations of the glass melt into the refractory crucible walls.

In the next section it will be shown that evaporation is neglectable and it is possible to calculate a kind of diffusion rate of the cations which can be compared for different cases.

3.2.2.2 Measurement method.

Measurements of the renewed glass in the experiments of 260 and 600 hours, have been made with X-ray Fluorescence (Philips PW 1400) using production standard calibration lines, which ensures a higher accuracy and reproducibility than the SEM/EDX measurements of part 3.2.1.

Two methods of sample preparation have been used. In the first

method, 5 grams of cullet of the renewed glass, which is poured out of the crucible during the test, is molten to a bead on a small platinum disk. The melting time has been 2 minutes at 1000 °C.

A second method is used to increase the reproducibility of these measurements. In this method 15 grams of cullet of the renewed glass, is ground to an average grainsize of 5 micrometer. 0.5 gram of this material is mixed with 2 grams of $\text{Li}_2\text{B}_4\text{O}_7$. The mixture of glass and $\text{Li}_2\text{B}_4\text{O}_7$ has been molten for 5 minutes at 1000 °C.

The Li_2O in the glass cannot be measured with X-ray Fluorescence. Therefore the Li_2O has been measured with Flame Atomic Absorption Spectroscopy (Philips SP 9).

For this analysis, 200 mg of the renewed glass is dissolved in HF and HClO_4 and evaporated. The residue is dissolved in 20 ml HNO_3 (6N) and filled up to 200 ml with water. The lithium in the resulting solution is measured using a calibration line (Com. Bur. of Reference).

All measurements have been performed in duplicate.

The difference in chemical composition of the glass before and after the test has been determined by this way. The difference may be due to evaporation or diffusion to or from the fused cast AZS, during residence of the glass melt in the crucible.

Table 3.6

Evaporation of lithium glass

temp. C	time hrs.	Li ₂ O weight %	Na ₂ O	K ₂ O	BaO	SrO	Al ₂ O ₃	SiO ₂	CaO	TiO ₂	Sb ₂ O ₃	Fe ₂ O ₃
0	0	3,85	3,31	3,73	8,32	8,33	4,96	65,6	0,96	0,20	0,38	0,069
			3,38	3,76	8,30	8,30	4,93	65,6	0,96	0,20	0,38	0,070
1350	92	3,83	3,24	3,70	8,35	8,24	4,97	65,9	0,96	0,20	0,38	0,070
			3,35	3,71	8,34	8,20	4,96	65,8	0,96	0,20	0,38	0,070
1425	94	3,83	3,28	3,70	8,35	8,23	4,94	65,9	0,96	0,20	0,37	0,071
			3,23	3,72	8,35	8,22	4,96	65,9	0,96	0,20	0,37	0,069
1500	93	3,83	3,34	3,71	8,34	8,26	4,98	66,0	0,96	0,20	0,35	0,069
			3,25	3,69	8,35	8,24	4,97	66,2	0,96	0,20	0,34	0,070

It can easily be shown that the amounts of material that have been evaporated are within the measuring accuracy for all three glass types used (see table 3.6 for lithium glass as an example).

So the change in the measured oxide contents in the glass, is predominantly due to the diffusion of cations and the increase of the corrosion products of fused cast AZS, like Al_2O_3 and ZrO_2 . The decrease of all the concentrations of the oxides, except for Al_2O_3 and ZrO_2 , by the dilution with the corrosion products from the fused cast AZS is on a relative scale the same for all studied oxides, except for a small deviation for Na_2O caused by the Na_2O content in the original AZS (see table 1.1). The amount of renewed glass in the crucibles and the dimensions and weight of the crucibles themselves are kept as constant as possible. In this way the decrease in the concentration of an oxide in the glass is a relative measure of the total diffusion in the crucible test set-up. This relative measure of the rate in the diffusion per oxide is expressed in electron equivalents per hour (e.e.h.). In other words: the e.e.h. is the decrease in molar content of a certain oxide of the glass divided by the residence time (in hours) of the glass during the test and multiplied by its valence.

The e.e.h. is a kind of "overall" value of the diffusion rate. The e.e.h. is a combination of a lot of effects like:

- The difference in partial Gibbs energy of the cation in the melt and the glassy phase of the AZS (driving force).
- The mobility of the cation.
- The diffusion of AZS material in the glass melt.
- The duration of the experiment with the increasing concentration of cations of the glass melt in the AZS.
- The interaction time of the glass melt between glass melt renewals with the AZS, which causes a decrease of diffusing cations in the glass melt and will decrease the driving force of the diffusion of the cations into the AZS.
- The wall thickness of the crucible (constant).
- The contact area of glass melt and AZS (constant).
- The interaction and inter-diffusion of the various cations.
- The temperature.

- The chemical composition of the glass melt.

The e.e.h. which is determined in this study is a relative measure for the diffusion rate of a cation in the AZS, and may only be compared when an identical test set-up and procedure (including time) is applied. With the standard test set-up and procedure, an approximation is made of the influence of glass melt composition and temperature on the diffusion rate of cations (e.e.h.) into new AZS, with an "infinite" quantity of glass melt and relatively large wall thickness of the fused cast AZS.

The relative diffusion rates that will be determined are not consistent with the diffusion theories with a $t^{0.5}$ dependence for a number of reasons, for instance the glassy phase of the fused cast AZS increases during the experiment, the effective diffusion coefficients are dependent on the chemical composition of the glassy phase of the fused cast AZS, also the equilibrium concentrations of oxides of the diffusing cations in the fused cast AZS are influenced by the diffusion of the cations and therefore changes during the test time.

In 3.2.2.3 the used assumptions are given to determine the e.e.h. of lithium, sodium, potassium, barium and strontium for new AZS, with a large wall thickness and an "infinite" quantity of glass melt (simulated by refreshing the melt after certain time intervals).

Annex 3 gives the measured values of Li^+ , Na^+ , K^+ , Ba^{2+} and Sr^{2+} in electron equivalents per hour, in table form and gives also an example of the calculation. In the figures of this chapter the calculated e.e.h. of the oxides of a renewed glass are placed in the time scale at the average of their residence time in the total test time, for example when a glass melt is poured in the crucible at 90 hours after the start of the test and poured out of the crucible 70 hours later at the total test time of 160 hours, the measured e.e.h. are placed in the time scale of the figures at $[90 \text{ (start time)} + 70/2 \text{ (average residence time)}] = 125 \text{ hours}$.

3.2.2.3 Results of glass analysis after refractory interaction and determination of e.e.h. values.

Figure 3.2.21 shows the determined diffusion rates expressed in e.e.h. values of Na^+ , K^+ , Ba^{2+} and Sr^{2+} for a 395 glass melt at 1500°C . The concentrations of Na_2O and K_2O show a marked reduction on the time scale, owing to the fact that the penetration depth tends to exceed the crucible wall thickness. This means that if the wall thickness is infinite, the diffusion rate would probably remain as it was in the first 200 hours.

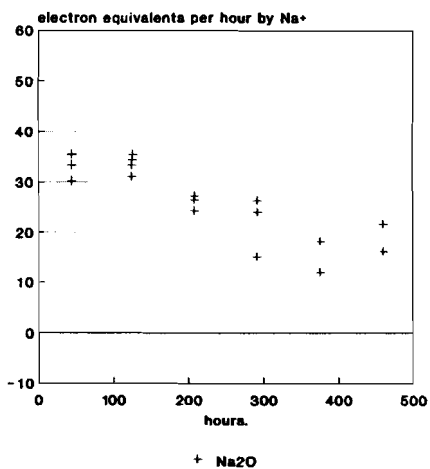
Relative diffusion rates from 395 glass into fresh fused cast AZS at 1500°C in electron equivalents per hour are:

Na^+	: 34	e.e.h.
K^+	: 48	
Ba^{2+}	: 9	
Sr^{2+}	: 15	

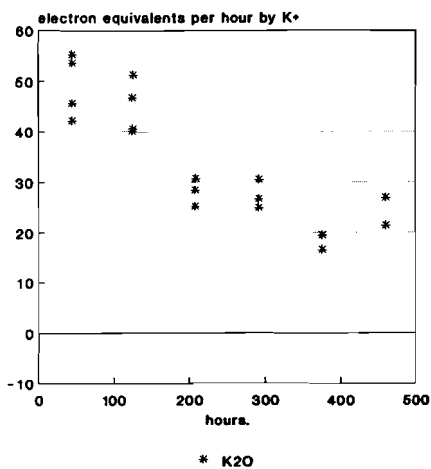
Figure 3.2.22 shows the relative diffusion rates of Na^+ , K^+ , Ba^{2+} and Sr^{2+} for a 395 glass melt at 1425°C . The diffusion rate of K_2O shows a strong reduction on the time scale, owing to the penetration depth tending to exceed the crucible wall thickness. The diffusion rate of Na_2O , however, shows an increase followed by stabilization, although its penetration depth also tends to exceed the crucible wall thickness. (The same phenomenon manifests itself with 395 glass-glass at 1350°C , figure 3.2.23). The glassy phase of the AZS contains about 3.5% Na_2O in its original state (local SEM measurements of untreated AZS 32 (ER 1681)). Figure 3.2.3 shows that part of the Na_2O in the AZS diffuses to the interface because the concentration of Na_2O at the outer wall side is lower than of the original AZS. After some time the diffusion of Na^+ from the glass melt is decisive. In practice the Na_2O from the AZS is a finite source and that from the glass by continuously charging is an 'infinite' source. Therefore, in this study, the diffusion rate is derived from the right hand section of the graph to minimize these initial counter diffusion effects.

Figure 3.2.21 The relative diffusion rates of Na^+ , K^+ , Ba^{2+} and Sr^{2+} for a 395 glass melt at 1500 °C.

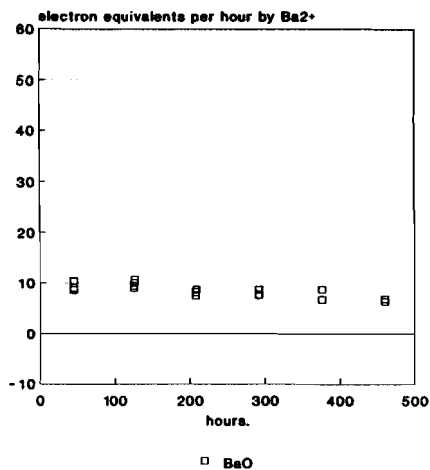
Diffusion of cations into AZS
395 glass, 1500 C



Diffusion of cations into AZS
395 glass, 1500 C



Diffusion of cations into AZS
395 glass, 1500 C



Diffusion of cations into AZS
395 glass, 1500 C

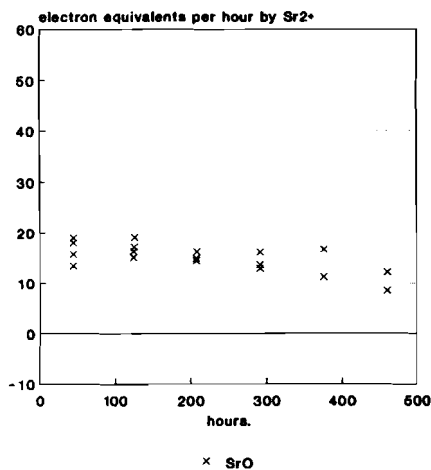


Figure 3.2.22 The relative diffusion rates of Na^+ , K^+ , Ba^{2+} and Sr^{2+} for a 395 glass melt at 1425 °C.

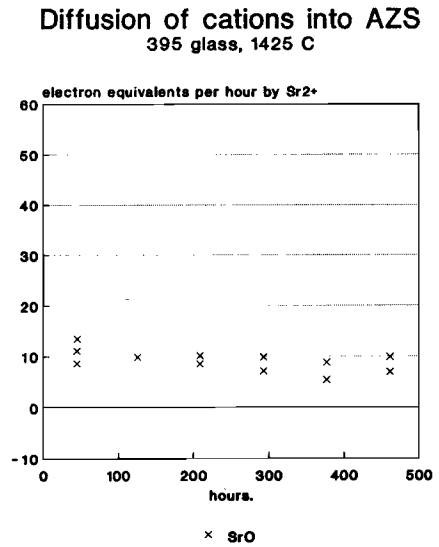
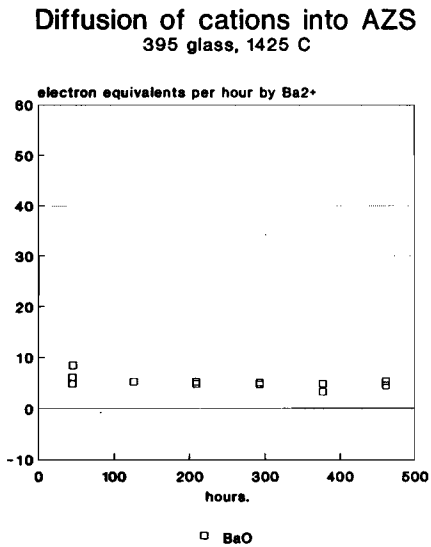
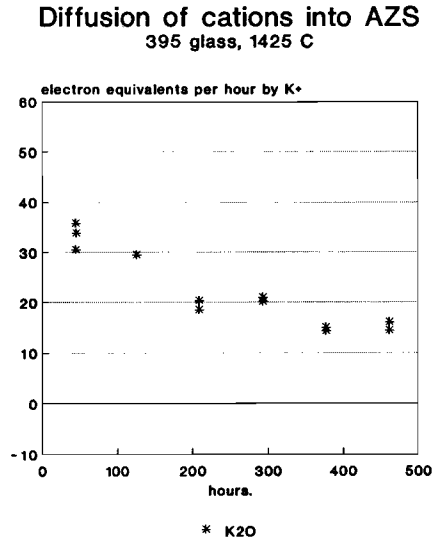
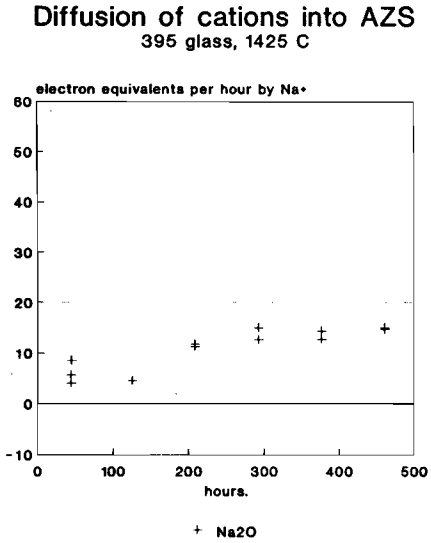
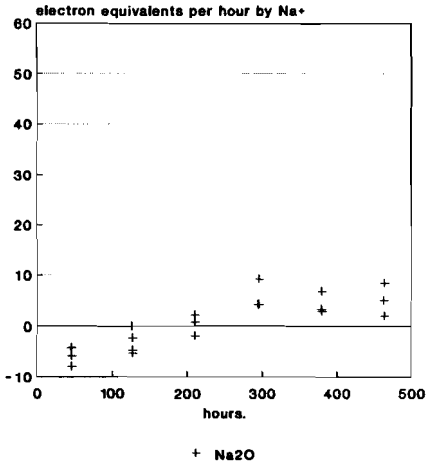
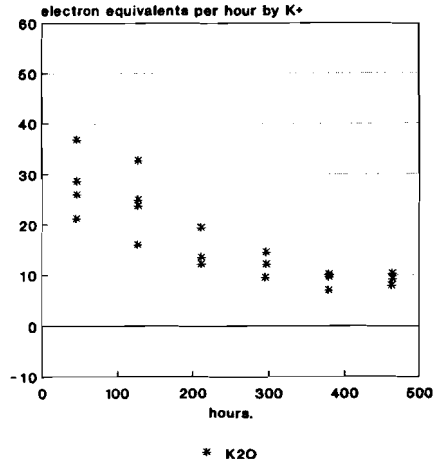


Figure 3.2.23 The relative diffusion rates of Na^+ , K^+ , Ba^{2+} and Sr^{2+} for a 395 glass melt at 1350 °C.

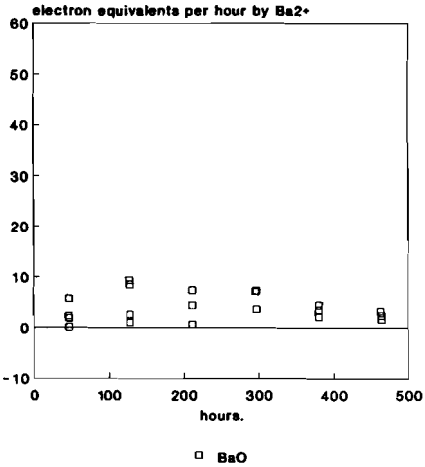
Diffusion of cations into AZS
395 glass, 1350 C



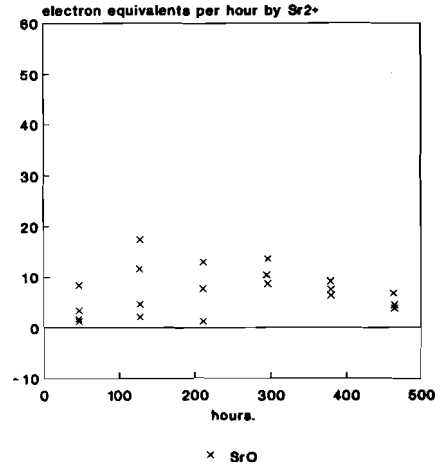
Diffusion of cations into AZS
395 glass, 1350 C



Diffusion of cations into AZS
395 glass, 1350 C



Diffusion of cations into AZS
395 glass, 1350 C



The penetration depth of sodium tends to exceed the crucible wall thickness (see figure 3.2.5) at this temperature after about 260 hours, therefore the in this way determined relative diffusion rate for sodium is probably somewhat too low.

The relative diffusion rates of 395 glass components into fresh fused cast AZS, at 1425°C in electron equivalents per hour are:

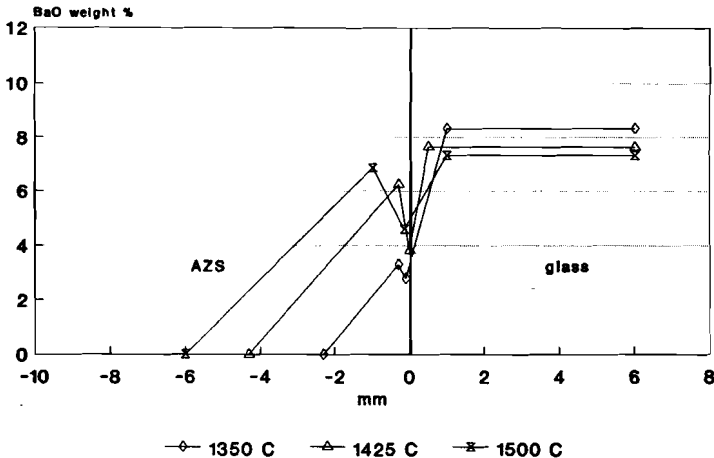
Na ⁺	: 14	e.e.h.
K ⁺	: 34	
Ba ²⁺	: 5	
Sr ²⁺	: 10	

Figure 3.2.23 shows the relative diffusion rates of Na⁺, K⁺, Ba²⁺ and Sr²⁺ for a 395 glass melt at 1350°C.

The behaviour of Na₂O and K₂O resembles that at 1425°C, the only difference is the even more exceptional behaviour of Na₂O. At first Na ions even diffuse from the AZS into the glass. The BaO and SrO analysis show large variations, even after the samples had

BaO diffusion in AZS
395 glass, 260 hr.

figure 3.2.24



2x renewed

been ground and mixed. This may indicate that there is a strong degree of segregation. The amount of barium diffusing into the AZS at 1350°C is much smaller than the amount diffusing at 1425 and 1500°C (see for example figure 3.2.24).

The area under the curves in the graphs in this figure is a factor of two to three times smaller at 1350°C than at 1425°C. The measurements carried out after the longest test period (figure 3.2.23) yield the smallest variation, the diffusion rate of Ba²⁺ at 1350 °C is nearly a factor of two lower than the diffusion measured at 1425°C.

The amount of strontium diffusing into the AZS at 1350°C is far lower than the diffusion rate of strontium at the higher temperatures, 1425 and 1500°C (see for example figure 3.2.17). The area under the curves in the graphs in this figure is three to seven times smaller at 1350°C than at 1425°C.

The measurements carried out after the longest test period (figure 3.2.23) yield the smallest variation, the diffusion rate is nearly a factor of two and a half lower than the diffusion rate at 1425°C. Diffusion rates of components of 395 glass into the fresh fused cast AZS, at 1350°C in electron equivalents per hour are:

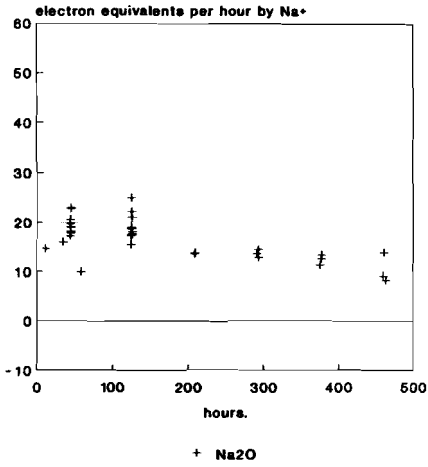
Na ⁺ :	4	e.e.h.
K ⁺ :	28	
Ba ²⁺ :	2	
Sr ²⁺ :	3	

Figure 3.2.25 shows the diffusion rates of Na⁺, K⁺, Ba²⁺ and Sr²⁺ for a 354 glass melt at 1425°C. The diffusion rate of K₂O shows a marked reduction on the time scale, owing to the penetration depth tending to exceed the crucible wall thickness.

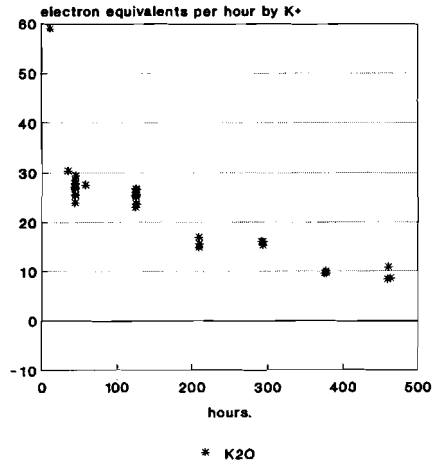
The diffusion rate of Na₂O shows a light tendency to drop. Those of BaO and SrO, again, show reasonable stability on the time scale.

Figure 3.2.25 The relative diffusion rates of Na^+ , K^+ , Ba^{2+} and Sr^{2+} for a 354 glass melt at 1425 °C.

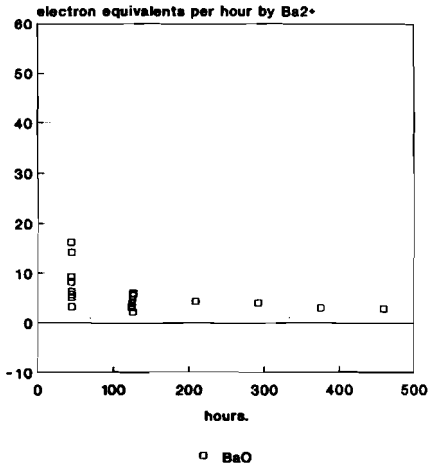
Diffusion of cations into AZS
354 glass, 1425 C



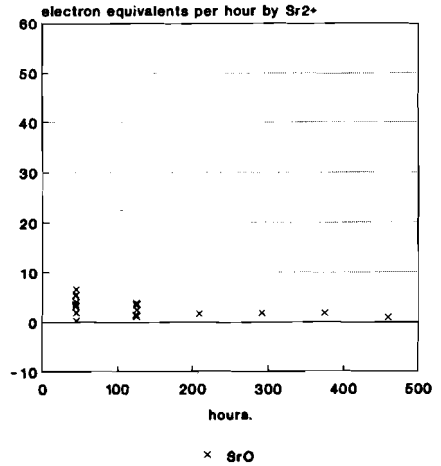
Diffusion of cations into AZS
354 glass, 1425 C



Diffusion of cations into AZS
354 glass, 1425 C



Diffusion of cations into AZS
354 glass, 1425 C



Diffusion rates of 354 glass at 1425°C into fresh fused cast AZS in electron equivalents per hour are:

Na⁺: 20 e.e.h.
 K⁺: 26
 Ba²⁺: 6
 Sr²⁺: 3

Figure 3.2.26 shows the relative diffusion rates of Na⁺ and K⁺ for a 354 glass melt at 1350°C.

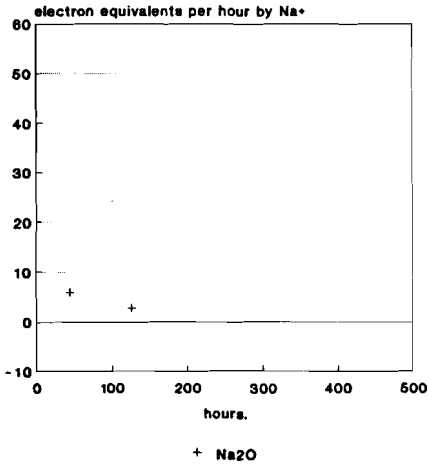
Since there are only two experiments done, there are only two measured e.e.h. values for each element, the reliability of the resulting e.e.h. is lower than usual.

The approximate relative diffusion rates for the case of 354 glass into fresh fused cast AZS at 1350°C given in electron equivalents per hour are here determined:

Na⁺: 4 e.e.h.
 K⁺: 18

Figure 3.2.26 The relative diffusion rates of Na⁺ and K⁺ for a 354 glass melt at 1350°C.

Diffusion of cations into AZS
 354 glass, 1350 C



Diffusion of cations into AZS
 354 glass, 1350 C

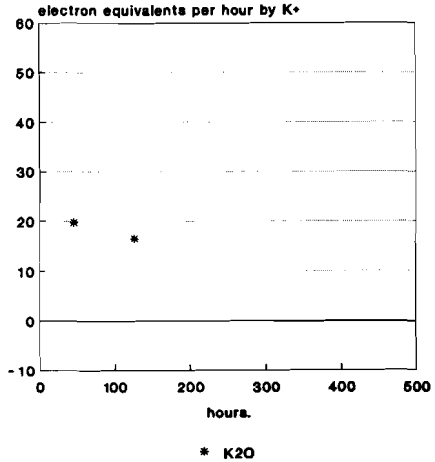
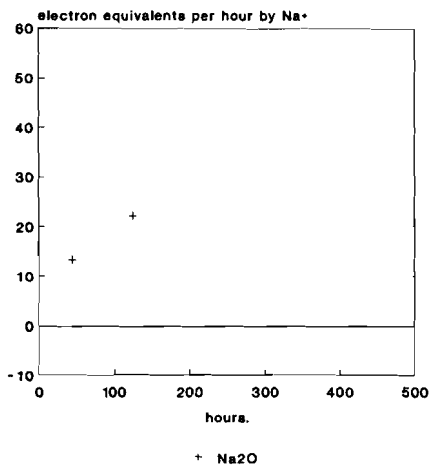
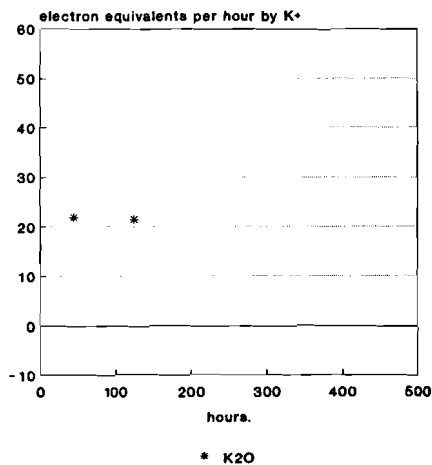


Figure 3.2.27 The relative diffusion rates of Na^+ , K^+ , Ba^{2+} and Sr^{2+} for lithium containing glass at 1500 °C.

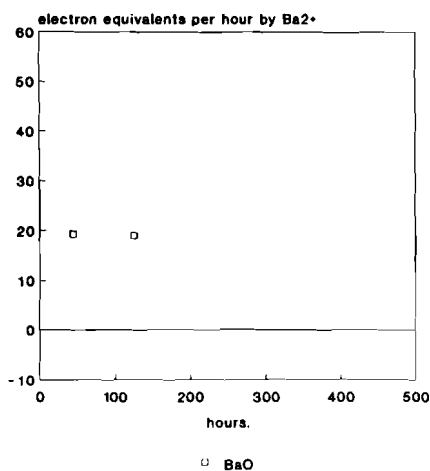
Diffusion of cations into AZS
Lithium glass, 1500 C



Diffusion of cations into AZS
Lithium glass, 1500 C



Diffusion of cations into AZS
Lithium glass, 1500 C



Diffusion of cations into AZS
Lithium glass, 1500 C

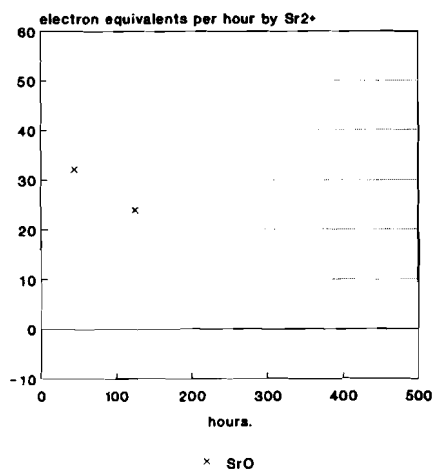


Figure 3.2.27 shows the relative diffusion rates of Na^+ , K^+ , Ba^{2+} and Sr^{2+} for lithium glass at 1500°C .

Since, again, there are only two experiments done, only two measured values for each element are available, the reliability of the resulting e.e.h. is lower than for the 395 glass.

Na_2O shows an increase in the diffusion rate values on the time scale at all the three temperatures (figures 3.2.27, 3.2.29 and 3.2.30) for this case.

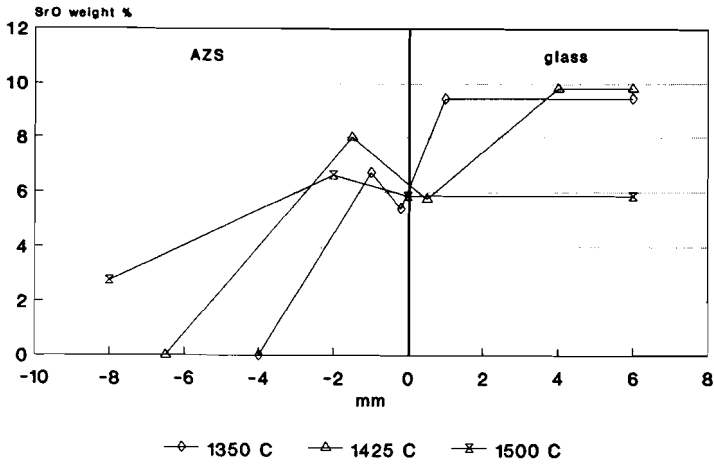
This effect is probably caused by the low Na_2O -content of the glass (annex 1). Due to this low Na_2O -content of the glass at the start of the experiments the Na^+ will diffuse from the AZS to the glass melt interface. This is the reason for the lower average Na^+ diffusion from the glass melt into the AZS during the first 90 hours. This is why, for lithium containing glass, the Na^+ diffusion rate, determined after a melting time of 125 hours is the best estimate.

The penetration depth of K^+ in lithium containing glass is so large, that the diffusion rates measured in this way are actually lower than the values when the penetration depth would not exceed the wall thickness.

The relative diffusion rate of SrO shows a drop on the time scale (figure 3.2.27). Figure 3.2.28 shows that the penetration depth after 260 hours at 1500°C just tends to exceed the crucible wall thickness. Since the glass used for the second measurement has been poured into the crucible after 160 hours, the effect of a finite wall thickness will have had only a slight effect. The concentration of Li_2O (figure 3.2.31) cannot be measured by using the SEM/EDX. If, however, the penetration depth of Li^+ is assumed to be the same as that of Na^+ or K^+ because of its small size, the shortest period would probably give the best indication. The measured relative diffusion rates into fresh fused cast AZS of lithium containing glass components, at 1500°C in electron

SrO diffusion in AZS
Lithium glass, 260 hr.

figure 3.2.28



2x renewed

equivalents per hour are:

Li⁺: 86 e.e.h.
 Na⁺: 22
 K⁺: 22
 Ba²⁺: 19
 Sr²⁺: 28

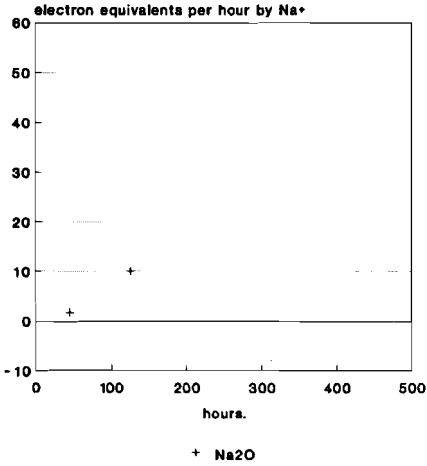
Figure 3.2.29 shows the diffusion rates of Na⁺, K⁺, Ba²⁺ and Sr²⁺ for a lithium glass melt at 1425°C.

The pattern is identical with that of figure 3.2.27 at 1500°C, with the difference that the penetration depth of SrO is smaller than the crucible wall thickness (figure 3.2.28).

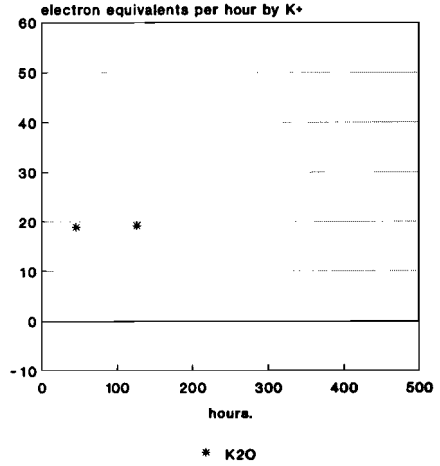
Figure 3.2.31, in turn, shows a drop in Li₂O-diffusion on the time scale, at a temperature of 1425 °C. This indicates that the

Figure 3.2.29 The relative diffusion rates of Na^+ , K^+ , Ba^{2+} and Sr^{2+} for lithium containing glass at 1425 °C.

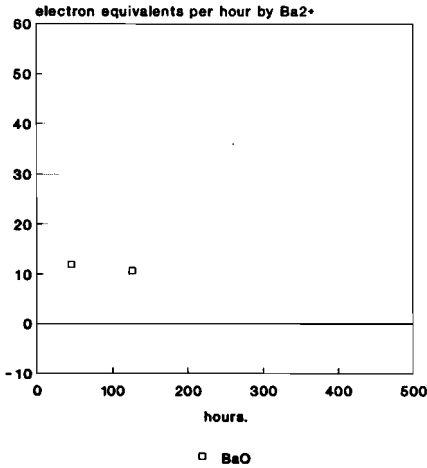
Diffusion of cations into AZS
Lithium glass, 1425 C



Diffusion of cations into AZS
Lithium glass, 1425 C



Diffusion of cations into AZS
Lithium glass, 1425 C



Diffusion of cations into AZS
Lithium glass, 1425 C

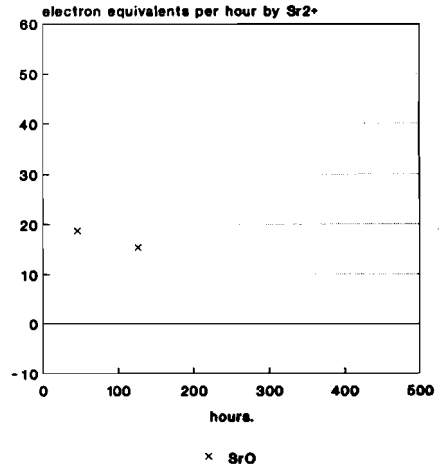
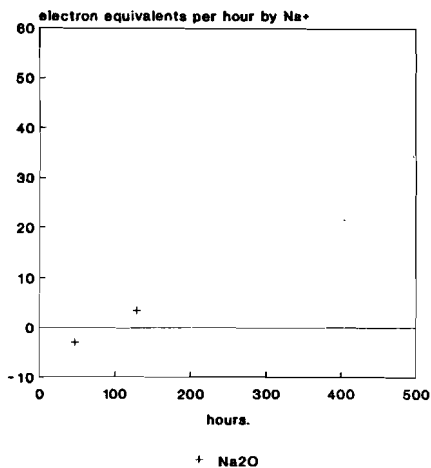
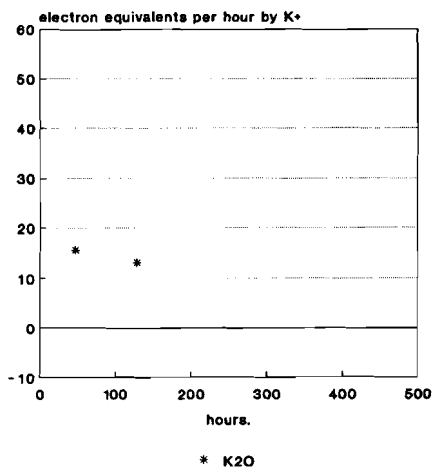


Figure 3.2.30 The relative diffusion rates of Na^+ , K^+ , Ba^{2+} and Sr^{2+} for lithium containing glass at 1350 °C.

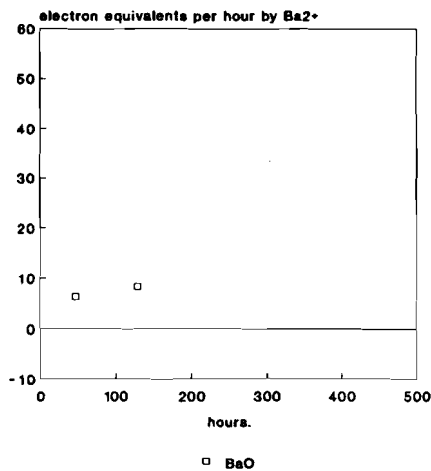
Diffusion of cations into AZS
Lithium glass, 1350 C



Diffusion of cations into AZS
Lithium glass, 1350 C



Diffusion of cations into AZS
Lithium glass, 1350 C



Diffusion of cations into AZS
Lithium glass, 1350 C

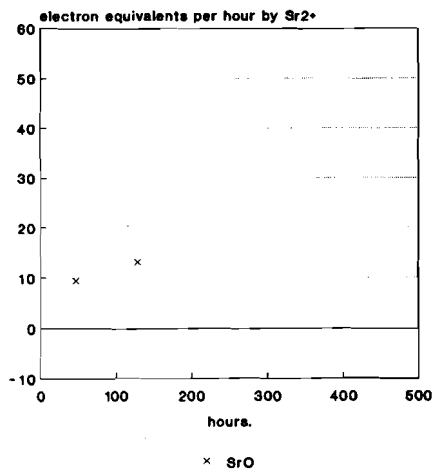
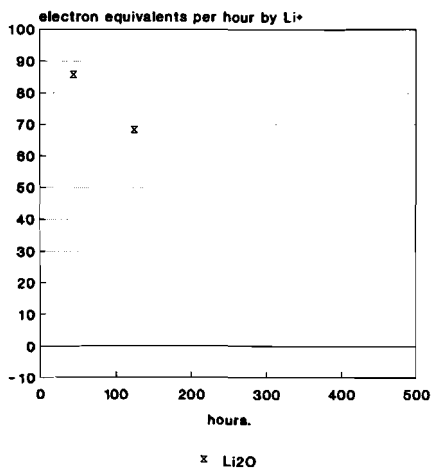
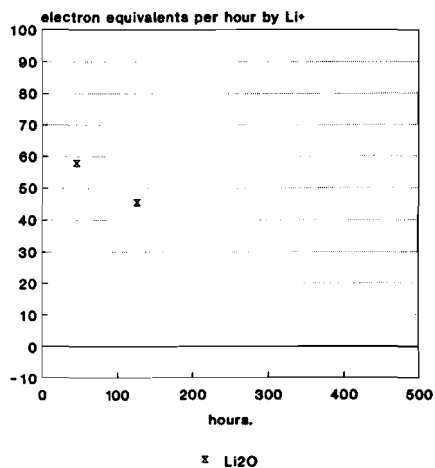


Figure 3.2.31 The relative diffusion rates of Li^+ for lithium containing glass at 1350, 1425 and 1500 °C.

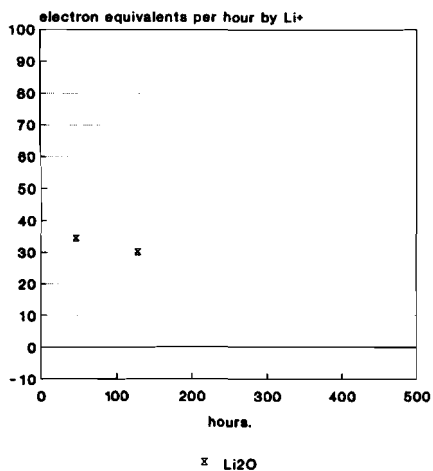
Diffusion of cations into AZS
Lithium glass, 1500 C



Diffusion of cations into AZS
Lithium glass, 1425 C



Diffusion of cations into AZS
Lithium glass, 1350 C



crucible wall is probably too thin.

The relative diffusion rates determined in this way for the case of lithium containing glass into fresh fused cast AZS at 1425°C in electron equivalents per hour are:

Li ⁺ :	58	e.e.h.
Na ⁺ :	10	
K ⁺ :	19	
Ba ²⁺ :	11	
Sr ²⁺ :	17	

Figure 3.2.30 shows the diffusion rates of Na⁺, K⁺, Ba²⁺ and Sr²⁺ for lithium glass at 1350°C.

The patterns are similar as those in figures 3.2.27 and 3.2.29. Figure 3.2.31, again, shows a drop in Li₂O-diffusion on the time scale, which is very slight at 1350°C.

The relative diffusion rates for the case of lithium containing glass into fresh fused cast AZS at 1350°C in electron equivalents per hour are:

Li ⁺ :	34	e.e.h.
Na ⁺ :	3	
K ⁺ :	14	
Ba ²⁺ :	7	
Sr ²⁺ :	11	

3.2.2.4 Discussion.

Table 3.8 summarizes the measured relative diffusion rates of cations into fresh fused cast AZS in electron equivalents per hour for the different cases presented in this study.

This table clearly shows that the relative drops in potassium diffusion rates by decreasing temperatures, are smaller than the relative drops in the diffusion rates for the other elements. The amount of diffused cations in the AZS is a combination of the fraction of glassy phase in the fused cast AZS, the concentration of the cation in the glassy phase and the penetration depth.

Table 3.8

cation	Li ⁺		
glass type	354 glass	395 glass	Li
1350°C	*	*	34
1425°C	*	*	58
1500°C	*	*	86
wt% in original glass as Li ₂ O	0	0	3.84
mol% in original glass as Li ₂ O	0	0	8.43
cation	Na ⁺		
glass type	354 glass	395 glass	Li
1350°C	4	4	3
1425°C	20	14	10
1500°C	*	34	22
wt% in original glass as Na ₂ O	9.43	6.84	3.30
mol% in original glass as Na ₂ O	10.34	7.72	3.50
cation	K ⁺		
glass type	354 glass	395 glass	Li
1350°C	18	28	14
1425°C	26	34	19
1500°C	*	48	22
wt% in original glass as K ₂ O	6.46	9.10	3.72
mol% in original glass as K ₂ O	4.66	6.75	2.59

cation	Ba ²⁺		
glass type	354 glass	395 glass	Li
1350°C	*	2	7
1425°C	6	5	11
1500°C	*	9	19
wt% in original glass as BaO	10.75	7.70	8.34
mol% in original glass as BaO	4.76	3.51	3.57

cation	Sr ²⁺		
glass type	354 glass	395 glass	Li
1350°C	*	3	11
1425°C	3	10	17
1500°C	*	15	28
wt% in original glass as SrO	3.01	9.59	8.25
mol% in original glass as SrO	1.97	6.47	5.23

The difference in behaviour of the potassium can be explained from the difference in penetration depths and the maximum potassium concentrations which can be absorbed in the AZS.

The penetration depths of all the cations drop as the temperature decreases. The relative penetration depth of sodium, however, drops stronger than those of the other cations, such as potassium. See figure 3.2.32, which shows the penetration depths of the maximum concentrations after 100 hours at different temperatures. The maximum concentrations of BaO and SrO in the glassy phase of the AZS drop strongly as the temperature decreases, while those of Na₂O and K₂O rise, although the maximum concentration of K₂O increases at lower temperature much stronger than that of Na₂O (see figure 3.2.33).

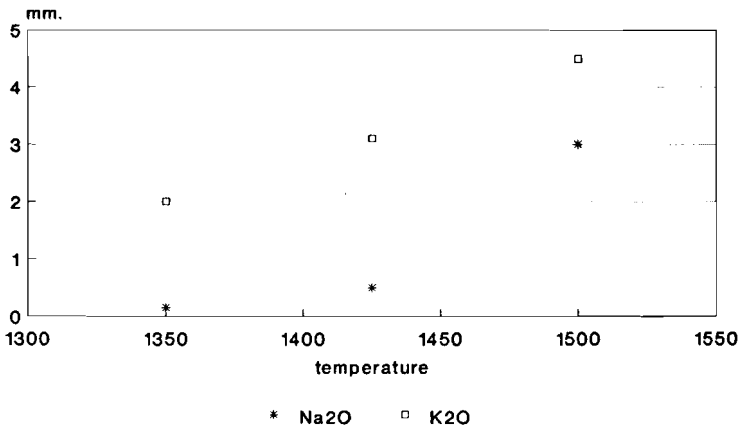
The two effects, decrease in penetration depth and maximum concentration bring about a drop in the "diffusion rates" of BaO and SrO determined in this way when the temperature decreases. The reduction in penetration depths of Na₂O and K₂O gives on one hand a reduction effect in the measured diffusion rates, and the increase in the maximum concentrations in the AZS on the other hand, would give a rise in the diffusion rates as the temperature decreases. As the rise in maximum concentration of Na₂O (figure 3.2.33) is far smaller than the exceptional relative reduction in penetration depth (figure 3.2.32), the diffusion rate of sodium shows a strong reduction as the temperature goes down. The rise in maximum concentration of K₂O (figure 3.2.33), however, is so high that it offsets part of the reduction in penetration depth (figure 3.2.32), which implies that the diffusion rate going with a drop in temperature shows a far smaller reduction than in the case of the other elements.

The strong rise in the e.e.h. values in the lithium glass is probably due to the diffusion of lithium in the glassy phase of the fused cast AZS having a significant influence on the viscosity of the glassy phase of the AZS and therefore on the diffusion of the other cations. The first part of this chapter shows that the penetration depth of lithium glass invariably far exceeds those of the situations for 354 and 395 glass. Another probable cause is the increase in equilibrium concentration of the cations in the glassy phase of the AZS with the cations in the glass melt due to the Li₂O diffusing into the AZS (see section 3.2.1.3 of this study), which increases the driving force for diffusion. Also the increase of the glassy phase of the AZS due to the diffusion of lithium, which dissolves the corundum (Al₂O₃) crystals, might be a cause for the larger e.e.h. values in the case of lithium glass melt AZS interaction.

The here determined relative diffusion rates are a measure for the flux of the positive charge transported by the cations in the glassy phase of the fused cast AZS.

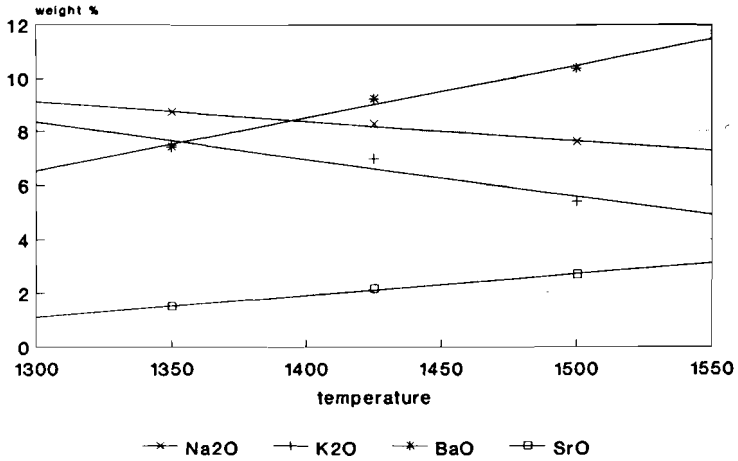
Penetration depth of maximum concentrations peaks in AZS-354 glass after 100 hrs.

figure 3.2.32



Maximum concentrations in AZS-354 glass after 100 hrs.

figure 3.2.33



The positive charge transported in the AZS is the rate determining step of the oxygen forming mechanism at the refractory/glass melt interface.

As already is mentioned in 3.2.2.2, the determined relative diffusion rates are not consistent with the diffusion theories with a time^{0.5} dependence for a number of reasons, for instance the glassy phase of the fused cast AZS grows during the experiment, the effective diffusion coefficients are dependent on the chemical composition of the glassy phase of the fused cast AZS, also the equilibrium concentrations of oxides of the diffusing cations in the fused cast AZS is influenced by the diffusion of the cations and therefore changes during the test time.

Summarizing it can be concluded that the relative diffusion rates, into fresh fused cast AZS, of the most important cations, for the case of T.V. screen glass have been determined in so called e.e.h., which is the positive charge transported by the cations in the fused cast AZS. The transported positive charge is proportional with the formation of oxygen at the interface fused cast AZS/glass melt and therefore important for the formation of bubbles and knots.

In chapter 4 the here determined values will be used in a model which predicts the formation of bubbles at the interface glass melt/fused cast AZS.

Literature references chapter 3.

- [1] A. Dietzel;
Zusammenhang zwischen Phasendiagramm, Reaktionsverlauf und Struktur von Schmelzen.
Glastech. Ber. **40** (1967) p. 378-381.
- [2] A.R. Cooper;
Model for multi-component diffusion.
J. Phys. Chem. Glasses **6** (1965) p. 55-61.
- [3] A.K. Varschneya, A.R. Cooper;
Diffusion in the system $K_2O-SrO-SiO_2$: III, Inter-diffusion coefficients.
J. Am. Ceram. Soc. **55** (1972) p. 312-318.
- [4] P.K. Gupta, A.R. Cooper;
The D matrix for multi-component diffusion.
Physica **54** (1971) p. 39-59.
- [5] V.A. Zhabrev, A.I. Isakov;
The inter-diffusion in silicate melts containing three cations.
Fiz. Khim. Stekla **12** (1986) p. 188-193.
- [6] V.A. Zhabrev, A.I. Isakov, G.A. Shashkina;
A study of three-cation diffusion with the interaction of alkali silicate melts.
Fiz. Khim. Stekla **12** (1986) p. 596-601.
- [7] K. Hunold, R. Brueckner;
Chemische Diffusion van Natrium- und Aluminimionen in Natrium-Alumosilicatschmelzen.
Glastech. Ber. **53** (1980) p. 207-219.
- [8] V.A. Zhabrev, A.I. Isakov;
Criteria determining the form of the diffusion path in glassy melts with three mobile cations.
Fiz. Khim. Stekla **14** (1988) p. 423-428.
- [9] A.R. Cooper, A.K. Varshneya;
Diffusion in the system $K_2O-SrO-SiO_2$: I, Effective binary diffusion coefficients.
J. Am. Ceram. Soc. **55** (1972) p. 312-318.

- [10] F. Novotny, M. Dragonn;
Anwendung der irreversiblen Thermodynamik auf die Loesung
der festen Phase in der Glasschmelze,
Silikattechnik **40** (1989) p. 373-376.

4. Effect of glass composition and temperature on glass defect potential originating from refractory.

4.1. Introduction.

According to chapter 2 the diffusion of cations appears to be the most probable rate determining step in the oxygen bubble forming mechanism at the refractory/glass melt interface.

In chapter 3, the diffusion process of the most important cations, for the case of T.V. screen glasses, into the glassy phase of the AZS was treated. The diffusion rates of the cations are experimentally estimated in so called electron equivalents per hour (e.e.h.), which is the positive charge transported by the cation into the fused cast AZS, determined in a standardised test set-up.

In the used test set-up all the crucibles were prepared using new fused cast AZS 32 material (ER 1681) and were, within small tolerances, of the same size and weight. Also, the amount of glass was kept as constant as possible. In this way it is not only possible to compare the diffusion rates of the different cations during one test, but also the diffusion rates of the cations of different tests, following the standardised procedure. In the standardised test procedure, three different glasses have been used with different chemical compositions and viscosities (annex 1). Of course, no absolute values of diffusion coefficients could be obtained with this test. With the measured relative values of the diffusion rates, it is possible to determine the influence of the chemical composition and viscosity on the formation rate of bubbles from the fused cast AZS, within the composition range of the glasses investigated.

The determined relations for the cation diffusion rate are used in a model which predicts the formation of bubbles at the interface glass melt/fused cast AZS. The creation of a model, including the required diffusion rate data, which predicts the glass defect potential of different T.V. screen glass melts in contact with fused cast AZS under different conditions, is one of the most

important objectives of this study.

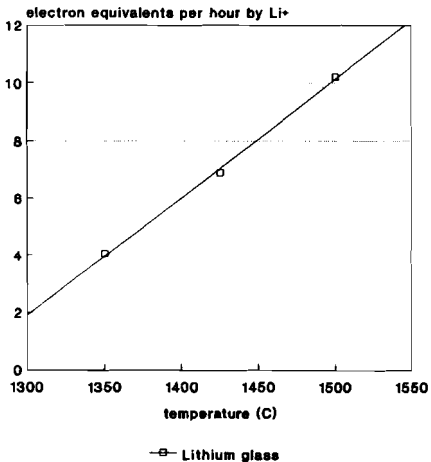
4.2. Results of measured cation diffusion.

- effect of composition, kind of cation, temperature level and viscosity of the glass melt.

The diffusion rate of a cation into the AZS is determined by its mobility and concentration in the AZS glassy phase in equilibrium with the glass melt. The temperature has a direct influence on the viscosity of the AZS glassy phase. The composition and therefore the viscosity of the glass melt can have an indirect influence on the viscosity of the AZS glassy phase as well, by the glass melt composition dependent diffusion of glass melt cations into the AZS which changes the composition of the glassy phase of the AZS. The diffusion rates in electron equivalents per hour, measured in the standard crucible set-up, can be represented in various ways. Although the diffusion of cations in the AZS glassy phase has been quantified, instead of listing the cation names (M^{n+}), the names of the cation oxides ($MO_{n/2}$) will be given.

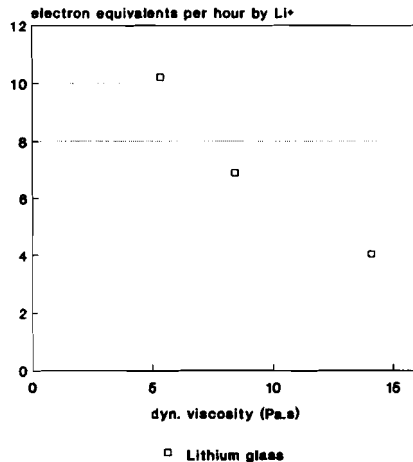
Figure 4.2.1 The relative diffusion rate for lithium.

Lithium figure 4.2.1.a



per mol per cent Li2O

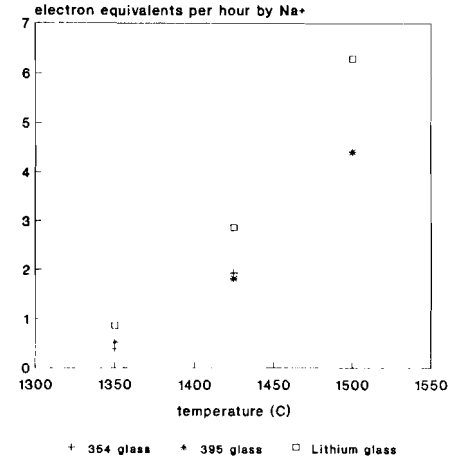
Lithium figure 4.2.1.b



per mol per cent Li2O

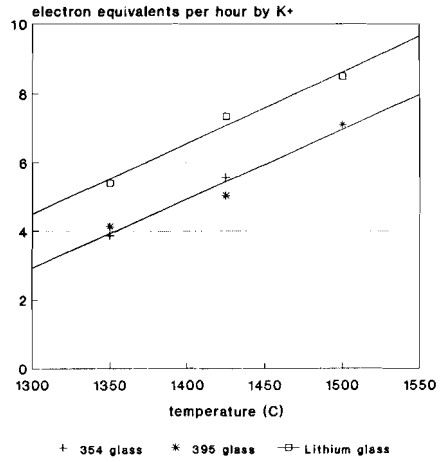
Figure 4.2.2 The relative diffusion rate of sodium, potassium, barium and strontium in e.e.h. versus temperature.

Sodium figure 4.2.2.a



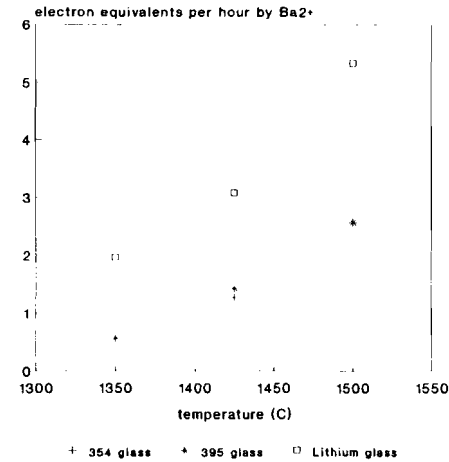
per mol per cent Na₂O

Potassium figure 4.2.2.b



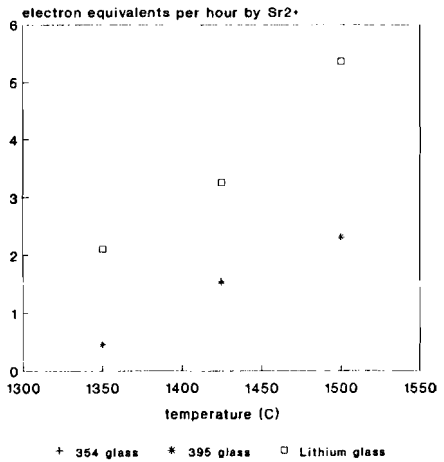
per mol per cent K₂O

Barium figure 4.2.2.c



per mol per cent BaO

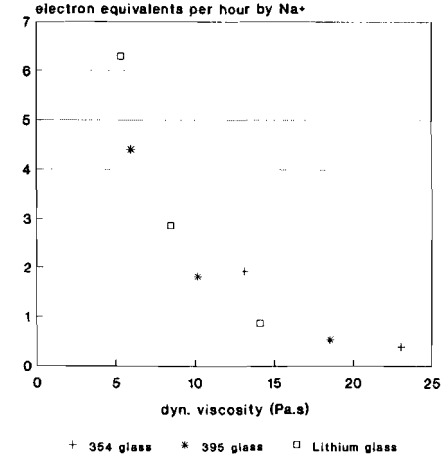
Strontium figure 4.2.2.d



per mol per cent SrO

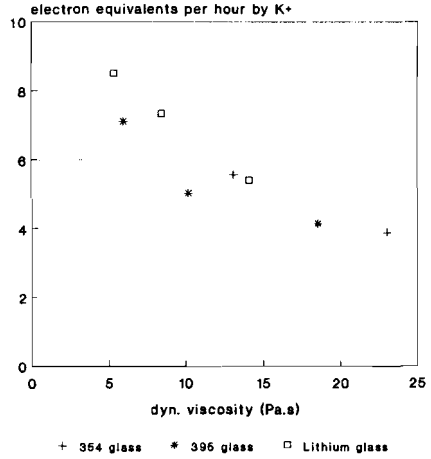
Figure 4.2.3 The relative diffusion rate of sodium, potassium, barium and strontium in e.e.h. versus viscosity.

Sodium figure 4.2.3.a



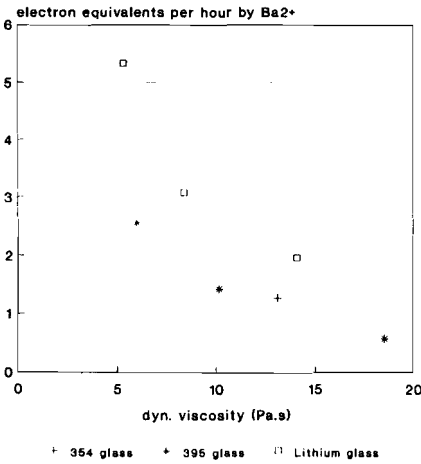
per mol per cent Na₂O

Potassium figure 4.2.3.b



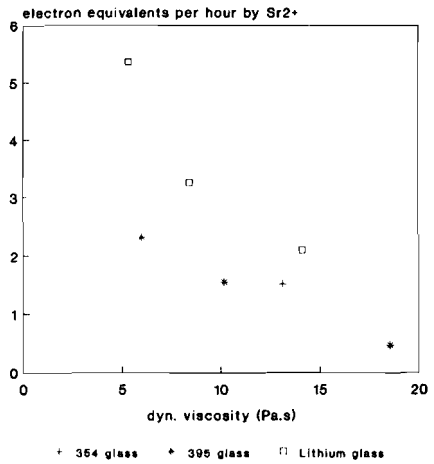
per mol per cent K₂O

Barium figure 4.2.3.c



per mol per cent BaO

Strontium figure 4.2.3.d



per mol per cent SrO

This has been done because all measurement results are in oxide fractions (given in mol% or weight%).

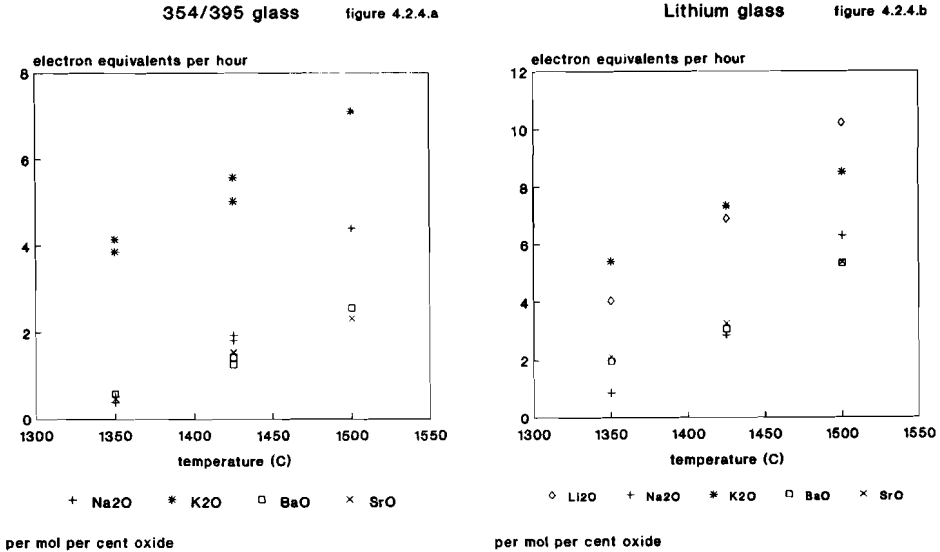
Figure 4.2.1, 4.2.2 and 4.2.3 show the e.e.h. values of Li_2O , Na_2O , K_2O , BaO and SrO in electron equivalents per hour (e.e.h.) per mol per cent in the glass composition, against the glass temperature and viscosity. Figure 4.2.1.a shows a linear relationship between the e.e.h. of Li_2O and the temperature.

There is no linear relationship between the viscosity and the e.e.h. of Na_2O (figure 4.2.3.a). The e.e.h. values for the cases of 395 and 354 glass are identical at a specific temperature. The e.e.h. values for Na, K, Ba and Sr using the lithium containing glass are markedly higher than those of 395 and 354 glass at a specific temperature (figure 4.2.2.a). For potassium there is a linear relationship between the e.e.h. values and temperature (figure 4.2.2.b). At a given temperature the e.e.h. values for potassium of 354 and 395 glass are identical and that of the lithium glass is higher. The e.e.h. values of barium and strontium show an identical tendency. Even at identical temperatures there is a wide difference in e.e.h. between 395 and 354 glass on one hand and lithium glass on the other hand (figure 4.2.2.c and 4.2.2.d).

The e.e.h. values plotted against the viscosity, which takes the shape of a curve with a rather narrow band (for the different glass compositions) for sodium and potassium (figure 4.2.3.a and 4.2.3.b), strongly diverges from the shapes for barium and strontium (figure 4.2.3.c and 4.2.3.d). For the same viscosity, the Ba^{2+} and Sr^{2+} diffusion rates from the lithium glass are much higher than from the other glasses.

The graph with the e.e.h. values of the oxides in zero-lithium glasses plotted against the temperature (figure 4.2.4.a) shows that the e.e.h. of K_2O is highest, far higher than those of the other oxides, notably at 1350°C . In glasses with a high Li_2O -content the e.e.h. values of all the four oxides are higher than at the same temperature, those of BaO and SrO the most strongest (figure 4.2.4.b). The e.e.h. of Li_2O itself is high too (Li^+ is a very small mobile cation). At 1350°C the e.e.h. of K_2O is less

Figure 4.2.4 The relative diffusion rate of lithium, sodium, potassium, barium and strontium in e.e.h.



dominant compared to the other oxides, than in the case of zero-lithium glasses.

Summarizing, it can be concluded that the determined relative diffusion rate for the cations in the Li_2O -containing glasses are higher than in the Li_2O -free glasses. Both figures 4.2.4.a and 4.2.4.b show an approximately linear relation between measured e.e.h. values and temperature between 1350 and 1500 °C.

The temperature dependency of the e.e.h. of the different cations are given by the following relations, which are the best fits of the values presented in the figures 4.2.4.a and 4.2.4.b.

e.e.h. values per mol per cent for Li₂O-free glasses, in fused cast AZS 32 material:

e.e.h. per mol per cent Na ₂ O	= -33.8450 + 0.025288*T	R=0.982
e.e.h. per mol per cent K ₂ O	= -23.3744 + 0.020228*T	R=0.980
e.e.h. per mol per cent BaO	= -17.4911 + 0.013295*T	R=0.984
e.e.h. per mol per cent SrO	= -16.1571 + 0.012364*T	R=0.994

e.e.h. values per mol per cent for Li₂O-containing glasses, in fused cast AZS 32 material:

e.e.h. per mol per cent Li ₂ O	= -51.5618 + 0.041122*T	R=0.999
e.e.h. per mol per cent Na ₂ O	= -40.2501 + 0.029830*T + 0.127461*[Li ₂ O]	R=0.975
e.e.h. per mol per cent K ₂ O	= -23.5880 + 0.020379*T + 0.192780*[Li ₂ O]	R=0.990
e.e.h. per mol per cent BaO	= -23.9845 + 0.017852*T + 0.237246*[Li ₂ O]	R=0.975
e.e.h. per mol per cent SrO	= -22.7870 + 0.017017*T + 0.249884*[Li ₂ O]	R=0.977

in which T is in degrees Centigrade, Li₂O in mol per cents and R is the correlation coefficient.

These equations have been verified in the following concentration ranges:

Li ₂ O	from 0	to 8.5 mol%
Na ₂ O	from 3.5	to 10.5 mol%
K ₂ O	from 2.5	to 6.8 mol%
BaO	from 3.5	to 4.8 mol%
SrO	from 2.0	to 6.5 mol%

For TV-screen glasses, these are the main oxides whose cations diffuse into the glassy phase of the AZS. In the current TV-screen glasses, other cations diffusing into this phase are only small in quantity.

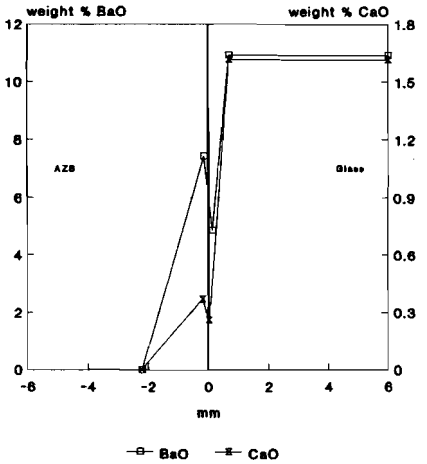
The other cations diffusing from T.V. glass melt into the glassy phase of fused cast AZS, are Ca^{2+} and Mg^{2+} . In a T.V. screen glass the concentrations of CaO and MgO are about 1 weight%. By way of estimation, the concentration profiles of CaO and MgO have been determined at various temperatures and for various periods. Figure 4.2.5 and 4.2.6 show them compared with those of BaO. Figure 4.2.5 shows the Y-axis scale (in weight%) of BaO and CaO so selected that their weight percentages in the glass coincide. The same 'standardized' graduation shows that the diffusion rate in weight percentages is a factor of 2.5 to 3 lower for CaO than for BaO. Figure 4.2.6 shows the concentration profiles of MgO compared with that of BaO. That of MgO expressed in weight% is a factor of 3.5 to 4 lower than that of BaO. The mol weights of BaO, CaO and MgO are 153.34, 56.08 and 40.30. The ratio between them is well in line with the ratio between the diffusion rates per weight% of the glass composition. For an estimate of the share of CaO and MgO in the total e.e.h. of the glass, in T.V. screen glass with its low CaO and MgO content, it is sufficient for this approach, to add the weight percentages of CaO and MgO to that of BaO for the calculation of the total e.e.h.

4.3 Practical application of the cation diffusion rules by a glass furnace model.

The cation diffusion is given in electron equivalents per hour (e.e.h.), which is the positive charge transported by the cations in the fused cast AZS in the standard crucible test set-up. The amount of positive charge transported in the AZS is a measure for the amount of oxygen formation at the interface glass melt/AZS. With the experimentally determined cation diffusion equations it is possible to make an estimation of the relative amount of transported positive charge by the diffusion of cations.

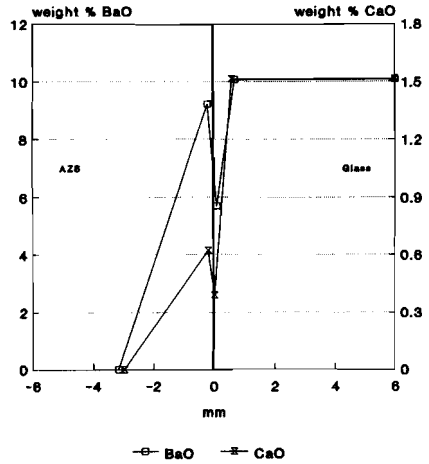
Figure 4.2.5 Comparison of the concentration profiles of BaO and CaO in the interface glass melt/fused cast AZS.

354 glass, 1350 C figure 4.2.5.a



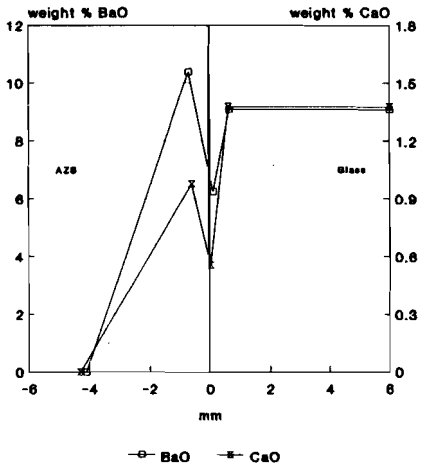
100 hrs.

354 glass, 1425 C figure 4.2.5.b



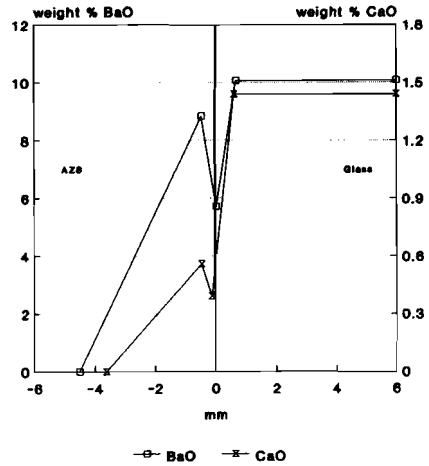
100 hrs.

354 glass, 1500 C figure 4.2.5.c



100 hrs.

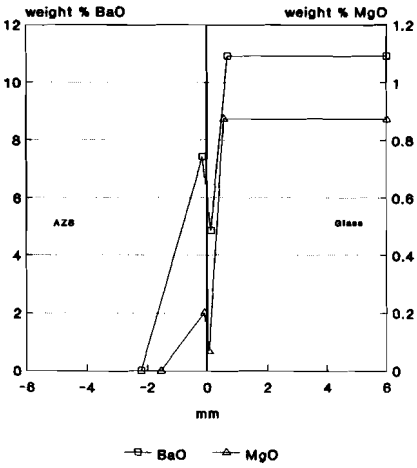
354 glass, 1425 C figure 4.2.5.d



260 hrs.

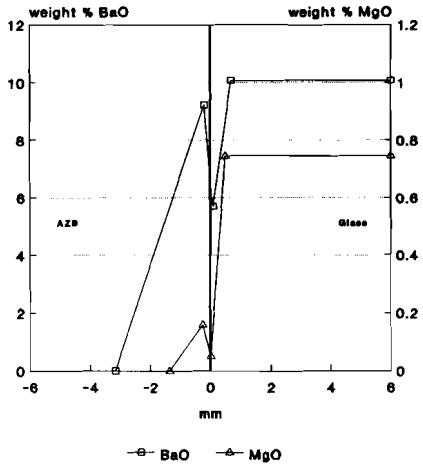
Figure 4.2.6 Comparison of the concentration profiles of BaO and MgO in the interface glass melt/fused cast AZS.

354 glass, 1350 C figure 4.2.6.a



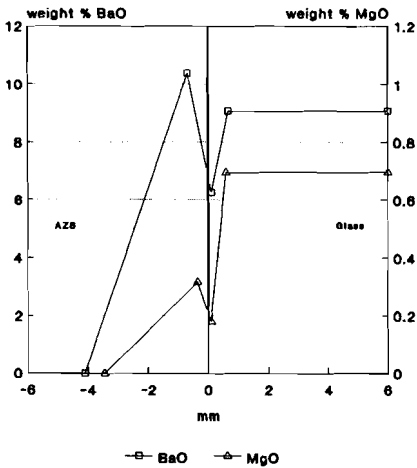
100 hrs.

354 glass, 1425 C figure 4.2.6.b



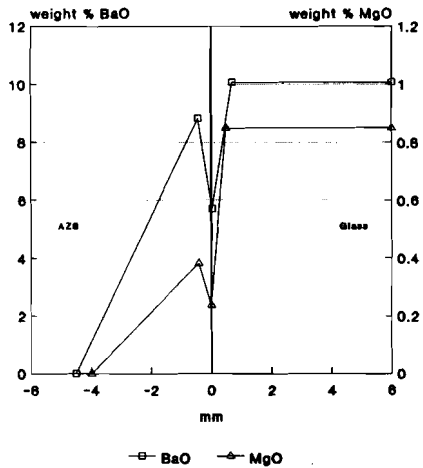
100 hrs.

354 glass, 1500 C figure 4.2.6.c



100 hrs.

354 glass, 1425 C figure 4.2.6.d

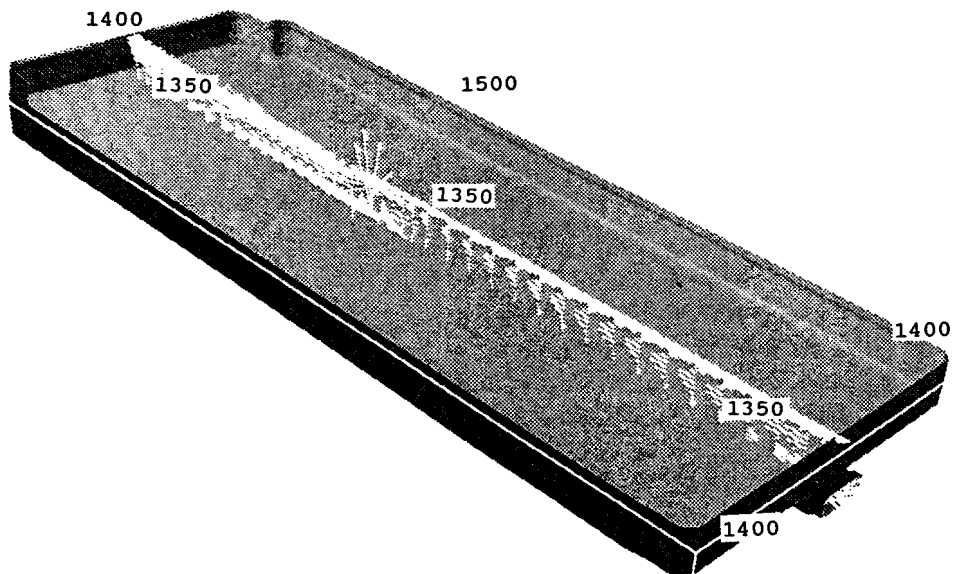


260 hrs.

To make such an estimation besides the chemical composition of the glass melt the contact temperature of the glass melt/fused cast AZS has to be known.

To illustrate the application of the model, let us assume a typical T.V. screen glass furnace with a glass output of 1.2 to 1.4 tons per day per mm^2 melting end surface, the industrial furnace is 19.4 m long, 6.7 m wide and its glass level 1.02 m high. The contact temperatures that will be used in the example have been checked with physical temperature measurements combined with computer model simulations.

Figure 4.2.7 In this picture of the glass bath of a melting end, the numbers give the contact temperatures in degrees Centigrade in the example of the model.



The temperature of the whole bottom is assumed to be 1350°C, that of the metalline (the three phase contact: glass melt, refractory and atmosphere) of front wall and rear wall 1400°C, that of the metalline near the hotspot 1500°C, and that of the palisade block surface, shows a linear gradient between the above temperatures. In the above mentioned furnace the total electron equivalents per hour per mol oxide, with new AZS and a Li₂O-free glass, are:
 Bottom area * e.e.h. at 1350°C + areas of front and rear walls * e.e.h. at 1375°C + side wall areas * e.e.h. at 1400°C.

e.e.h. of	bottom	front and rear walls	side walls	total
Na ₂ O	38.2	12.7	61.7	112.5
K ₂ O	511.3	60.7	195.7	767.6
BaO	59.4	10.8	44.4	114.6
SrO	69.4	11.5	45.6	126.6

The values in the table apply to the above furnace and its temperatures. The share of K₂O is obviously far higher than those of the other oxides. This difference in the share of the various oxides implies that the glass composition has a strong effect on the total e.e.h., thus on the oxygen gas formation potential at the AZS interface, of a glass melt in an industrial furnace. By way of example, the table below shows the difference between 354 and 395 glass for the complete furnace.

There is a marked difference between the two glass types, which is mainly caused by the difference in the potassium content.

glass	354 glass			395 glass		
	weight%	mol%	e.e.h.	weight%	mol%	e.e.h.
Na ₂ O	9.35	10.25	1153	6.70	7.56	851
K ₂ O	6.45	4.67	3585	9.10	6.77	5197
CaO	1.50			0.35		
BaO	10.70	5.87	673	7.70	3.79	434
MgO	1.00			0.25		
SrO	3.00	1.96	248	9.50	6.39	809
total			5659			7291

4.4 Discussion.

The strong rise in e.e.h. values using a lithium glass might be due to the fact that lithium glass has a lower viscosity or to the interaction between Li₂O and the AZS leading to a rapid decrease in the AZS glassy phase viscosity due to Li⁺ penetration. The difference in the so called melting point (which is by definition the temperature at which the melt has a viscosity of 10 Pa.S) between 354 and 395 glass is comparable with that between 395 glass and lithium glass. (The melting point of 354 glass is 1465 °C, that of 395 glass is 1427 °C and that of lithium glass 1400 °C). The e.e.h. values per mol of cation, of 354 and 395 glass are comparable at identical temperatures, which points out that the velocity-determining step: the diffusion of glass melt cations in the glassy phase of the AZS is left rather unaffected by the difference in composition between 354 glass and 395 glass. The Li₂O in the lithium glass affects the properties of the glassy phase in the AZS, in such a way that the diffusion rates of all the cations are increased (see 3.2.2.4 of this study). The total summation of e.e.h. values of a glass in the described

model, gives an indication of the amount of oxygen formed by the diffusion rate controlled mechanism of oxygen formation at the interface AZS/glass melt.

A glass is capable of absorbing or releasing oxygen, expressed in moles per unit of time and per unit of AZS surface area. There are two ways in which a glass can absorb oxygen: physically and chemically (Lit. 1). When oxygen is dissolved physically, the oxygen molecules dissolve in the glass melt interstitially, as if the melt is an inert, more or less open matrix. The oxygen can also dissolve in the glass by an oxidation reaction of polyvalent cations in the glass melt. This is called chemical dissolution. The quantity of oxygen which can be absorbed by the glass melt depends mainly on the temperature, the redox of the glass and the concentration of Sb, Ce, Fe and S (Lit. 2). For instance, the equilibrium of the reaction



shifts to the right hand side when the temperature decreases.

As long as the local potential for oxygen absorption by complete dissolution is equal to or higher than the supply, no oxygen bubbles will be generated. After the tests with 354 glass at 1350 °C, hardly any bubbles with oxygen were found. It is, therefore, supposed, as a first approximation, that a TV-screen glass, with about 0.4 weight% Sb_2O_3 and 0.05 weight% Fe_2O_3 , is still capable of absorbing the oxygen atoms arising from interaction between 354 glass and AZS at 1350°C. For the furnace used in the model this implies an absorption capacity of 4601 e.e.h. (4601 e.e.h is equal to the total e.e.h. value of 354 glass at 1350 °C, about 25 e.e.h. per m^2 , multiplied by the total glass melt/AZS interaction area in the model).

The potential of glass defect formation owing to interaction between AZS and 354 glass is (from calculation example 5659 - 4601) 1058 and between AZS and 395 glass is (7291 - 4601) 2690, which means a glass defect ratio owing to the interaction between fused cast AZS and 354 glass to 395 glass of 1 to 2.5.

The above calculation is only an estimate, with the hypothesis of the oxygen absorption capacity having a strong effect on the glass

defect potential ratio. An intensive study to quantify the effects of oxygen absorption by the glass melt would improve the accuracy of this estimation. In industrial practice, the mentioned ratio of glass defects due to the interaction of fused cast AZS, for the two mentioned glasses (354 glass and 395 glass) corresponds with the relative amount of glass rejects.

The bubbles originating from the melting end were doubled. The knots out of the melting end were more than doubled. The sum of the two glass defects originating from fused cast AZS/glass melt interaction in the 395 glass was approximately 2.5 times larger than the sum of both mentioned glass defects when 354 glass was melted in the same furnace.

Similar observations of increase of glass defects due to fused cast AZS/glass melt interaction have been made when smaller increases of K_2O content in the glass were applied. Of course, the larger the increase of K_2O content the larger the glass defect increase.

Generally, in an industrial furnace, there is a temperature difference over the fused cast AZS block: between the glass melt touching surface inside and the colder outside surface of the block. This temperature decrease over the refractory block will lower the diffusion of cations in the glassy phase in the interior of the fused cast AZS.

Starting with new AZS, the amount of electron equivalents produced, will drop (slowly) because the chemical composition of the glassy phase in the AZS and the oxides in the glass melt will become better in balance.

Previously it has been shown that potassium ions have by far the highest diffusion rates (due to the larger driving force) among of the investigated cations at 1350 °C. This means that deep in the block at temperature levels where the diffusion rates of the other cations is almost zero, potassium still may have a substantial diffusion rate. Therefore it will take more time to obtain a balance (an apparent equilibrium, the reaction kinetics are stopped by the low mobilities) between the potassium oxide in the

glass melt and the fused cast AZS compared with the other oxides in the glass melt. In practice a complete chemical balance will not be reached on account of the AZS corrosion, which increases the local block temperature. The tests in which the e.e.h. values have been derived, have been performed under static and isothermal conditions. The corrosion rates or wear of fused cast AZS in non static conditions, like in an industrial furnace, are higher than under static conditions. At the same temperature, a glass melt with a low viscosity will give a larger corrosion rate (lit. 3-6), therefore a higher diffusion rate and more production of oxygen. A rise in temperature will increase the temperature of the refractory causing a change in the equilibrium of the polyvalent ions (to the lower valence state) in the fused cast (Lit. 7-9), thereby releasing oxygen. Also the diffusion of cations will increase because the apparent equilibrium of the concentration profiles will shift deeper into the refractory, the difference between the existing concentration profiles and the apparent equilibrium concentration profiles of the higher temperature increases the driving force for the diffusion of cations. At a drop in temperature the opposite will occur, there will be a temporary "over-saturation" of the local concentration of the cations and therefore a decrease in driving force for diffusion. A furnace in which during a long period, a specific glass composition has been molten, the fused cast AZS is in "apparent balance" with this specific glass. In the case of a change in glass composition the fused cast is out of "balance" with the new glass composition. As an example, the glasses (354 and 395 glass) used in this chapter for the e.e.h. calculation, have about the same total amount of alkali oxides ($\text{Na}_2\text{O} + \text{K}_2\text{O}$) expressed in weight%. When for instance a sodium oxide rich glass like 354 glass has been molten for a long time in a furnace and in this furnace the glass is changed to a potassium rich glass like 395 glass, initially the amount of positive charge by diffusion of potassium into the fused cast will be partly compensated by the diffusion out of the fused cast into the glass melt of sodium, consequently the electron transfer will be relatively small and

therefore also the oxygen bubble formation (comparable with the bubble formation with the previous 354 glass). The charge compensation by the sodium diffusion from the glassy phase of the fused cast AZS will decrease relatively fast because of the limited amount of sodium oxide in the fused cast AZS. The diffusion of potassium from the glass melt, however, continues thereby, increasing the formation of glass defects from the interface glass melt/AZS. This explains why in industrial practice the number of glass defects, after such a glass change, is higher after a few months than in the first few weeks. The diffusion of sodium in the glassy phase of the fused cast AZS to the glass melt has been derived in chapter 3, figure 3.2.23 of this study. Under regular conditions, most of the glass defects arise owing to the interaction between glass and AZS in the high-temperature areas. If the AZS interacts with a "high-potassium" glass, the lower-temperature (1320 - 1350 °C) interaction area (furnace bottom) may also take a substantial share in the total glass fault rate (see chapter 6 for examples of industrial furnaces). Note that not all the defects arising in the glass, end up in the product or are a cause for rejection. The chance of survival of bubbles and knots depends on aspects like their source, their original size, the composition of the defect, the composition of the glass melt, the temperature of the glass melt, the redox state of the glass melt, the exchange of gases from the generated oxygen bubble with the melt, residence time and glass flow patterns in the melting tank. In the T.V. screen glass production, it is their ultimate size and location in the screen which decides whether they are a cause of product rejection.

Literature references chapter 4.

- [1] R.H. Doremus;
Diffusion in glasses and melts.
J. of Non-Cryst. Solids **62** (1977) p. 263-292.
- [2] R.G.C. Beerkens, H. de Waal;
Mechanism of oxygen diffusion in glass melt containing
variable-valence ions.
J. Am. Cer. Soc. **73** (1990) p. 1857-1861.
- [3] R. Brueckner;
Wechselwirkungen zwischen Glasschmelze und
Feuerfestmaterial.
Glastech. Ber. **53** (1980) p. 77-88.
- [4] M. Dunkl, Brueckner;
Corrosion of refractory materials by a container glass melt
under the influence of various convection flows.
Glastech. Ber. **62** (1989) p. 10-19.
- [5] S. Ozgen, E. Aydin, M. Orhon;
The relation between the type of alkali oxide in glass and
refractory corrosion.
Int. Conf. on glass XV (1989) p. 283-286.
- [6] B. Krabel, R. Brueckner;
Convection flow dependent corrosion of refractory material
in glass melts and comparison to theoretical relations.
Int. Coll. on Refractories XXXVI (1993) p. 45-49.
- [7] F.W. Kraemer;
Analysis of gases evolved by AZS refractories and by
refractory/glass melt reactions. Techniques and results.
Contribution to the bubble forming mechanism of AZS
material.
Glastech. Ber. **65** (1992) p. 93-98.
- [8] E.L. Swarts;
Bubble generation at glass/refractory interfaces. A review
of fundamental mechanisms and practical considerations.
Glastech. Ber. **65** (1992) p. 87-92.

[9] M. Dunkl;

Studies on the glassy and reaction phases given off by fused cast AZS blocks and their effects on the glass quality. Glastech. Ber. 62 (1989) p. 389-395.

5. Bubble formation during the laboratory-scale tests.

5.1. Introduction.

In the laboratory-scale tests, described in chapter 3 of this study, the formation of O₂-bubbles has been shown.

The objective of the experiments described in this chapter is to determine the influence of temperature and glass melt composition on the number of bubbles, their size (diameter) and gas content, in the laboratory-scale (crucible) tests. The results can be used as starting parameters for a flow model which includes the position of bubbles in the glass melt bath and the gas exchange between bubbles and the glass melt.

The number of bubbles generated and their diameter, in relation to the temperature, gives an indication of the importance of the fraction of bubbles from fused cast AZS in the total glass defects.

Another objective of the experiments described in this chapter is the investigation of the glass defect potential tendency of a glass melt/AZS interaction by direct counting the number of bubbles at the end of a crucible experiment.

Although the original gas content of a bubble can change dramatically during its residence time in the glass melt (Lit. 1-8), the gas composition of the relatively fresh bubbles can confirm the existence of an electrochemical mechanism for the bubble formation.

Another parameter which has been investigated here, is the effect of the duration of the interaction between glass melt and fused cast AZS on the number, size and gas composition of the bubbles.

5.2. Experimental method.

The crucible + glass samples obtained from the tests, described in chapter 3 'Cation diffusion into fused cast AZS' have been cut into slices, polished and photographed. Next the bubbles were counted and their diameters measured. The gas composition of a

part (a randomly taken sample) of the generated bubbles in the crucible have been analyzed.

The gas composition and the volumetric diameter of the bubble have been analyzed by breaking a bubble in a high vacuum chamber and analyzing the gas content of the broken bubble with a Balzers QMG 420 quadrupole mass spectrometer. The volumetric diameter has been determined by measuring the increase in pressure of the known chamber volume immediately after the breaking of the bubble in the high vacuum chamber, assuming that the pressure in the bubble at room temperature is 1/3 bar and the gas of the bubble is an ideal gas. The diameter of the bubbles is calculated with the equation $P \cdot V / T = \text{constant}$. The assumption that the gas in the bubble has a pressure of 1/3 bar has been checked by analyzing numerous spherical bubbles and is understandable because at about 900 K the diameter of the bubble is frozen in and further gas exchange is neglectable.

5.3. Test results.

Annex 4 shows the results of the analysis and annexes 1 and 5 present the compositions of the glass types used.

The **number** of bubbles, in the glass slices, differs widely from test to test, also within the duplicate tests. Figure 5.1 shows the number of bubbles plotted against the temperatures. The samples tend to contain more bubbles as the temperature increases. The dispersion at a given temperature is very large. The so called t-test (annex 6) shows that the average counts at 1350 and 1425°C differ significantly ($t[30]=3.041$). The difference between the number of bubbles at 1425 and 1500°C is not significant ($t[27]=1.198$). That between the number at 1350 and 1500°C, again, is significant ($t[19]=3.226$).

The results of figure 5.1 show that the method of counting the number of bubbles at the end of the test is not suitable for detecting the difference in glass defect potential because of the large variation of for instance the number of bubbles counted in

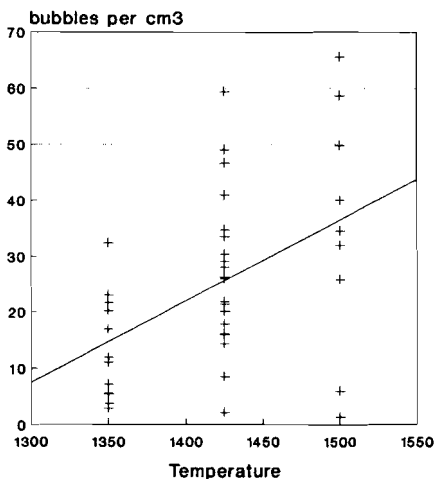
duplicate tests (annex 4). Even the influence of the temperature on the number of bubbles can only be proven statistically after a large number of tests.

The **diameter** of the bubbles increases as the temperature rises. Figure 5.2 shows the average diameters (arithmetic) of the five largest bubbles found in each test. The average diameter of the five largest bubbles is described in the figures as the diameter range. No difference between the different glasses except for lithium glass has been detected.

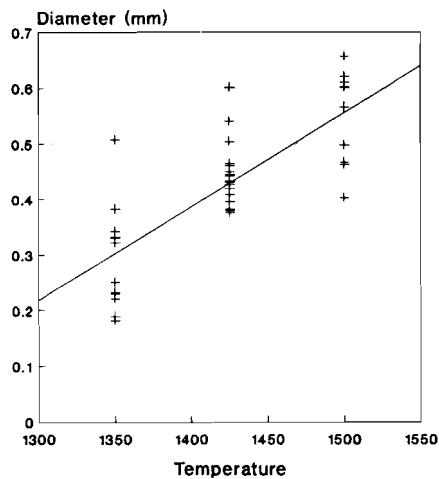
Figure 5.1 Number of bubbles per cm³ determined in the crucible experiments with different glasses at different temperatures.

Figure 5.2 Average diameter of the five largest bubbles determined in the crucible experiments with different glasses at different temperatures.

Number of bubbles figure 5.1
ER 1681 crucible



Bubble diameter range figure 5.2
ER 1681 crucible



average diameter of 5 largest bubbles in sample.

Remark: The lithium glass is the only glass melt of which the results of the experiments is slightly different, the number of bubbles at the end of the test is low and the average diameter is the largest of all tested glasses.

The t-test results of all the experiments, point to a significant difference in average diameter between 1350 and 1425°C ($t[30]=5.767$), and between 1425 and 1500°C ($t[27]=3.988$).

Figure 5.3 The relation between the average diameter of the bubbles prepared for gas content analysis and the average diameter of the five largest bubbles determined in the sample.

Figure 5.4 The relation between the average diameter of the bubbles prepared for gas analysis and the average diameter of the successfully analyzed bubbles, showing that the analyzed bubbles are representative.

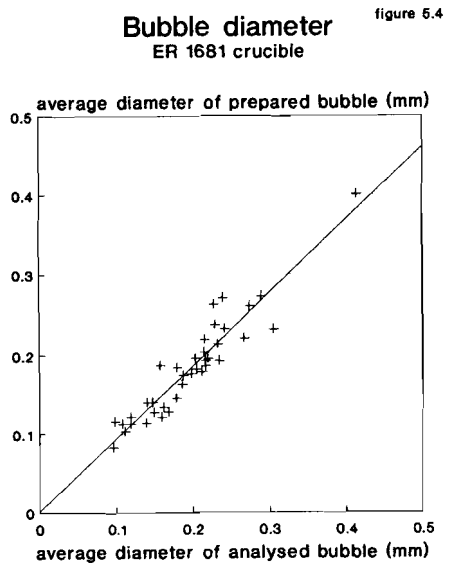
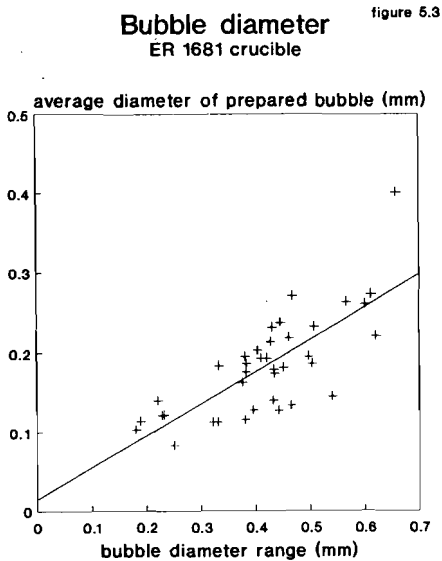


Figure 5.3 proves there is a linear relationship between the average diameter of the five largest bubbles in the sample and the randomly taken sample of the average diameter of bubbles prepared for gas composition analyses. The linear relationship indicates that the largest bubbles, which are large enough to cause reject in for example TV-screen production are a part of the population of the analyzed bubbles.

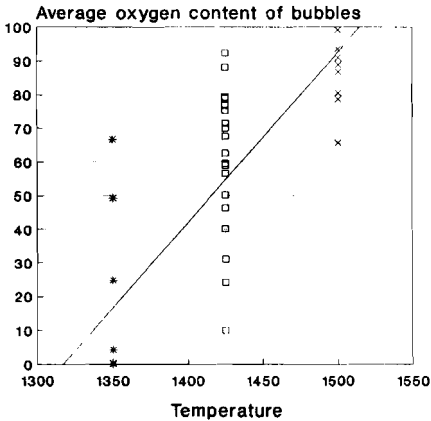
The bubbles prepared for analyses have been taken randomly in the neighbourhood of the glass/AZS interface. Not all the prepared bubbles have been successfully analyzed, figure 5.4 shows that there is no significant difference between the average diameter of the prepared and the successfully analyzed bubbles.

Figure 5.5 Average (arithmetic) oxygen content of the analyzed bubbles of the tests with different glasses at different temperatures.

Figure 5.6 Relation between the average oxygen content of the bubbles and the average diameter of the analyzed bubbles.

Bubbles
ER 1681 crucible

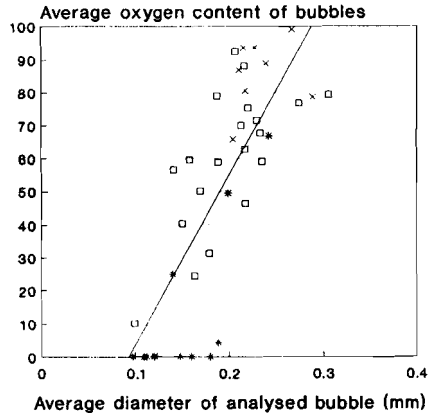
figure 5.5



* 1350 C □ 1425 C × 1500 C

Bubbles
ER 1681 crucible

figure 5.6



* 1350 C □ 1425 C × 1500 C

This justifies the assumption that the gas content of the analyzed bubbles is representative for the gas content of the randomly prepared bubbles.

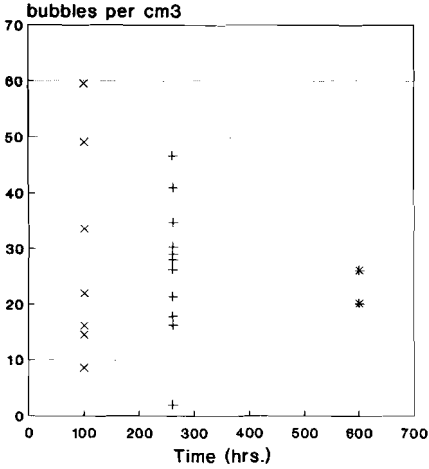
From the analysis it is obvious that the average **gas composition** of the bubbles depends on the test temperature and diameter. The higher the temperature and the larger the diameter, the higher the oxygen content (figures 5.5 and 5.6). Bubbles from various tests at 1350 °C hardly contain oxygen gas. At tests at 1500°C there are hardly any bubbles analyzed without oxygen as the main component.

The effect of the **test duration** is investigated by experiments in which the AZS crucible has been exposed longer than 100 hours to the molten glass, the glass melt has been exchanged several times during such an experiment. The last renewal of the glass melt has been performed approximately 100 hours before the end of the test. In this way in all the tests the residence time of the glass in the crucible in which the bubbles have been investigated has been equal. The residence time of the bubbles is much smaller than the mentioned 100 hours due to their (Stokes) rising speed. The rising speed of a bubble with a diameter of 0.2 mm is for example 2 cm/h at melting point temperature (viscosity 10 Pa.s), which means that such a bubble reaches the surface within 2 hours under these conditions.

The effect of test duration (the total time the AZS has been exposed to the molten glass) on the number of bubbles, present at the end of the test time, at a specific temperature is not significant (figure 5.7). Nor has it any significant effect on the average diameter of the five largest bubbles (range in annex 4) of the prepared sample (figure 5.8). There is no significant difference in the average diameters of the bubbles between the various test duration times (figure 5.9). There is also no significant difference in average oxygen content on the time scale between 100 and 260 hours ($t[16]=1.156$), but there is a significant difference between 260 and 600 hours ($t[11]=2.106$) and

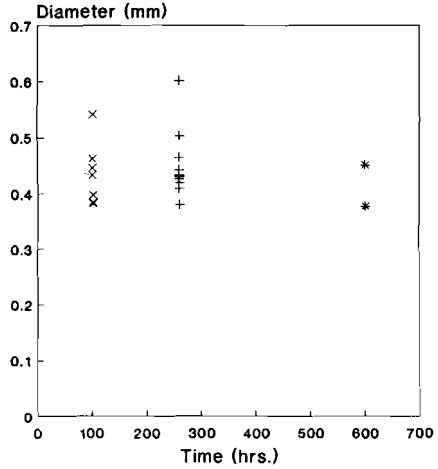
Figure 5.7 - 5.10 The number, the average diameter of the five largest, the average diameter of the analyzed and the average oxygen content of the bubbles in relation with the duration of the experiment.

Number of bubbles figure 5.7
ER 1681 crucible



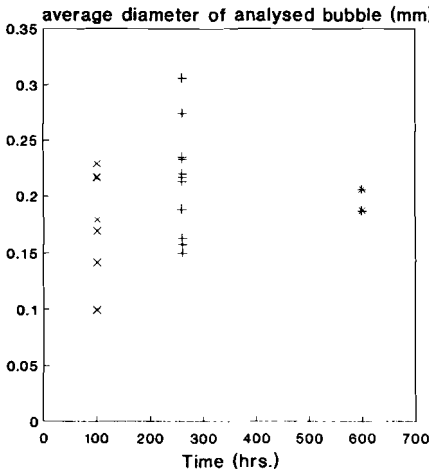
test temperature 1425 C

Bubble diameter range figure 5.8
ER 1681 crucible



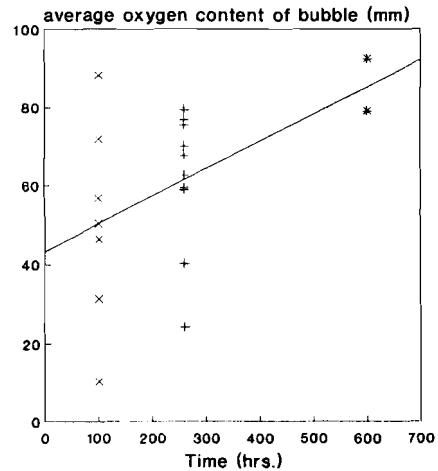
test temperature 1425 C

Bubble diameter figure 5.9
ER 1681 crucible



test temperature 1425 C

Bubbles figure 5.10
ER 1681 crucible



test temperature 1425 C

between 100 and 600 hours ($t[7]=1.989$). Although the t-test with the experiments of a test duration of 600 hours is very disputable because there are only two measurements of this test duration. A tendency to obtain higher O_2 levels in these bubbles has been observed for larger test periods (figure 5.10), although also here the small number of measurements of the experiments with a test duration of 600 hours makes the observation disputable.

Summarising, it can be concluded from figure 5.1, 5.5 and annex 4 that for the bubbles found in the crucible experiments no relation between these bubble characteristics and the glass melt composition could be established.

A temperature increase, increases the number of bubbles, their diameter and oxygen content in the crucible experiments.

5.4 Discussion

A rise in temperature is accompanied by an increase in the average bubble diameter and a drop in glass viscosity and consequently, a reduction in the average time a bubble takes to reach the glass surface to be released. If the change in viscosity caused by increasing levels of corrosion products in the glass is ignored and the glass density is assumed to remain unchanged at the various temperatures, the ratio of the residence time of a bubble with the determined average diameter can be calculated. The ratio between the periods of residence time for a bubble of the average (constant) diameter in the melt is 11 to 3 to 1 at 1350, 1425 and 1500°C.

The number of bubbles found in the glass slices, however, increases as the temperature rises, in spite of the strong reduction in expected residence time in the glass melt. Thus, the amount of bubbles formed, at the end of the test duration, is probably about 25 times higher at 1500 than at 1350°C.

This increase can be explained by the results presented in chapter 4 of this study. There are two factors; first the increase of the diffusion rate of cations from the glass melt into the AZS which

increases the formation of oxygen at the interface glass melt/AZS. The second important factor is the reduced capability of the glass melt to absorb oxygen at increasing temperatures, because of the higher O_2 fugacity of the glass melt, mainly caused by the redox reactions of polyvalent ions (antimony, iron) in the melt producing oxygen gas at elevated temperatures. The second factor is also important for the observed decrease in diameter and oxygen content of the bubbles with decreasing test temperatures. During the residence time of the bubbles in the glass melt the oxygen from the bubbles is diffusing into the glass melt. At lower temperatures, the oxygen fugacity of the melt is larger and thus the driving force for this diffusion is increased. Also the average residence time of the bubbles is increased by the larger viscosity at lower temperatures.

Meden and v.d. Pas (Lit. 9) have determined the average life time of 100% oxygen bubbles, of bubbles consisting of oxygen and other gases and of non-oxygen bubbles in similar crucible tests. Their conclusion also was that the oxygen in the bubbles is absorbed as the bubble remains longer in the glass at the investigated high temperatures. Apart from a minor number of bubbles arising, for example, from pores and cavities in the refractory, most of the bubbles started as pure oxygen bubbles. The present investigation shows to the same tendency, although the amount of oxygen bubbles found after tests at 1350°C is too low for the same conclusion to be definite. At higher temperatures, the number of analyzed oxygen bubbles is high enough for this conclusion to be fully justified. However, the wide spread in the results makes the present method of counting and analyzing bubbles unsuitable as a simple way of judging the tendency for differences in glass defect potential of glasses with different glass composition.

The dynamic blister test proposed by Dunkle (Lit. 10), in which with the help of lenses, objectives, mirrors and a video camera, all the bubbles which are formed in the glass melt in a refractory crucible are followed in-situ, is probably a better method of determining the bubble generating potential of a glass melt/refractory combination.

With this method, measurements of the bubble formation rate at the fused cast AZS 32 in contact with a glass melt show a decrease in bubble generation after 260 hours at 1400 °C. These results in the Dunkl test method agree well with the proposed mechanism and the measured cation diffusion decrease in time in a crucible experiment described in chapter 3 of this study.

Simply counting the number of bubbles at the end of the test is only suitable to demonstrate very large differences in the bubble generation potential.

Summarising, it can be concluded that the applied test method is suitable to get an insight in the bubble formation mechanism and the gas exchange of the bubble in the molten glass at different temperatures. The used test is hardly suitable as a quantitative method for determining bubble formation tendencies.

The number of generated bubbles, their diameter and gas content can be used as a starting parameter for a model which calculates the rise of bubbles in the glass melt and the gas exchange between bubbles and glass melt. It is recommended to link such a future model with a 3-D model of a glass furnace. The result can give a good estimation of the contribution of the bubbles from fused cast AZS to the total glass defect number of industrial glass production. Such a future model would be a very powerful tool for glass quality control in industrial glass production.

Literature references chapter 5.

- [1] F.W. Kraemer;
Bubble defect diagnosis by means of a mathematical model.
Coll. papers, XIV Intl. Congr. on Glass (1986) p. 288-295.
- [2] F.W. Kraemer;
Mathematical models of bubbles growth and dissolution in
glass melts.
Gas bubbles in glass; I. Comm. on Glass (1985) p. 92-126.
- [3] L. Nemeč;
The refining of glass melts.
Glass Tech. **15** (1974) p. 153-156.
- [4] C.H. Greene, D.R. Platts;
Behaviour of bubbles in oxygen and sulfur dioxide in soda
lime glass.
J. Am. Cer. Soc. **52** (1969) p. 106-109.
- [5] R.G.C. Beerkens;
Chemical equilibrium reactions as driving forces for growth
of gas bubbles during refining.
Glastech. Ber. **63K** (1990) p. 222-241.
- [6] J.M. Hermans, A.C. Verbeek;
Gasaustausch zwischen Blasen und geschmolzenem Glas.
67 Glastechnische Tagung, Koningswinter (1993) p. 34-38.
- [7] H.O. Mulfingher;
Zum Verhalten von Blasen in Glasschmelzen.
Glastech. Ber. **45** (1972) p. 238-243.
- [8] H.O. Mulfingher;
Gasanalytische Verfolgung des Lautervorganges im Tiegel und
in der Schmelzwanne.
Glastech. Ber. **49** (1976) p. 232-245.
- [9] G. Meden, T. v.d. Pas;
Invloed van het uitstoken van ZAC 1681 op de mate van
belvorming (Effect of firing out ZAC 1681 on intensity of
bubble formation).
OC 81/350.

[10] M. Dunkl;

TC-11 meeting (Refractories) in Madrid d.d. 04-10-1992.

6. Knot formation mechanism and characterization.

6.1 Introduction.

A knot is a vitreous particle with a composition deviating from the composition of the bulk of the glass, and consequently, a different index of refraction, which brings about a local lens effect.

The vitreous particle may contain crystals.

Objective of this chapter is to show the relation between the chemical composition of the knots in the glass products and their origin in order to find the source of these important glass defects. In T.V. screen glass production, for instance, a product with a knot with a diameter of 1 mm. is in most cases a reject.

A knot, originating from fused cast AZS in TV-screen glass has a higher Al_2O_3 -content than the bulk glass, which leads to a viscosity and surface energy of the knot higher than for the bulk glass. The density of these knots, however, is lower than that of the bulk (TV-screen) glass.

In the literature review of chapter 2 the gas formation (bubbles) in the refractory and at the interface refractory/glass melt is found to be the most important cause of pushing liquid phase out (exudation) of the fused cast AZS.

This means that, the mechanism and rate of bubble formation investigated in the previous chapters of this study, is also determining for the knot formation at the interface glass melt/fused cast AZS.

For the elimination of a knot defect problem in the practice of industrial glass production, an indication of the origin of the knot in the furnace is very helpful.

In this chapter, the chemical composition of knots in products fabricated in the past will be investigated. The dissolving of knots will be investigated and the preservation and/or change of the chemical composition of the knot during its residence time in the glass melt. The effect of the local temperature and the chemical composition of the glass melt on the chemical composition

of the interface glass melt/AZS is also studied in this chapter. By combining information on the chemical composition of the knots with data on the chemical composition of the glass melt/AZS interface obtained from laboratory experiments, the last part of the chapter will show the possibility to link a production knot defect problem to its origin temperature area where it has been formed in the furnace.

6.2 Knots in TV-screen glass products.

Of the knots in products fabricated in the past few years the chemical composition of the glassy phase, the location in the screen, the size and the kind of crystals (if present) they contain have been determined. No relation could be established between the knots location and size, chemical composition or containing crystals. Nor between the knots size and location, chemical composition or containing crystals. However, a relation has been found between the Al_2O_3 content of the glassy phase of the knot and, for instance, the content of BaO , SiO_2 , K_2O and ZrO_2 of the glassy phase of the knot.

The applied analysis is identical with the SEM/EDX method described in chapter 3, part 3.2.1.1. Only the sample preparation is different, a straightforward polishing treatment of the knot is applied.

The concentration of Al_2O_3 of a large number of analyzed knots in the TV-screens plotted in a graph, against the concentration of one of the other components, for instance BaO , SiO_2 , K_2O and ZrO_2 , has a distinct shape.

Figure 6.1.a to 6.1.d show the Al_2O_3 related to measured BaO concentrations (in weight%) of knots in TV-screens. The knots in the TV-screens from an industrial Philips furnace PTA plotted in a graph (figure 6.1.a), having the distinct shape of a crescent with tips up. The knots in the TV-screens from furnace PBA (figure 6.1.b) have a similar shape. The knots in TV-screens from furnace PAB (figure 6.1.c) are almost exclusively high- Al_2O_3 ones (more than 15 wt%), which means that only half of the crescent is

Figure 6.1.a The BaO versus Al₂O₃ concentration (in weight%) of knots, of furnace PTA, in TV-screen glass.

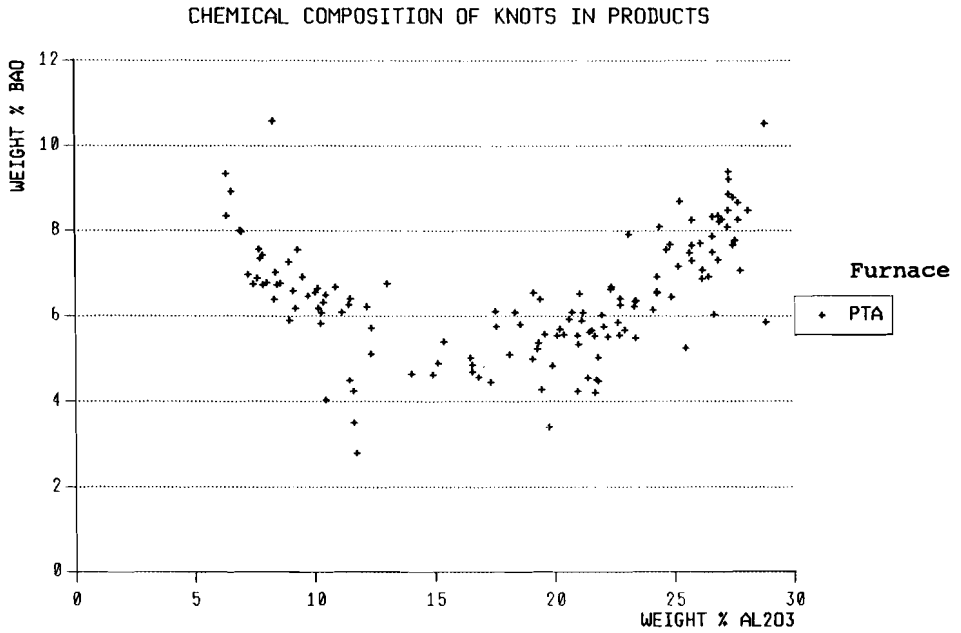


Figure 6.1.b The BaO versus Al₂O₃ concentration (in weight%) of knots, of furnace PBA, in TV-screen glass.

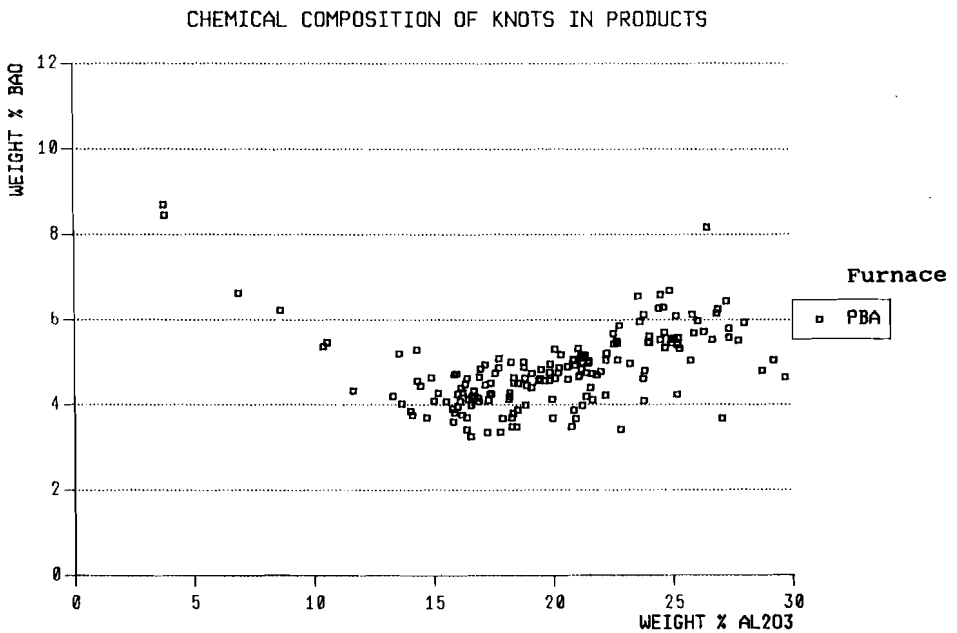


Figure 6.1.c The BaO versus Al₂O₃ concentration (in weight%) of knots, of furnace PAB, in TV-screen glass.

CHEMICAL COMPOSITION OF KNOTS IN PRODUCTS

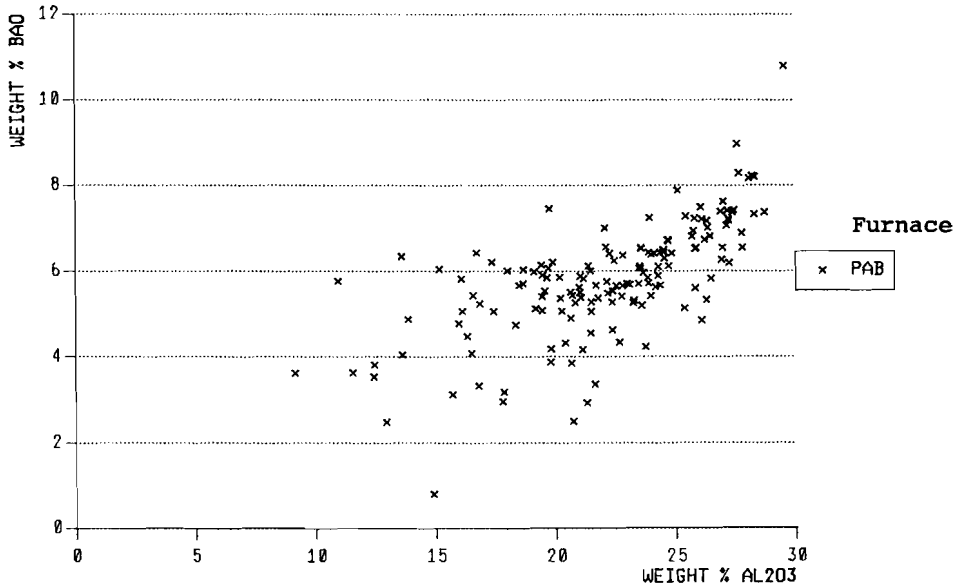
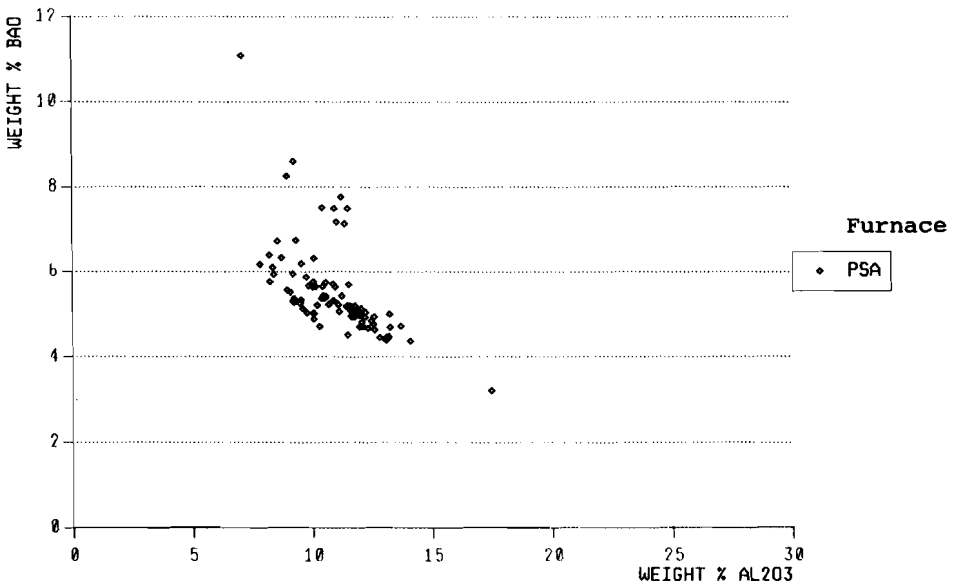


Figure 6.1.d The BaO versus Al₂O₃ concentration (in weight%) of knots, of furnace PSA, in TV-screen glass.

CHEMICAL COMPOSITION OF KNOTS IN PRODUCTS



visible. The knots in the screens from furnace PSA (figure 6.1.d) had a few incidents as source (calamities). All but one of these analyzed knots in the PSA products have a low Al_2O_3 -content (less than 15 wt%), again only half of the crescent shows up.

All the knots from all the furnaces together form the whole crescent again, despite the difference in glass type melted in these furnaces.

Table 6.1 shows that the variation in BaO-contents of these glasses is rather wide.

Table 6.1

The main components of the glasses molten in the different furnaces in weight% (nominal values).

furnace	glass type	SiO_2	Al_2O_3	Na_2O	K_2O	BaO
PTA	328	66.1	2.9	7.0	6.4	12.3
PBA	346	63.8	3.3	9.1	6.5	8.7
PAB	354 glass	63.9	3.3	9.5	6.5	10.7
PSA	346	63.8	3.3	9.1	6.5	8.7

Figure 6.2 shows the linear relationship between the concentrations (in weight%) of Al_2O_3 and SiO_2 in the knots.

Figure 6.3 showing the K_2O -content against the Al_2O_3 -content in a large number of analyzed knots yields a crescent as in the case of BaO, although in the present case one with tips down.

All the "pure" glasses in table 6.1 are free from ZrO_2 , although the knots do contain this component (figure 6.4).

Apart from some parts of the refractory in the forehearth, AZS is the only furnace material which contains ZrO_2 . Thus this is a very strong indication that the AZS is the source of the knots.

Figure 6.4 also shows that high ZrO_2 -concentrations (> 4 wt%) are most likely to occur when the Al_2O_3 -content is low (< 20 wt%).

Figure 6.2 The SiO_2 versus Al_2O_3 concentration (in weight%) of knots in TV-screen glass.

CHEMICAL COMPOSITION OF KNOTS IN PRODUCTS

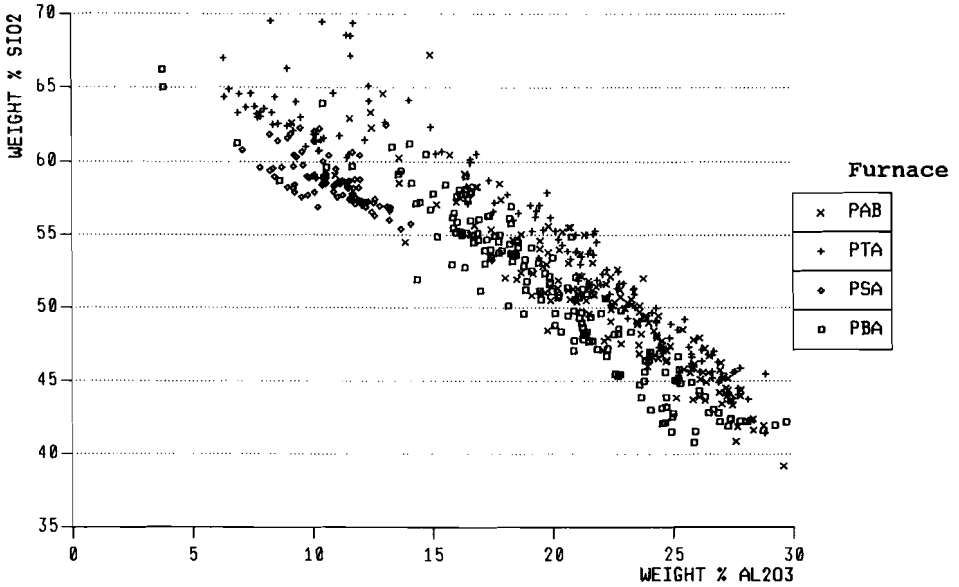


Figure 6.3 The K_2O versus Al_2O_3 concentration (in weight%) of knots in TV-screen glass.

CHEMICAL COMPOSITION OF KNOTS IN PRODUCTS

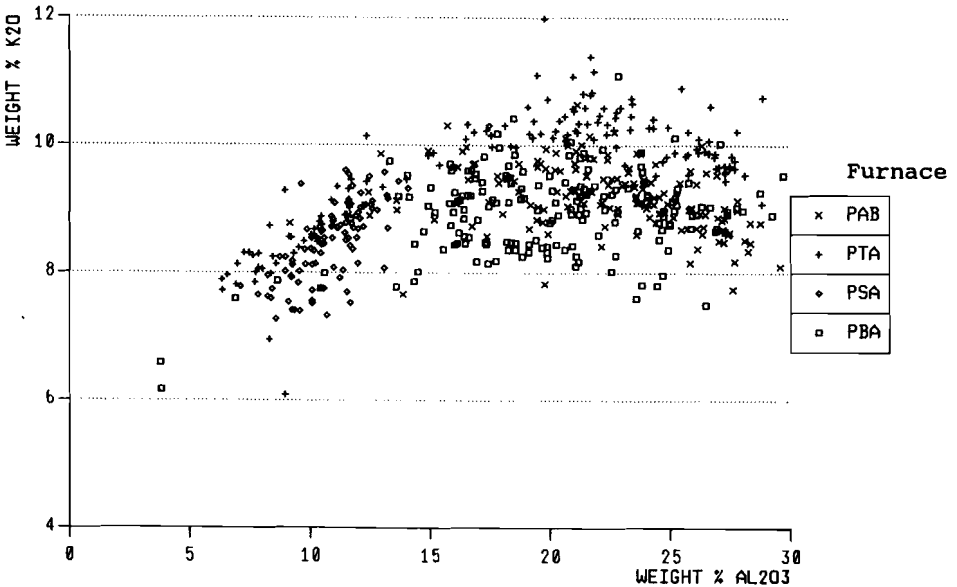
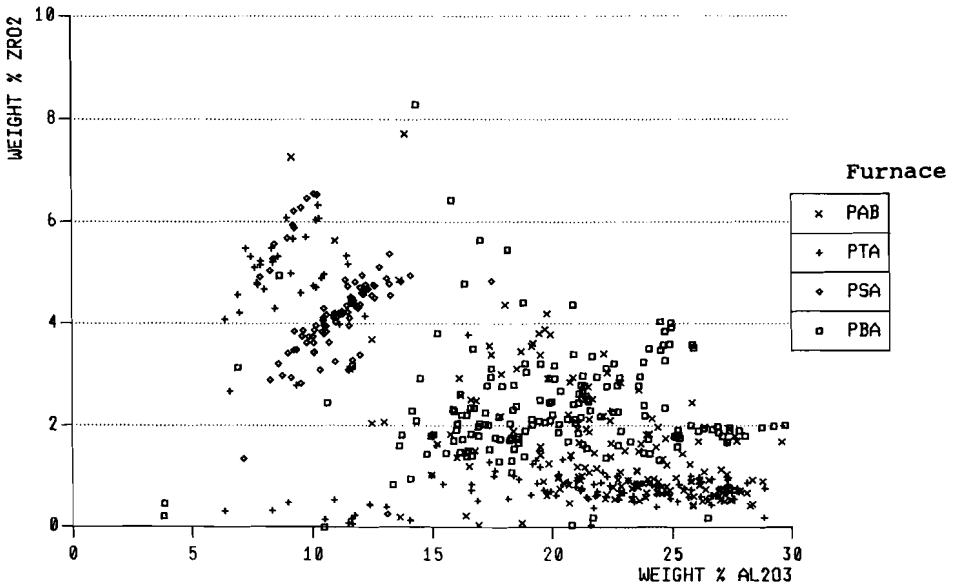


Figure 6.4 The ZrO_2 versus Al_2O_3 concentration (in weight%) of knots in TV-screen glass.

CHEMICAL COMPOSITION OF KNOTS IN PRODUCTS



The solubility of ZrO_2 in the glass increases when the Al_2O_3 -content decrease which is also reported by Manfredi and McNally (Lit. 1).

Often the knots contain inclusions, the most common sort of inclusion is recrystallized ZrO_2 .

6.3 Dissolution of knots

Tests have been carried out introducing synthetic knots in glass melts in order to investigate the knot dissolution process. The knots in the bulk of the glass show a different dissolution behaviour than the knots at the glass surface.

Dissolution of knots in the bulk of the glass

The diffusion profiles remain relatively stable on the time scale. The knot ascends in the molten glass, because its density is lower than that of the bulk glass. Besides, its viscosity increases strongly as the Al_2O_3 -content increases. The ascending velocity of the knot in the molten glass raises drag forces at the border of the knot. The lower the viscosity of the material the larger the transport of this material due to the drag forces. The combination of the ascending knot with an increasing viscosity at the border going to the inside of the knot, yield an effective diffusion rate that increases as the Al_2O_3 -content in the concentration profile drops. The result is that instead of a flattening of the concentration profiles on the time scale, a kind of balance arises with stability of the slope of the diffusion profiles on the time scale (figure 6.5). The diameter of the knot (diameter with constant high Al_2O_3 content) of course, decreases on the time scale.

Dissolution of knots at the glass surface

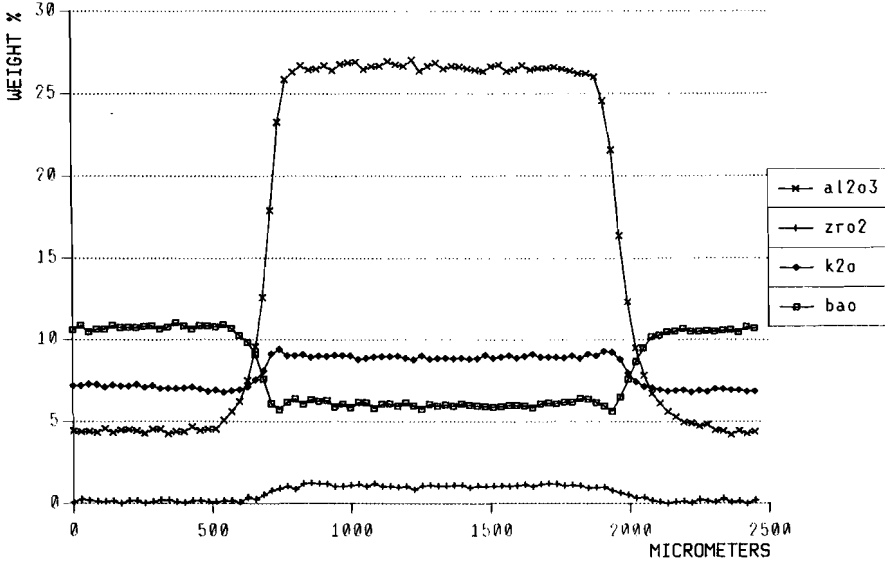
The lower density of the knots causes them to rise to the glass surface. Owing to the higher surface tension of the knot glass (0.350 N/m against 0.290 N/m at 1400°C) the bulk glass melt tends to cover the knot glass. This phenomenon is similar with the 'Marangoni effect', which occurs at the three phase contact point: glass melt, AZS and atmosphere (metalline). The described phenomenon accelerates the dissolution of the knots in a similar way as the Marangoni effect accelerates the metalline corrosion (Lit. 2).

The difference in dissolution behaviour is shown in figure 6.6 for the knots dissolving in the bulk of the glass and in figure 6.7 for those dissolving at the glass surface.

Figure 6.8 shows the results of the analysis of the concentration profiles of a knot dissolving at the surface.

Figure 6.5 Concentration profiles for different components in synthetic knots after different periods of time, at 1350 °C, present in the bulk of 354-glass (the synthetic knots have different original diameters).

SYNTHETIC KNOT DISSOLVING FOR 1 HOUR,
AT 1350 C IN THE BULK OF THE GLASS.



SYNTHETIC KNOT DISSOLVING FOR 8 HOURS,
AT 1350 C IN THE BULK OF THE GLASS.

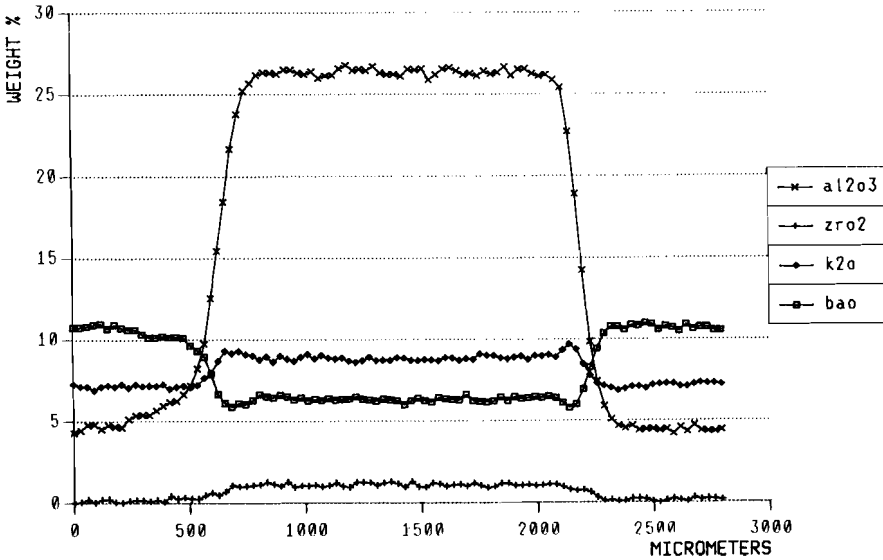
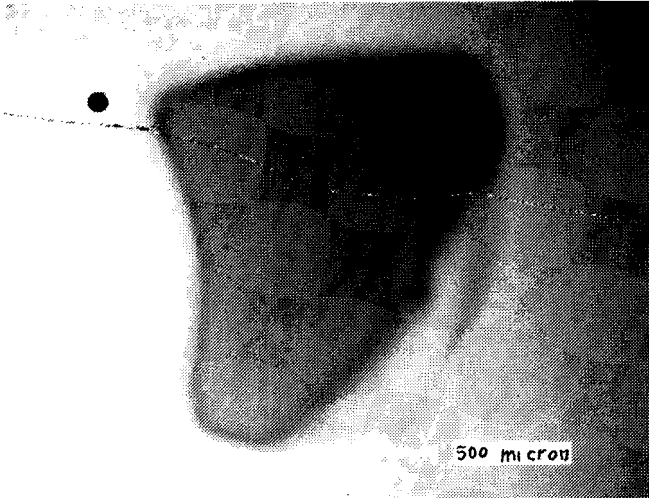


Figure 6.6 Photographs of synthetic knots dissolving for different time periods, at 1350 °C, in the bulk of the glass.

Dissolution of a knot in the bulk, of the glass for 2 hours at 1350 °C.



Dissolution of a knot in the bulk, of the glass for 4 hours at 1350 °C.

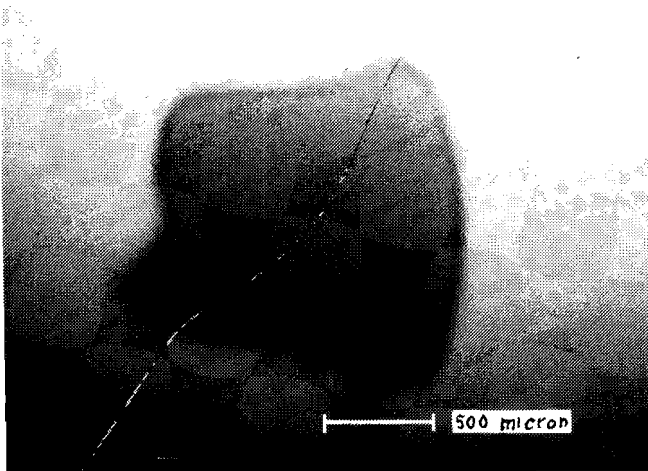
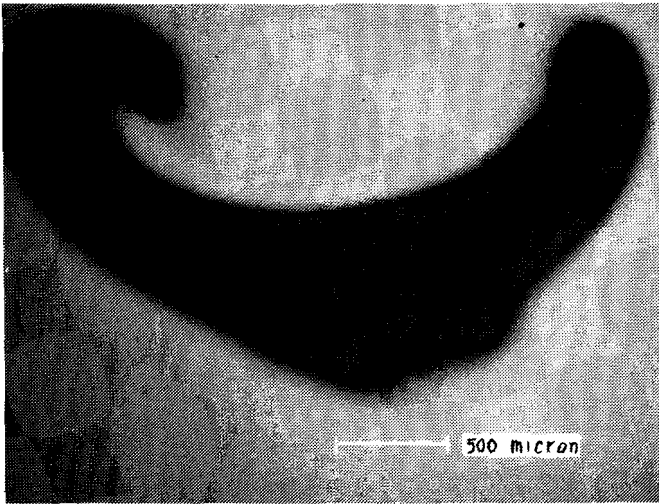
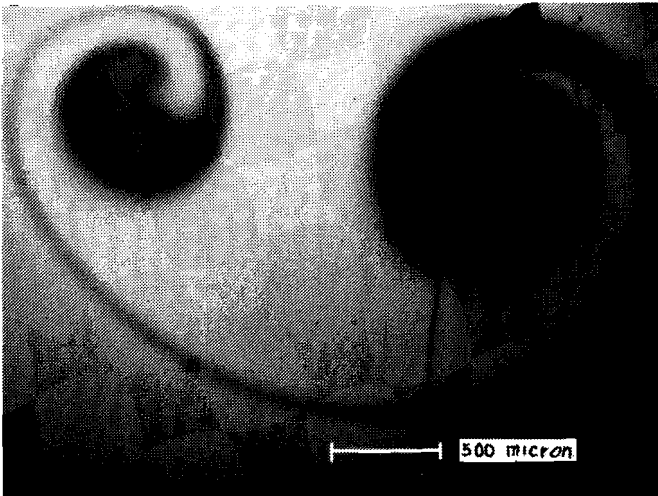


Figure 6.7 Photographs of synthetic knots dissolving for different time periods, at 1350 °C, at the glass surface (vertical cut).

Dissolution of a knot at the glass surface for one hour at 1350 °C.



Dissolution of a knot at the glass surface for two hour at 1350 °C.



Both in the bulk of the glass and at the surface the chemical composition of the knot remains stable until the slopes of the concentration profiles meet after a certain time period (figure 6.8). For example, in figure 6.8 the slopes of the concentration profiles at 1700 micrometer meet and the concentration does not remain stable, the slopes of the concentration profiles at around 1150 micrometer do not meet and therefore the chemical composition of the knot material between the two concentration profiles is still equal to the original chemical composition.

These results are in agreement with the investigations of Uemura and Tabuchi (Lit. 3).

Even tests at 1425 instead of 1350°C did not yield any change in chemical composition of the cores of the knots.

Figure 6.8

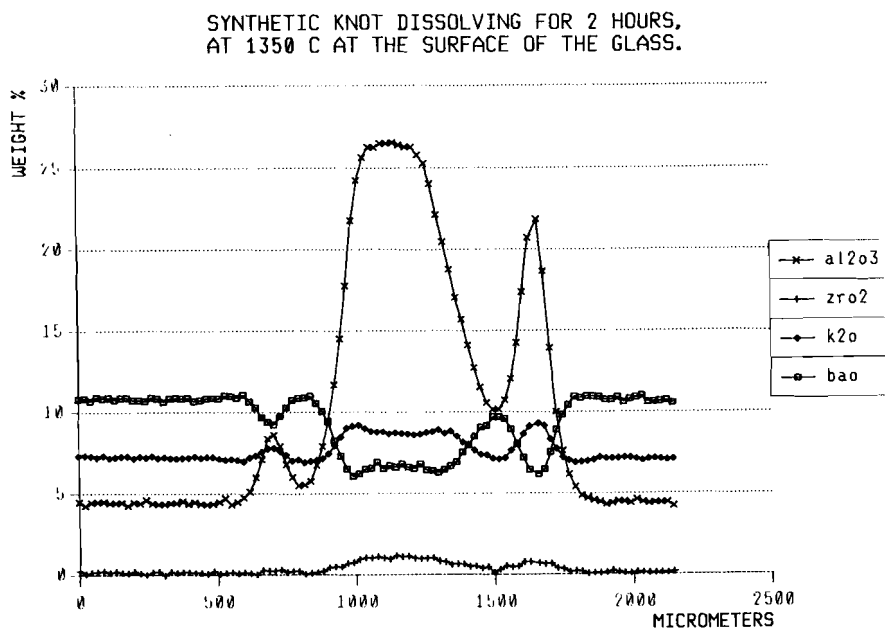


Table 6.2 shows the results of the SEM/EDX analyses of the chemical composition of the core of the knot under various conditions.

The chemical composition is not affected by either time or temperature. If the composition of a knot remains stable until the slopes of the concentration profiles meet, the knots in the products have the same chemical core composition compared to their original state (at least, as long as the slopes of the concentration profiles do not meet).

The preservation of the chemical composition of the knot is a very important condition for the identification method of the source of the knot later in this chapter.

Table 6.2 The chemical composition of the core of a synthetic knot after experiments investigating the knot dissolution process in molten glass.

tempe- rature	time (in hours)		SiO ₂ in weight%	Al ₂ O ₃ in weight%	K ₂ O in weight%	BaO in weight%
		glass	63.85	3.3	6.45	10.7
1350°C	1	knot	47.42	26.55	8.96	6.07
	2	knot	47.07	26.60	9.06	6.12
	4	knot	46.75	26.38	9.44	6.38
	6	knot	46.71	26.37	8.97	6.54
	8	knot	47.58	26.36	8.88	6.37
1425°C	1	knot	46.86	26.48	8.96	6.48
	2	knot	46.93	26.69	8.96	6.30

6.4 Concentration profiles of AZS-to-glass interface

Chapter 3 'Cation diffusion into fused cast AZS' shows the concentration profiles of Na_2O , K_2O , BaO and SrO at the AZS/glass melt interface after a test. The physical properties of the interface and the knots arising from it are strongly affected by the Al_2O_3 content. The interface, in this case, is defined as the layer stretching from the glass end at the point where the Al_2O_3 -content starts to increase until the AZS end where it reaches its maximum in the glassy phase.

Figure 6.9 shows the effect of convection at the various temperatures, with 'w' is the velocity at which a rod (diameter 21 mm) revolves in a crucible with an inner diameter of 70 mm. The forced convection has hardly any effect on the Al_2O_3 concentration profile in the defined interface.

Figure 6.10 shows the effect of the test time on the interface concentration profiles at the various temperatures. The schedule of glass renewal has been the same as described in 3.2 of chapter 3 in this study. After 100 hours, further exposure no longer has a large effect on the defined interface itself. The temperature, however, does affect the interface profiles. Higher temperatures result in more penetration of the profile into the AZS and gives slightly higher Al_2O_3 concentration peaks.

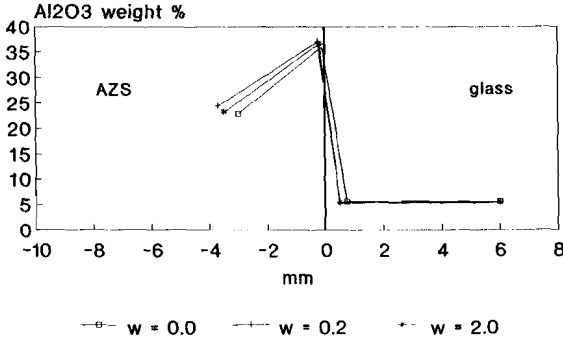
All the graphs are those of the concentration profiles on the inner crucible side wall (glass side).

Figure 6.11 shows the difference of the Al_2O_3 concentration profiles between the side wall and bottom location. The interface layer on the bottom is about half as thick as that on the side wall due to the lower density of the interface layer compared to the glass melt. At 1350°C , the interface layer on the side wall is about 1 mm thick and on the bottom about 0.5 mm. In both cases (side wall and bottom) the interface layer is thick enough for the formation of knots which have the same diameter. Annex 2, table 6 shows the concentration profiles in a table.

Figure 6.9 The effect of forced convection on the chemical composition of the interface glass melt/fused cast AZS 32/33, at various temperatures.

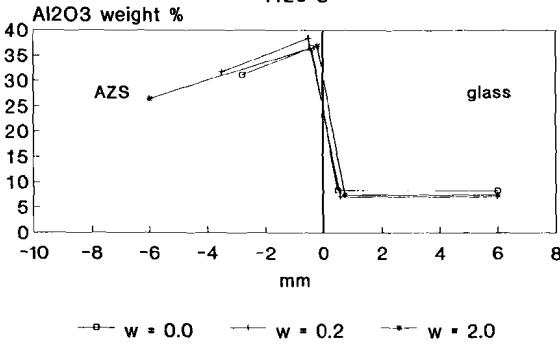
Concentration profiles of Al_2O_3 .

354 glass, 100 hrs. melting time.
1350 C



Concentration profiles of Al_2O_3 .

354 glass, 100 hrs. melting time.
1425 C



Concentration profiles of Al_2O_3 .

354 glass, 100 hrs. melting time.
1500 C

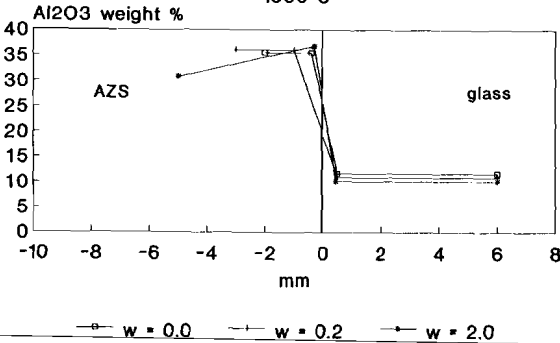
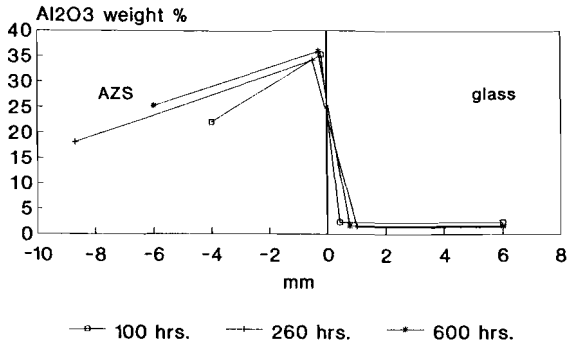
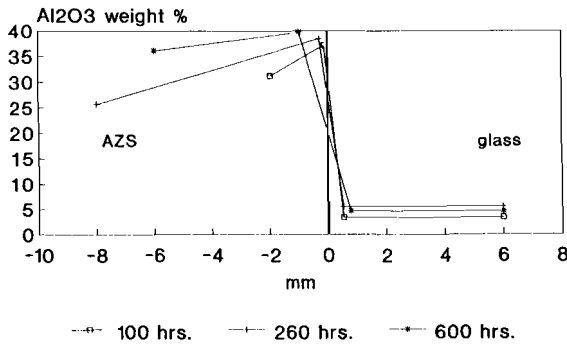


Figure 6.10 The effect of test duration on the chemical composition change of the interface glass melt/fused cast AZS 32/33, at various temperatures.

Concentration profiles of Al_2O_3 .
395 glass, 1350 C.



Concentration profiles of Al_2O_3 .
395 glass, 1425 C.



Concentration profiles of Al_2O_3 .
395 glass, 1500 C.

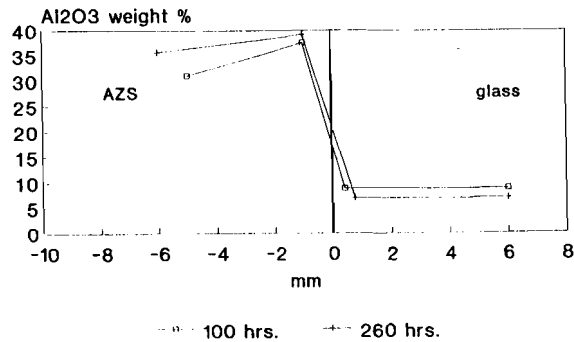
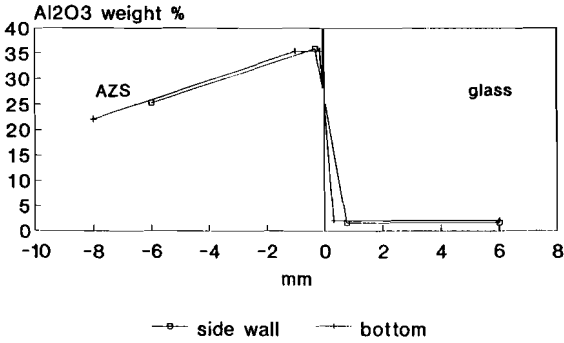


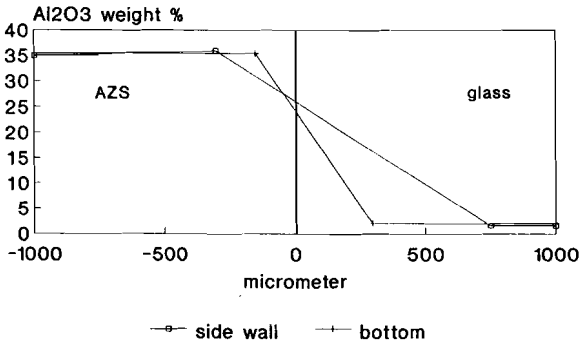
Figure 6.11 The difference, of the interface glass melt/fused cast AZS 32/33, between side wall and bottom.

concentration profiles of Al₂O₃.
395 glass, 1350 C.



600 hrs.

Concentration profiles of Al₂O₃.
395 glass, 1350 C.



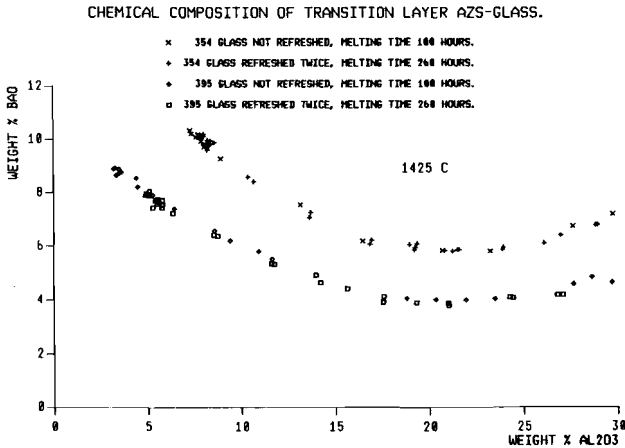
600 hrs.

6.5 Chemical composition of the interface glass melt/fused cast AZS.

The curves presenting the BaO concentrations versus Al_2O_3 concentrations (in weight%), of the knots in products, in figure 6.1 is crescent-shaped.

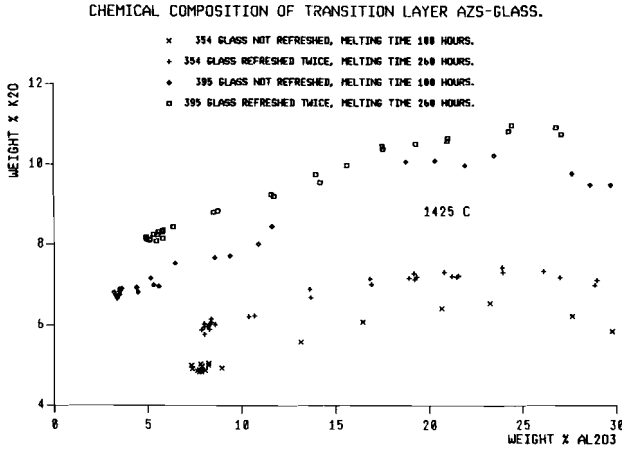
With the results of measurements which have been made, of the glass/AZS interface composition going from low Al_2O_3 (glass side) to high Al_2O_3 concentration (AZS side), of the crucible samples, plotted in the same way, the crescent shows up again (figure 6.12).

figure 6.12



The position of this crescent depends (figure 6.12) on the composition of the glass, but in the case of BaO, not on time. The crescent-shaped curves of the K_2O versus Al_2O_3 concentrations (in weight%) of the knots in the products (figure 6.3) can be derived from the chemical composition of the interface (figure 6.13) in a similar way. In this case, however, it is not only the glass composition that affects the position of the crescent, also the test duration and number of glass renewals.

Figure 6.13



The glass-to-crucible interface, of experiments with the glass (354 or 395 glass) twice renewed and a total melting time of 260 hours contains more K_2O with identical Al_2O_3 -concentrations, compared to the experiments with a total melting time of 100 hours without glass renewal.

Figure 6.14, too, shows the extent to which the BaO -to- Al_2O_3 ratio is stable for a specific glass type (395 glass, annex 1), at a specific temperature, on the time scale. These graphs also show that the crescent remains stable even with a total melting time of 600 hours and six renewals.

In chapter 3 in this study, it was shown that the BaO -content in the interface increases as the temperature rises. The same effect shows up with the BaO -content of the interface plotted against the Al_2O_3 -content. Figure 6.15 and 6.16 show the dependence of the interface composition on the temperature for 354 glass and 395 glass (Annex 1). The chemical composition of the interface agrees with that of the original composition of the knots and most often with the final composition of the central part of the larger

Figure 6.14 The concentration of BaO versus Al₂O₃ of the interface glass melt/fused cast AZS 32/33, at various temperatures and test durations.

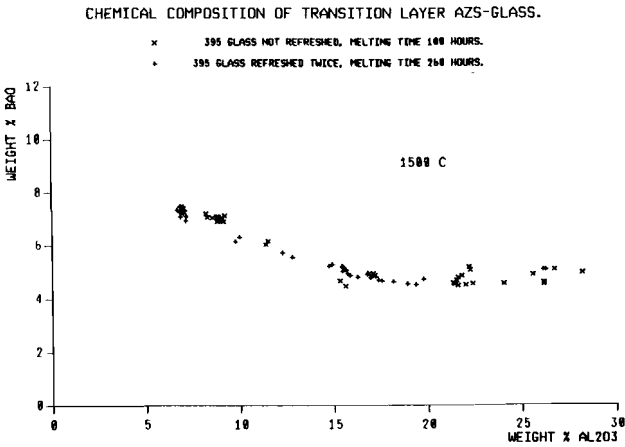
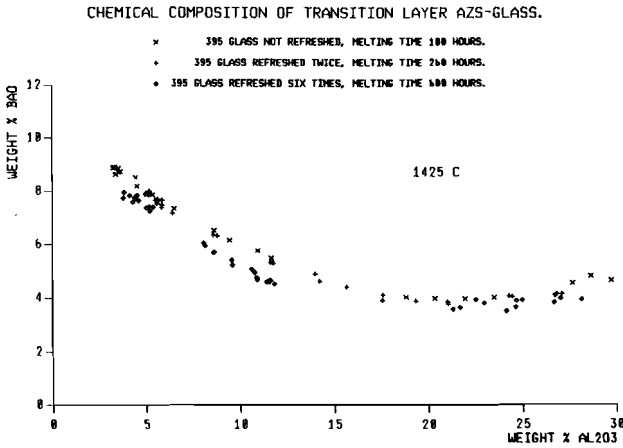
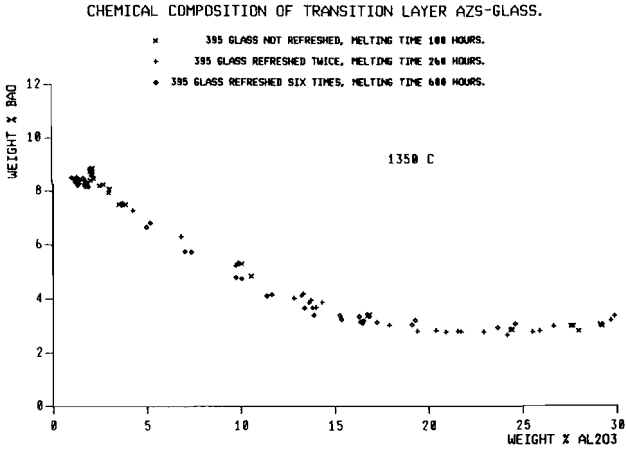
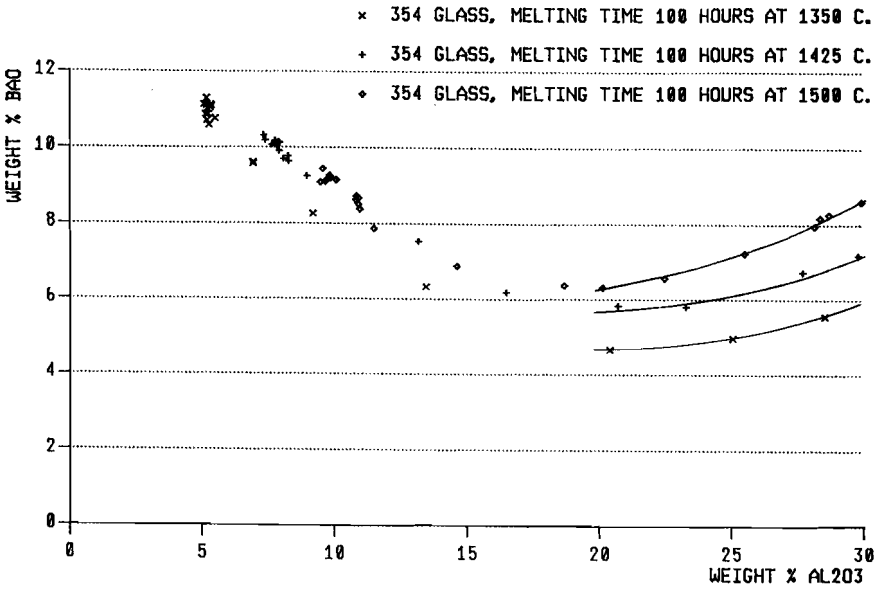


Figure 6.15 and 6.16 The dependence, of the concentration of BaO versus Al_2O_3 , of the interface glass melt/fused cast AZS on the temperature.

CHEMICAL COMPOSITION OF TRANSITION LAYER AZS-GLASS.

figure 6.15



CHEMICAL COMPOSITION OF TRANSITION LAYER AZS-GLASS.

figure 6.16

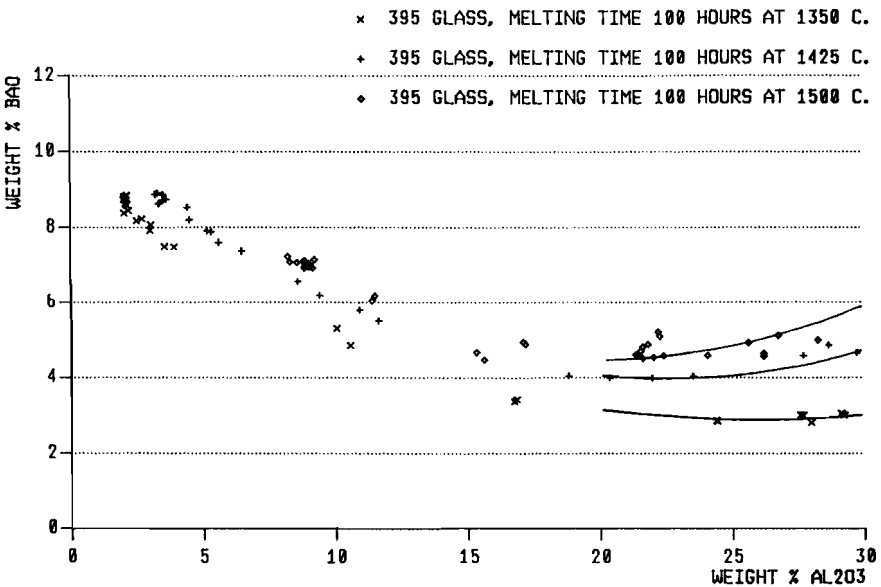


Figure 6.17

A bubble in the interface squeezes a part of the interface layer, which contains ZrO_2 crystals, into the bulk of the glass.



knots which are mainly responsible for the reject of the glass product. As described in previous chapters, cation diffusion in the AZS causes oxygen bubble formation in the interface. A bubble in this interface can force an interface particle into the bulk glass (figure 6.17) (Lit. 4 and 5). On account of its high surface tension (due to the high Al_2O_3 concentration compared to the bulk of the glass), this particle becomes spherical. This means the formation of such a bubble can be accompanied with the formation of a knot.

6.6 Examples of knots in industrial TV-screen glass production and their sources.

The combination between the stability in chemical composition of the knot core during dissolution, resulting in preservation of the original composition of the glass-to-AZS interface, and the temperature dependence of BaO versus Al_2O_3 in this interface, allows an estimate of the temperature at which the knot has been formed.

Figure 6.18 shows clear knots (without crystals) found in glass products from furnace PAB arising in the first year after the overhaul. A comparison between the position of the BaO versus Al_2O_3 concentration of the knots in figure 6.18 and the curves in figure 6.15 proves that most of the knots have arisen between 1425 and 1500°C, which points to palisade blocks in the melting end as the most likely source.

Figure 6.19 shows the knots arising during the 395 glass-glass run in PAC. A comparison of their location with the curves in figure 6.16 proves that the knots have arisen around 1350°C, which probably points to the colder bottom as the source.

Chapter 4 'Effect of glass composition and temperature on glass defect potential originating from refractory' shows that, at bottom temperatures (1300 - 1380 °C), oxygen bubble formation accelerates by the mechanism described for a glass with a high K_2O -content.

Figure 6.18 and 6.19 Examples of the Al_2O_3 against BaO concentration in TV-screens.

figure 6.18

CHEMICAL COMPOSITION OF CLEAR KNOTS IN PRODUCTS DURING START UP OF PAB FURNACE WITH 354 GLASS.

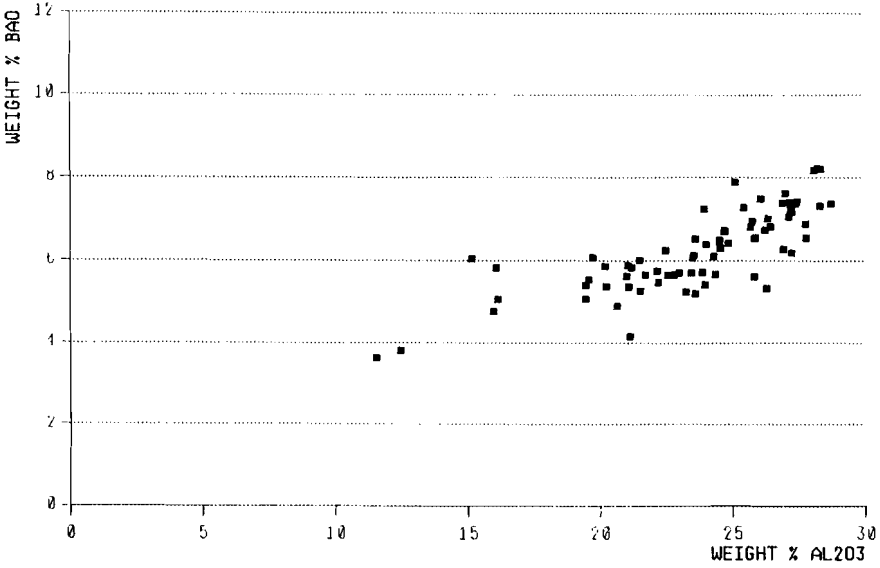
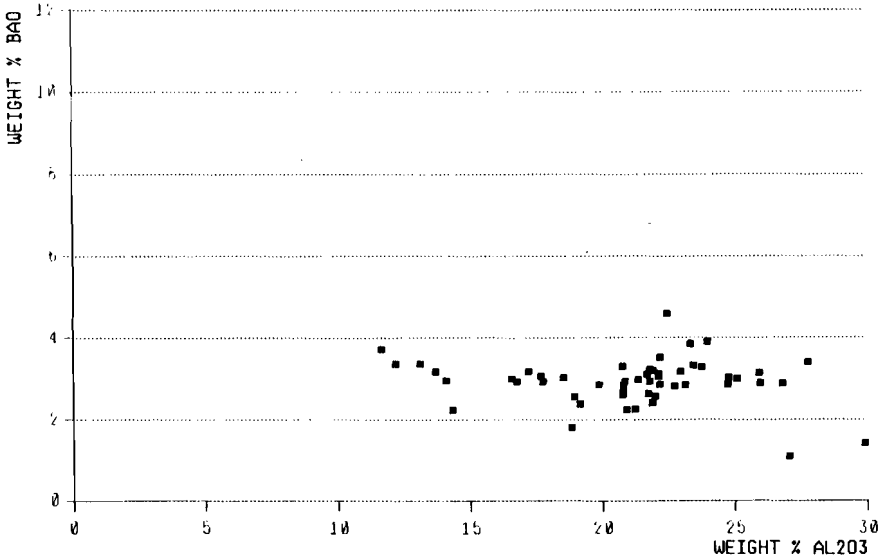


figure 6.19

CHEMICAL COMPOSITION OF KNOTS IN PRODUCTS DURING 395 GLASS RUN IN PAC FURNACE.



The K_2O content is far higher in 395 glass (9.1 weight%) than in 354 glass (6.5 weight%), this results in hardly any knots arising from the bottom by this mechanism for the case of 354 glass and far more knots are generated in the 395 glass which is in close agreement with the knot analysis. The absence of knots originating from higher temperature areas in figure 6.19 does not mean that no knots have been formed in high temperature areas. The knots in products are always a combination of formation rate and chance of survival in the glass melt. In the example of the 395 glass the lower formation rate at bottom temperatures is compensated by a high chance of survival, which points to a source close to the throat of the melting end.

In the beginning of the present chapter it has already been pointed out that the knots in glass from the PSA furnace (figure 6.1 to 6.4) are originating from a few specific incidents (calamities): namely glass level fluctuations. The presence of about 10 weight% Al_2O_3 and a high (4-5 weight%) ZrO_2 concentration, indicates that the origin of the knots comes from above glass level (metalline, silica superstructure). Maximum Al_2O_3 -contents in knots originating from the bottom of the PAC furnace are on average about 20 weight% and the knots originating from the palisade blocks of the PAB furnace have an average maximum Al_2O_3 concentration in the knots of about 25 weight%. These knots with their sources are frequently observed for TV screen glass producing furnaces.

If no temperature curves of a specific glass type or any similar type are available, the Al_2O_3 -content may provide a very rough indication of the potential source in the tank, for knots originating from below glass level in TV glass melts (remark: knots originating from refractories of the superstructure (above the glass level) are not the subject of this study).

Literature references chapter 6.

- [1] L.J Manfredo, R.N. McNally;
The Corrosion resistance of high-ZrO₂ fusion-cast
Al₂O₃-ZrO₂-SiO₂ glass refractories in soda-lime glass.
J. of Mat. Science **19** (1984) p. 1272-1276.
- [2] H. Jebesen-Marwedel;
Dynaktive Flüssigkeitspaare.
Glastech. Ber. **29** (1956) p. 233-238.
- [3] H. Uemura, H. Tabuchi;
Characterization of typical knots in window glass.
J. of non-Cryst. Solids **38 & 39** (1980) p. 791-796.
- [4] M. Dunkl;
Studies on the glassy and reaction phases given off by
fused-cast AZS blocks and their effects on glass quality.
Glastech. Ber. **62** (1989) p. 389-395.
- [5] D. Walrod;
A Study of the driving force behind AZS glassy phase
exudation.
Cer. Eng. Science Proc. **10** (1989) p. 338-347.

Annex 1

Composition and properties of investigated glasses.

Chemical composition	Glass 354	Glass 395	Glass lithium
SiO ₂	63,85 weight %	62,06 weight %	65,86
Al ₂ O ₃	3,33	0,80	4,96
Li ₂ O	-	-	3,84
Na ₂ O	9,43	6,84	3,30
K ₂ O	6,46	9,10	3,72
MgO	1,05	0,28	-
CaO	1,48	0,37	0,96
SrO	3,01	9,59	8,25
BaO	10,75	7,70	8,34
ZrO ₂	-	2,10	-

Properties

Density in kg/m ³ at room temperature	2679 kg/m ³	2750 kg/m ³	2672
Viscosity:			
strain point (10 ^{13.5} Pa.S)	474 °C	497 °C	451
annealing point (10 ¹² Pa.S)	507	528	481
softening point (10 ^{6.6} Pa.S)	685	706	649
working point (10 ³ Pa.S)	1015	1017	958
melting point (10 Pa.S)	1465	1427	1400

Constants Fulcher equation: $10 \log \mu = A + (B/(T - C))$

μ = viscosity in dPaS

T = temperature in °C

A	-1,756	-2,064	-1,638
B	4879,317	5055,011	4522,540
C	165,184	183,028	155,642

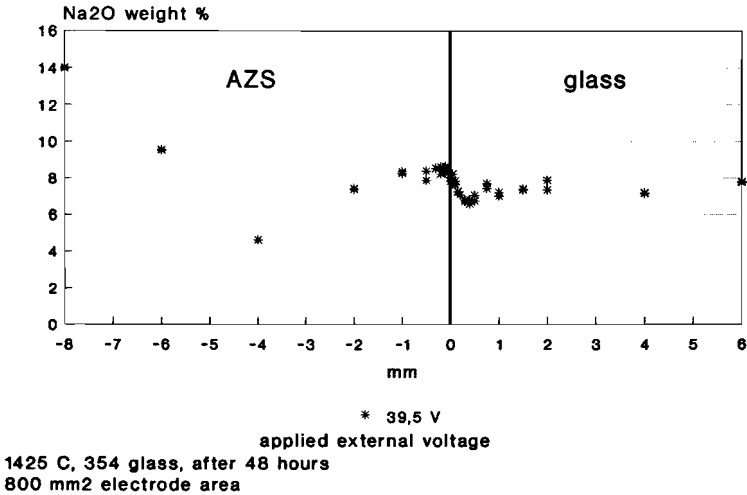
Annex 2.

In this annex the large amount of measurements concerning the concentration profiles is presented in figures and tables. As explained in chapter 3, every concentration profile of an oxide consists of about 50 spot measurements. When the spot measurements are individually printed, like in figure 2.1 it can become very confusing when several concentration profiles are shown in one picture.

Experiment 127

Na₂O diffusion

figure A 2.1



Also the data in a table become very comprehensive. To concentrate the essential information and increase the surveyability, the measurement spots of figure A 2.1 are transformed to a figure with straight lines, like figure A 2.2. Such a figure can also be brought more easily into a table presentation.

Explanation of tables.

experiment	: number of the test.
glass	: used glass (cullet).
time	: test duration.
voltage	: applied external potential.
surface	: the surface of the electrode in the glass melt.
cation	: oxide of cation under investigation.
start pt.	: the measurement starts in the glass at 6000 micrometer from the first zirconia nodules, the start point (start pt.) is the distance from the first zirconia nodules where the concentration changes.
C bulk	: concentration of the oxide between 6000 micrometer and start point in weight%.
C top/bot	: concentration of oxide at maximum or minimum peaks in weight%.
distance	: distance in micrometer between C bulk and C top/bot or between C top/bot and the next C top/bot.
cum. dist.	: cumulative distance which gives the position in the sample of the measured concentration with regard to the first zirconia nodules.

An example explains the tables: Figure A 2.2 gives the concentration profile of the Na_2O of experiment 127. In table 1 this is the fifth row.

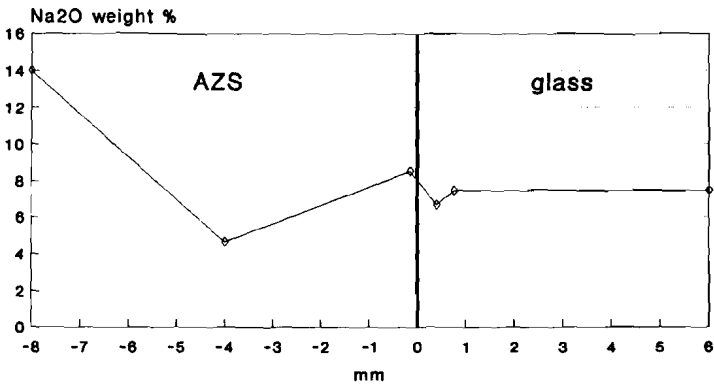
Experiment 127; the glass used was 354 glass, the duration of the experiment 48 hours, the applied external voltage 39.5 V with a glass electrode with a surface of 800 mm². The concentration profile of Na_2O is shown in figure A 2.2. The measurement starts at 6000 micrometer from the first ZrO_2 nodules of the interface glass melt/AZS in the glass, until 750 micrometer (start pt. micro) from the ZrO_2 nodules a stable concentration of 7.48 weight% (C bulk wght%). A drop in the concentration down to 6.69 weight% (C top/bot wght%), the slope in the concentration decrease is 350 micrometer (distance micro) long. The concentration 6.69 weight% is reached at 400 micrometer (cum. dist. micro) from the

first ZrO_2 nodules. An increase in the concentration to 8.50 weight% (C top/bot wght%) across 550 micrometer (distance micro), the 8.50 weight% is reached at -150 micrometer (cum. dist. micro), 150 micrometer in the AZS material. Then a concentration drop again to 4.62 weight% (C top/bot wght%) across a distance of 3850 micrometer (distance micro), the 4.62 weight% Na_2O is reached at -4000 micrometer (cum. dist. micro), 4000 micrometer in the AZS material. The final increase in concentration to 13.99 weight% (C top/bot wght%) has been across 4000 micrometer (distance micro) and the measurement has been done at 8000 micrometer (cum. dist. micro) in the AZS material. All measurements in the fused cast AZS have been done in the glassy phase.

Experiment 127

Na₂O diffusion

figure A 2.2



—○— 39.5 V

applied external voltage

1425 C, 354 glass, after 48 hours
800 mm² electrode area

Experiment	glass	time hrs.	voltage V	surface mm ²	cation	start pt. micro	C bulk wght%	C top/bot wght%	distance micro	cum.dist. micro	C top/bot wght%	distance micro	cum.dist. micro	C top/bot wght%	distance micro	cum.dist. micro	C top/bot wght%	distance micro	cum.dist. micro
162	354	48,0	0,0	0	Na2O	1000	6,81	5,74	700	300	7,57	600	-300	2,49	5700	-6000	2,75	2000	-8000
168	354	48,0	1,0	800	Na2O	2000	6,47	5,50	1850	150	7,41	300	-150	3,14	5850	-6000			
143	354	49,5	2,5	800	Na2O	1500	6,62	5,67	1200	300	8,20	450	-150	5,01	3850	-4000	7,50	2000	-6000
140	354	48,0	5,0	800	Na2O	1000	6,29	5,51	700	300	7,76	800	-500	4,50	4500	-5000	9,24	3000	-8000
127	354	48,0	39,5	800	Na2O	750	7,48	6,69	350	400	8,50	550	-150	4,62	3850	-4000	13,99	4000	-8000
162	354	48,0	0,0	0	Na2O	1000	6,81	5,74	700	300	7,57	600	-300	2,49	5700	-6000	2,75	2000	-8000
144	354	48,5	2,5	20	Na2O	4000	7,63	6,55	3950	50	8,25	450	-400	3,57	5600	-6000			
173	354	48,0	39,5	20	Na2O	750	6,29	5,40	350	400	7,93	550	-150	4,38	3850	-4000	6,73	2000	-6000
162	354	48,0	0,0	0	K2O	750	5,71	7,23	550	200	6,09	700	-500	6,74	1500	-2000	1,25	6000	-8000
168	354	48,0	1,0	800	K2O	750	5,14	7,33	700	50	5,95	150	-100	7,00	1200	-1300	3,15	4700	-6000
143	354	49,5	2,5	800	K2O	500	4,96	6,92	300	200	4,92	250	-50	6,40	1450	-1500	2,61	4500	-6000
140	354	48,0	5,0	800	K2O	500	4,85	6,85	350	150	5,06	300	-150	6,16	1850	-2000	2,32	6000	-8000
127	354	48,0	39,5	800	K2O	750	4,78	6,93	600	150	5,43	300	-150	5,99	350	-500	2,06	7500	-8000
162	354	48,0	0,0	0	K2O	750	5,17	7,23	550	200	6,09	700	-500	6,74	1500	-2000	1,25	6000	-8000
144	354	48,5	2,5	20	K2O	200	5,13	6,83	400	-200	6,23	300	-500	7,00	800	-1300	4,04	4700	-6000
173	354	48,0	39,5	20	K2O	500	5,10	7,30	300	200	5,50	350	-150	6,72	850	-1000	2,13	5000	-6000
162	354	48,0	0,0	0	BaO	1500	11,13	4,28	1300	200	5,45	350	-150	0,05	2050	-2200	0,05	5800	-8000
168	354	48,0	1,0	800	BaO	1500	10,49	3,92	1450	50	5,44	150	-100	0,18	3900	-4000	0,18	2000	-6000
143	354	49,5	2,5	800	BaO	1000	10,13	4,67	800	200	8,01	250	-50	0,07	2150	-2200	0,07	3800	-6000
140	354	48,0	5,0	800	BaO	1500	10,00	4,34	1300	200	7,22	350	-150	0,00	2350	-2500	0,00	5500	-8000
127	354	48,0	39,5	800	BaO	1000	10,48	4,18	800	200	6,10	350	-150	0,33	5850	-6000	0,64	2000	-8000
162	354	48,0	0,0	0	BaO	1500	11,13	4,28	1300	200	5,45	350	-150	0,05	2050	-2200	0,05	5800	-8000
144	354	48,5	2,5	20	BaO	300	9,61		300	0	4,74	300	-300	0,10	2700	-3000	0,10	3000	-6000
173	354	48,0	39,5	20	BaO	1000	10,48	4,05	800	200	6,31	300	-100	0,09	1900	-2000	0,09	4000	-6000
162	354	48	0	0	Al2O3	1000	4,24	35,15	1500	-500	22,54	5500	-6000	23,24	2000	-8000			
168	354	48	1	800	Al2O3	500	6,00	34,68	700	-200	22,07	5800	-6000						
143	354	49,5	2,5	800	Al2O3	750	6,37	35,47	850	-100	25,95	3900	-4000	29,66	2000	-6000			
140	354	48	5	800	Al2O3	750	6,54	36,12	1050	-300	25,00	4700	-5000	32,43	3000	-8000			
127	354	48	39,5	800	Al2O3	750	6,69	33,02	900	-150	22,87	3850	-4000	36,48	4000	-8000			
162	354	48	0	0	Al2O3	1000	4,24	35,15	1500	-500	22,54	5500	-6000	23,24	2000	-8000			
144	354	48,5	2,5	20	Al2O3	200	5,65	33,81	700	-500	23,14	5500	-6000						
173	354	48	39,5	20	Al2O3	500	5,73	35,78	600	-100	25,51	3900	-4000	29,76	2000	-6000			

Annex 2 Table 1

Experiment	time	temp.	glass	parameter	Na2O start pt.	Na2O conc. bulk	Na2O conc. top/bot	Na2O dist. micro	Na2O cum. dist.	Na2O conc. top/bot	Na2O dist. micro	Na2O cum. dist.	Na2O conc. top/bot	Na2O dist. micro	Na2O cum. dist.	Na2O conc. top/bot	Na2O dist. micro	Na2O cum. dist.
16	100	1350	354		750	8,00	6,65	600	150	8,65	150	0				4,04	3000	-3000
21	100	1425	354		750	7,00	6,60	400	350	8,00	550	-200				7,17	2600	-2800
26	100	1500	354		750	5,99	5,71	250	500	7,02	625	-125				6,72	1875	-2000
43	100	1350	354	alter temp	750	7,90	6,62	600	150	8,60	300	-150				2,52	4850	-5000
28	100	1425	354	alter temp	1000	7,00	6,71	700	300	8,41	1300	-1000						
32	100	1500	354	alter temp	400	5,94	5,94	0	400	8,06	3400	-3000				7,76	1000	-4000
50	100	1350	354	w=0.2	750	7,87	6,49	550	200	8,89	500	-300				4,48	3400	-3700
25	100	1425	354	w=0.2	1000	7,00	6,34	700	300	8,42	350	-50				7,29	3450	-3500
37	100	1500	354	w=0.2	0	6,00	6,00	0	0	8,25	3000	-3000						
66	100	1350	354	w=2.0	400	7,68	6,74	200	200	8,65	400	-200				4,14	3300	-3500
62	100	1425	354	w=2.0	400	6,59	6,02	200	200	8,30	1000	-800				4,37	5200	-6000
67	100	1500	354	w=2.0	750	5,96	5,41	250	500	7,43	1000	-500	7,43	3500	-4000	6,68	1000	-5000
142	260	1350	354*	2xrenewed	500	7,94	7,04	200	300	9,30	800	-500				1,88	7500	-8000
90	260	1425	354	2xrenewed	500	6,99	5,44	200	300	7,90	600	-300	7,90	1700	-2000	6,30	5000	-7000
106	260	1425	354	2xrenewed	750	6,88	6,09	650	100	8,14	2100	-2000				6,16	3000	-5000
101	260	1425	354	2xrenewed	500	7,21	6,40	350	150	8,03	250	-100	8,03	1900	-2000	7,03	3000	-5000
103	260	1425	354	2xrenewed	200	7,00	6,55	100	100	8,08	400	-300	8,08	1700	-2000	5,25	5000	-7000
133	600	1425	354*	6xrenewed	750	7,20	6,86	550	200	8,97	4200	-4000				8,46	1000	-5000
134	600	1425	354*	6xrenewed	0	6,81	6,81	0	0	8,38	1000	-1000	8,38	4000	-5000			
81	100	1350	395		300	6,47	5,25	150	150	6,72	250	-100				1,83	3900	-4000
79	100	1425	395		400	5,60	5,05	200	200	6,78	1200	-1000				5,28	1000	-2000
80	100	1500	395		500	4,96	4,57	350	150	5,94	650	-500				5,07	4500	-5000
150	260	1350	395	2xrenewed	1000	6,70	5,39	1000	0	7,06	500	-500				1,30	8200	-8700
92	260	1425	395	2xrenewed	500	5,49	4,95	350	150	6,15	300	-150	6,15	1850	-2000	3,25	6000	-8000
153	260	1500	395	2xrenewed	750	4,61	4,44	350	400	6,63	4400	-4000				6,04	2000	-6000
161 repeat	600	1350	395	6xrenewed	500	6,76	5,85	350	150	7,16	1150	-1000				4,18	5000	-6000
161	600	1350	395	6xrenewed	750	5,53	4,56	600	150	5,17	450	-300	5,17	1700	-2000	2,72	4000	-6000
186	600	1350	395	6xrenewed	400	5,20	4,47	250	150	4,72	150	0	4,72	2000	-2000	3,63	4000	-6000
148 repeat	600	1425	395	6xrenewed	1000	4,99	4,67	1000	0	6,38	2000	-2000				5,74	4000	-6000
148	600	1425	395	6xrenewed	750	5,83	4,58	900	-150	6,11	1850	-2000	6,11	2000	-4000	5,58	2000	-6000
187	260	1350	Lithium	2xrenewed	750	2,39	2,39	0	750	4,24	4750	-4000				2,93	4000	-8000
180	260	1425	Lithium	2xrenewed	2000	2,11	2,11	0	2000	3,84	10000	-8000						
200	260	1500	Lithium	2xrenewed	2000	3,39	2,93	500	1500	4,48	9500	-8000						

Experiment	time	temp.	glass	parameter	K2O start pt.	K2O conc. bulk	K2O conc. top/bot	K2O top/bot dist.	K2O micro	K2O cum.dist.	K2O conc. top/bot	K2O top/bot dist.	K2O micro	K2O cum.dist.	K2O conc. top/bot	K2O top/bot dist.	K2O micro	K2O cum.dist.
16	100	1350	354		500	5,33	7,50	375	125	6,00	300	-175	8,11	1825	-2000	6,93	1000	-3000
21	100	1425	354		500	4,95	6,65	575	-75	4,90	300	-375	7,11	2425	-2800			
26	100	1500	354		750	4,77	5,45	750	0	3,70	500	-500	4,59	1500	-2000			
43	100	1350	354	alter temp	500	5,20	8,79	350	150	5,92	250	-100	7,64	1900	-2000	4,60	3000	-5000
28	100	1425	354	alter temp	400	4,92	6,54	300	100	4,32	300	-200	5,93	800	-1000			
32	100	1500	354	alter temp	600	4,77	5,76	500	100	3,76	600	-500	6,50	3500	-4000			
50	100	1350	354	w=0.2	500	5,14	7,51	350	150	5,28	300	-150	7,20	1850	-2000	6,26	1700	-3700
25	100	1425	354	w=0.2	500	4,85	6,63	350	150	4,19	300	-150	7,38	3350	-3500			
37	100	1500	354	w=0.2	500	4,67	5,55	450	50	4,03	1050	-1000	5,45	2000	-3000			
66	100	1350	354	w=2.0	400	4,92	7,23	350	50	5,11	250	-200	6,97	1800	-2000	5,90	1500	-3500
62	100	1425	354	w=2.0	750	4,75	6,66	600	150	5,35	350	-200	6,50	2800	-3000	4,90	3000	-6000
67	100	1500	354	w=2.0	500	4,56	5,76	350	150	3,65	400	-250	5,10	4250	-4500	4,90	500	-5000
142	260	1350	354*	2xrenewed	500	5,70	7,83	400	100	5,94	300	-200	8,90	2300	-2500	5,47	5500	-8000
90	260	1425	354	2xrenewed	500	5,97	7,37	550	-50	5,90	650	-700	8,46	4300	-5000	8,33	2000	-7000
106	260	1425	354	2xrenewed	500	5,86	7,13	600	-100	5,31	400	-500	8,01	3500	-4000	8,01	1000	-5000
101	260	1425	354	2xrenewed	500	6,00	7,59	450	50	5,33	350	-300	8,15	4700	-5000			
103	260	1425	354	2xrenewed	500	5,87	7,00	550	-50	5,17	450	-500	8,13	3500	-4000	8,13	3000	-7000
133	600	1425	354*	6xrenewed	400	6,28	7,31	500	-100	5,86	900	-1000	7,85	4000	-5000			
134	600	1425	354*	6xrenewed	2000	6,20	7,41	2300	-300	5,89	700	-1000	7,26	4000	-5000			
81	100	1350	395		300	7,29	11,32	200	100	9,59	300	-200	11,05	800	-1000	6,95	3000	-4000
79	100	1425	395		400	6,90	10,10	250	150	7,34	300	-150	10,67	1850	-2000			
80	100	1500	395		400	6,29	7,96	500	-100	6,32	900	-1000	8,70	3000	-4000	8,48	1000	-5000
150	260	1350	395	2xrenewed	750	7,80	11,28	850	-100	10,86	400	-500	11,50	2000	-2500	6,92	6200	-8700
92	260	1425	395	2xrenewed	500	8,22	10,90	550	-50	8,09	250	-300	11,94	3700	-4000	10,73	4000	-8000
153	260	1500	395	2xrenewed	750	7,18	8,82	1050	-300	6,52	700	-1000	10,50	5000	-6000			
161 repeat	600	1350	395	6xrenewed	750	8,47	11,83	1250	-500			-500	11,83	3500	-4000	10,73	2000	-6000
161	600	1350	395	6xrenewed	500	8,62	18,54	800	-300	11,07	5700	-6000						
186	600	1350	395	6xrenewed	400	8,69	20,03	700	-300	12,01	5700	-6000						
148 repeat	600	1425	395	6xrenewed	750	8,30	10,98	1250	-500	9,47	500	-1000	12,03	5000	-6000			
148	600	1425	395	6xrenewed	750	8,11	10,73	950	-200	8,62	300	-500	12,12	5500	-6000			
187	260	1350	Lithium	2xrenewed	1000	3,17	3,81	1200	-200	2,81	800	-1000	5,17	5000	-6000	4,95	2000	-8000
180	260	1425	Lithium	2xrenewed	4000	3,17	3,66	3700	300	2,50	1600	-1300	4,87	6700	-8000			
200	260	1500	Lithium	2xrenewed	200	3,10	3,10	0	200	2,13	4200	-4000	3,13	4000	-8000			

Experiment	time	temp.	glass	parameter	BaO start pt.	BaO conc. bulk	BaO conc. top/bot	BaO dist. micro	BaO cum. dist.	BaO conc. top/bot	BaO dist. micro	BaO cum. dist.	BaO conc. top/bot	BaO dist. micro	BaO cum. dist.	BaO conc. top/bot	BaO dist. micro	BaO cum. dist.
16	100	1350	354		750	10,83	4,88	600	150	6,90	250	-100	0,45	1900	-2000	0	1900	-2000
21	100	1425	354		750	9,82	6,10	850	-100	7,94	200	-300	0,71	2500	-2800	0	2500	-2800
26	100	1500	354		750	9,00	6,51	750	0	11,38	1000	-1000	7,81	500	-1500			
43	100	1350	354	alter temp	750	10,74	5,00	600	150	6,60	300	-150	0,15	2850	-3000	0	2000	-2150
28	100	1425	354	alter temp	625	10,05	5,82	500	125	9,25	300	-175	4,84	825	-1000			
32	100	1500	354	alter temp	750	9,07	5,87	600	150	9,97	650	-500	0,74	3500	-4000	0	3500	-4000
50	100	1350	354	w=0.2	750	10,97	4,66	600	150	7,97	300	-150	0,30	3550	-3700	0	2350	-2500
25	100	1425	354	w=0.2	650	10,21	5,55	500	150	10,25	300	-150	0,55	3350	-3500	0	3350	-3500
37	100	1500	354	w=0.2	600	9,01	6,30	450	150	9,53	1150	-1000	2,99	2000	-3000	0	3000	-4000
66	100	1350	354	w=2.0	500	11,13	4,89	450	50	8,19	250	-200	0,35	3300	-3500	0	2000	-2200
62	100	1425	354	w=2.0	750	10,18	5,29	550	200	9,46	400	-200	0,25	5800	-6000	0	3000	-3200
67	100	1500	354	w=2.0	500	9,19	6,31	350	150	10,67	450	-300	0,28	4700	-5000	0	4000	-4300
142	260	1350	354*	2xrenewed														
90	260	1425	354	2xrenewed	500	9,90	5,84	450	50	8,21	550	-500	0,07	6500	-7000	0	4000	-4500
106	260	1425	354	2xrenewed	750	10,11	5,25	850	-100	8,35	400	-500	0,11	4500	-5000	0	3000	-3500
101	260	1425	354	2xrenewed	750	10,27	5,51	650	100	9,08	400	-300	0,65	4700	-5000	0	4700	-5000
103	260	1425	354	2xrenewed	750	9,99	6,25	700	50	9,61	550	-500	0,25	6500	-7000	0	4500	-5000
133	600	1425	354*	6xrenewed														
134	600	1425	354*	6xrenewed														
81	100	1350	395		750	8,65	2,85	650	100	3,81	300	-200	0,20	3800	-4000	0	1200	-1400
79	100	1425	395		500	8,51	4,01	350	150	6,23	300	-150	0,76	1850	-2000	0	1500	-1650
80	100	1500	395		400	7,03	4,55	500	-100	5,75	400	-500	0,19	5500	-6000	0	3500	-4000
150	260	1350	395	2xrenewed	1000	8,34	2,77	1100	-100	3,30	200	-300	0,07	3700	-4000	0	2000	-2300
92	260	1425	395	2xrenewed	500	7,66	3,82	500	0	6,25	300	-300	0,17	5700	-6000	0	4000	-4300
153	260	1500	395	2xrenewed	1000	7,34	4,60	1150	-150	6,86	850	-1000	0,58	5000	-6000	0	5000	-6000
161 repeat	600	1350	395	6xrenewed	750	8,19	2,88	850	-100	3,51	100	-200	0,27	3800	-4000	0	2000	-2200
161	600	1350	395	6xrenewed	750	8,30	0,42	1050	-300	1,18	700	-1000	0,04	5000	-6000	0	1500	-2500
186	600	1350	395	6xrenewed	500	7,77	3,22	350	-50	3,90	100	-150	0,08	5850	-6000	0	2000	-2150
148 repeat	600	1425	395	6xrenewed	750	7,64	3,60	1050	-300	5,05	700	-1000	0,54	5000	-6000	0	4500	-5500
148	600	1425	395	6xrenewed	750	7,37	3,06	900	-150	5,44	350	-500	0,00	5500	-6000	0	4000	-4500
187	260	1350	Lithium	2xrenewed	1500	7,86	6,74	1700	-200	8,04	800	-1000	0,05	7000	-8000	0	3500	-4500
180	260	1425	Lithium	2xrenewed	4000	8,02	6,12	3500	500	7,94	1000	-500	0,44	7500	-8000	0	6500	-7000
200	260	1500	Lithium	2xrenewed	4000	6,57	6,11	3500	500	7,43	1500	-1000	2,85	7000	-8000	0	11800	-12800

Annex 2 Table 4

Experiment	time	temp.	glass	parameter	SrO start pt.	SrO conc. bulk	SrO conc. top/bot	SrO dist. micro	SrO cum.dist.	SrO conc. top/bot	SrO dist. micro	SrO cum.dist.	SrO conc. top/bot	SrO dist. micro	SrO cum.dist.	SrO conc. top/bot*	SrO dist. micro*	SrO cum.dist.
16	100	1350	354		500	3,73	1,22	400	100	1,76	200	-100	0,18	1900	-2000	0	1900	-2000
21	100	1425	354		500	3,27	1,53	350	150	1,76	150	0	0,15	2800	-2800	0	3000	-3000
26	100	1500	354		1000	3,45	1,85	1000	0	2,99	1000	-1000	1,85	500	-1500			
43	100	1350	354	alter temp	750	3,57	1,20	650	100	1,40	200	-100	0,00	2900	-3000	0	1900	-2000
28	100	1425	354	alter temp	500	3,46	1,46	450	50	2,00	200	-150	0,78	850	-1000			
32	100	1500	354	alter temp	1000	3,14	1,16	1000	0	2,50	500	-500	0,60	3500	-4000	0	3500	-4000
50	100	1350	354	w=0.2	750	3,81	1,10	700	50	1,50	100	-50	0,50	1950	-2000	0	2500	-2550
25	100	1425	354	w=0.2	600	3,57	1,43	500	100	2,50	300	-200	0,31	3300	-3500	0	3300	-3500
37	100	1500	354	w=0.2	400	3,02	1,80	500	-100	2,50	900	-1000	0,82	2000	-3000	0	3000	-4000
66	100	1350	354	w=2.0	500	3,76	1,27	500	0	1,37	500	-500	0,04	3000	-3500	0	2000	-2500
62	100	1425	354	w=2.0	1000	3,38	1,28	1000	0	2,40	300	-300	0,00	5700	-6000	0	3000	-3300
67	100	1500	354	w=2.0	1500	3,10	1,93	1500	0	2,78	300	-300	0,06	4700	-5000	0	4000	-4300
142	260	1350	354*	2xrenewed														
90	260	1425	354	2xrenewed	500	3,31	1,43	700	-200	2,12	300	-500	0,00	5500	-6000	0	3000	-3500
106	260	1425	354	2xrenewed	500	3,38	1,23	700	-200	1,95	100	-300	0,00	4700	-5000	0	2700	-3000
101	260	1425	354	2xrenewed	750	3,38	1,38	750	0	1,82	300	-300	0,20	4700	-5000	0	4500	-4800
103	260	1425	354	2xrenewed	500	3,30	1,50	550	-50	1,97	450	-500	0,06	4500	-5000	0	4000	-4500
133	600	1425	354*	6xrenewed														
134	600	1425	354*	6xrenewed														
81	100	1350	395		400	11,26	2,54	350	50	2,54	250	-200	0,06	3800	-4000	0	800	-1000
79	100	1425	395		750	11,41	4,24	550	200	4,24	700	-500	0,79	1500	-2000	0	1500	-2000
80	100	1500	395		400	9,24	3,76	600	-200	5,59	300	-500	0,51	5500	-6000	0	3500	-4000
150	260	1350	395	2xrenewed	1000	11,57	1,92	1100	-100	2,07	100	-200	0,00	600	-800	0	600	-800
92	260	1425	395	2xrenewed	500	9,74	3,31	550	-50	5,33	450	-500	0,41	3500	-4000	0	2500	-3000
153	260	1500	395	2xrenewed	1000	10,55	4,37	1150	-150	7,57	850	-1000	0,04	5000	-6000	0	3500	-4500
161 repeat	600	1350	395	6xrenewed	750	9,05	1,35	850	-100	1,61	100	-200	0,00	1800	-2000	0	1200	-1400
161	600	1350	395	6xrenewed	750	11,74	0,08	1050	-300	0,72	700	-1000	0,00	3000	-4000	0	1000	-2000
186	600	1350	395	6xrenewed	500	11,01	1,97	600	-100	2,64	50	-150	0,00	5850	-6000	0	1200	-1350
148 repeat	600	1425	395	6xrenewed	1000	10,74	3,04	1300	-300	4,21	700	-1000	0,00	5000	-6000	0	4000	-5000
148	600	1425	395	6xrenewed	750	10,05	1,96	950	-200	4,59	300	-500	0,00	5500	-6000	0	2000	-2500
187	260	1350	Lithium	2xrenewed	1000	9,45	5,40	1200	-200	6,73	800	-1000	0,05	3000	-4000	0	3000	-4000
180	260	1425	Lithium	2xrenewed	4000	9,82	5,76	3500	500	8,00	2000	-1500	0,08	6500	-8000	0	5000	-6500
200	260	1500	Lithium	2xrenewed	0	5,86	5,86	0	0	6,64	2000	-2000	2,77	6000	-8000	0	10300	-12300

Concentration profiles of Al₂O₃.

Experiment	time	temp.	glass	parameter	start pt.	bulk conc.	dist. micro	cum. dist.	conc. top/bot	dist. micro	cum. dist.	conc. top/bot	dist. micro	cum. dist.	conc. top/bot
16	100	1350	354		750	5,57	850	-100	35,91				2900	-3000	22,87
21	100	1425	354		500	8,38	900	-400	36,60				2400	-2800	31,15
26	100	1500	354		500	11,70	900	-400	35,50	1600	-2000	35,50			
50	100	1350	354	w = 0.2	500	5,23	750	-250	36,95				3450	-3700	24,41
25	100	1425	354	w = 0.2	600	7,08	1100	-500	38,49				3000	-3500	31,77
37	100	1500	354	w = 0.2	500	10,94	1500	-1000	36,07	2000	-3000	36,07			
66	100	1350	354	w = 2.0	500	5,40	700	-200	36,55				3300	-3500	23,15
62	100	1425	354	w = 2.0	750	7,45	950	-200	36,95				5800	-6000	26,47
67	100	1500	354	w = 2.0	450	10,20	750	-300	36,77				4700	-5000	30,84
81	100	1350	395		400	2,31	600	-200	35,32				3800	-4000	22,08
79	100	1425	395		500	3,34	650	-150	37,14				1850	-2000	31,12
80	100	1500	395		400	8,84	1400	-1000	37,56				4000	-5000	31,08
150	260	1350	395		1000	1,38	1500	-500	34,17				8200	-8700	18,09
92	260	1425	395		500	5,50	800	-300	38,42				7700	-8000	25,66
153	260	1500	395		750	6,97	1750	-1000	39,19				5000	-6000	35,74
161	600	1350	395		750	1,61	1050	-300	35,93				5700	-6000	25,30
186	600	1350	395		750	3,47	1050	-300	35,87				5700	-6000	28,87
148	600	1425	395		750	4,64	1750	-1000	39,75				5000	-6000	36,07
186	600	1350	395	bottom	300	2,08	450	-150	35,42	850	-1000	35,42	7000	-8000	22,11

Annex 2 Table 6

Annex 3

Table of calculated e.e.h. of the crucible experiments.

An example of the calculation of the e.e.h. (electron equivalents per hour):

As example the calculation of the e.e.h. of potassium in the experiment 161 (first row of the table) will be given.

In the glass (cullet) before the start of the experiment, the content of K_2O is 9.09 weight%, after the glass melt was 90.5 hours in contact with the fused cast AZS crucible at 1350 °C, the K_2O content in the glass was 7.80 weight% (average of a duplicate measurement). The difference between the K_2O content before and after the glass melt contact with the AZS crucible is 1.29 weight%.

The average mole weight of the glass is 69.92 and the mole weight of K_2O is 94. The change in K_2O in the glass is therefore $(1.29 \cdot 69.92) / 94 = 0.96$ mole%.

The contact time is 90.5 hours, the decrease of K_2O per hour is $0.96 / 90.5 = 10.6 \cdot 10^{-3}$ mole%/hour.

The decrease in K_2O in the glass melt represents the diffusion of two K^+ cations in the glassy phase of the AZS and, to keep the electro neutrality conditions, two electrons. So the change of the K_2O content in the glass melt in the crucible gives a migration of $2 \cdot 10.6 \cdot 10^{-3} = 21.2 \cdot 10^{-3}$ electrons/hour.

The measured values are only valid for the standard test set-up and can only be used as a relative value, it is therefore more convenient to multiply all so calculated values with 10^{+3} and use these values as electron equivalents per hour (e.e.h.).

The e.e.h. of K_2O in the experiment 161 is therefore 21.2 e.e.h.

Annex 3 Table 1

experiment	glass	method	temp	delta time	aver. time	Li2O el.eq/hr	Na2O el.eq/hr	K2O el.eq/hr	BaO el.eq/hr	SrO el.eq/hr
161	395	cullet	1350	90,50	45,250		-4,24	21,20	2,32	1,6
161	395	cullet	1350	72,50	126,750		0,00	16,00	9,33	11,5
161	395	cullet	1350	95,50	210,750		2,24	12,16	7,37	12,8
161	395	cullet	1350	72,50	294,750		4,20	9,54	7,12	10,2
161	395	cullet	1350	95,50	378,750		3,30	6,94	4,40	9,0
161	395	cullet	1350	72,00	462,500		5,02	7,86	3,11	6,6
186	395	cullet	1350	92,00	46,000		-5,88	28,62	5,76	8,2
186	395	cullet	1350	69,75	126,875		-5,16	23,78	8,45	17,3
186	395	cullet	1350	97,75	210,625		-1,84	13,46	4,35	7,6
186	395	cullet	1350	72,75	295,875		4,20	12,06	7,29	13,4
186	395	cullet	1350	95,50	380,000		2,96	10,04	3,45	7,3
186	395	cullet	1350	72,00	463,750		2,02	9,20	1,46	3,7
186	395	powder	1350	92,00	46,000		-7,96	36,78	0,05	3,3
186	395	powder	1350	69,75	126,875		-2,26	32,64	0,92	2,0
186	395	powder	1350	97,75	210,625		0,82	19,40	0,47	1,1
186	395	powder	1350	72,75	295,875		9,30	14,42	3,64	8,5
186	395	powder	1350	95,50	380,000		6,86	9,58	2,06	6,2
186	395	powder	1350	72,00	463,750		8,46	10,22	2,28	4,3
150	395	cullet	1350	92,00	46,000		-4,16	25,96	1,79	1,1
150	395	cullet	1350	70,20	127,100		-4,66	24,90	2,54	4,6
148	395	cullet	1425	88,25	44,125		4,08	30,52	4,76	8,5
148	395	cullet	1425	72,25	124,375					
148	395	cullet	1425	95,75	208,375		11,78	18,48	4,68	8,4
148	395	cullet	1425	72,25	292,375		14,98	20,18	4,55	7,0
148	395	cullet	1425	95,75	376,375		14,36	14,30	3,15	5,3
148	395	cullet	1425	72,25	460,375		14,68	14,42	4,43	6,8
148	395	powder	1425	88,25	44,125		5,76	35,82	6,01	11,0
148	395	powder	1425	72,25	124,375					
148	395	powder	1425	95,75	208,375		11,30	20,28	5,15	10,1
148	395	powder	1425	72,25	292,375		12,64	21,00	5,00	9,7
148	395	powder	1425	95,75	376,375		12,72	15,00	4,73	8,7
148	395	powder	1425	72,25	460,375		14,98	16,06	5,25	9,7
85/92	395	cullet	1425	90,00	45,000		8,60	33,80	8,40	13,4
85/92	395	cullet	1425	70,00	125,000		4,60	29,40	5,10	9,8
174	395	cullet	1500	88,00	44,000		35,50	45,56	8,83	15,6
174	395	cullet	1500	71,50	123,750		33,28	40,06	8,82	15,0
174	395	cullet	1500	95,50	207,250		26,46	25,16	7,42	14,3
174	395	cullet	1500	73,00	291,500		26,26	24,92	7,73	13,5
174	395	cullet	1500	96,00	376,000		18,20	16,54	6,62	11,1
174	395	cullet	1500	71,50	459,750		21,76	21,36	6,78	12,1
174	395	powder	1500	88,00	44,000		35,38	53,50	10,18	17,9
174	395	powder	1500	71,50	123,750		31,08	46,72	9,27	16,2
174	395	powder	1500	95,50	207,250		24,32	28,36	8,04	14,8
174	395	powder	1500	73,00	291,500		15,14	26,70	8,70	16,0
174	395	powder	1500	96,00	376,000		11,98	19,44	8,66	16,6
174	395	powder	1500	71,50	459,750		16,24	26,84	6,26	8,4
174	395	powder	1500	95,50	207,250		33,36	55,24	10,27	18,8
201	395	powder	1500	89,00	44,500		35,40	51,24	10,54	18,9
201	395	powder	1500	72,00	125,000		27,28	30,70	8,58	16,1
201	395	powder	1500	94,25	208,125		24,04	30,48	7,59	12,8
201	395	powder	1500	72,25	291,375		30,22	42,06	8,46	13,4
153	395	cullet	1500	88,08	44,042		34,38	40,54	9,91	17,0
153	395	cullet	1500	72,83	124,500					

Annex 3 Table 2

experiment	glass	method	temp	delta time	aver. time	Li2O eleeq/hr	Na2O eleeq/hr	K2O eleeq/hr	BaO eleeq/hr	SrO eleeq/h
142	354	cullet	1350	90,00	45,000		6,00	19,80		
142	354	cullet	1350	72,00	126,000		2,80	16,60		
109	354	cullet	1425	90,00	45,000		22,80	29,40	5,20	0,3
109	354	cullet	1425	71,00	125,500		18,60	26,00	3,90	1,1
109	354	cullet	1425	95,00	208,500		13,80	17,00	4,30	1,7
109	354	cullet	1425	71,00	291,500		13,60	16,00	4,00	1,8
109	354	cullet	1425	97,00	375,500		11,40	9,60	3,00	1,8
109	354	cullet	1425	71,00	459,500		9,00	8,40	2,80	0,9
133	354	cullet	1425	89,50	44,750		17,80	25,40		
133	354	cullet	1425	71,00	125,000		18,80	25,40		
133	354	cullet	1425	97,00	209,000		13,60	14,80		
133	354	cullet	1425	72,00	293,500		12,80	16,00		
133	354	cullet	1425	96,00	377,500		13,40	9,60		
133	354	cullet	1425	75,00	463,000		8,20	8,60		
134	354	cullet	1425	89,25	44,630		19,00	28,00		
134	354	cullet	1425	72,00	125,250		25,00	26,80		
134	354	cullet	1425	96,25	209,380		13,80	15,60		
134	354	cullet	1425	71,75	293,380		14,40	15,20		
134	354	cullet	1425	96,00	377,250		12,60	10,00		
134	354	cullet	1425	70,25	460,380		13,80	10,80		
102	354	cullet	1425	90,00	45,000		23,00	25,60	14,30	6,6
102	354	cullet	1425	71,00	125,500		22,20	26,80	4,80	3,5
104	354	cullet	1425	90,00	45,000		18,00	26,80	6,20	3,3
104	354	cullet	1425	72,00	126,000		17,60	23,60	6,10	3,6
106	354	cullet	1425	89,00	44,500		20,60	28,40	9,20	5,4
106	354	cullet	1425	73,00	125,500		19,00	25,20	5,90	3,9
108	354	cullet	1425	89,00	44,500		19,80	24,00	16,30	5,6
108	354	cullet	1425	71,00	124,500		17,20	25,40	3,20	1,3
112	354	cullet	1425	89,00	44,500		19,80	27,00	8,30	3,2
112	354	cullet	1425	71,00	124,500		15,40	23,00	4,10	1,5
101	354	cullet	1425	90,00	45,000		19,20	27,80	6,30	4,1
101	354	cullet	1425	72,00	126,000		18,00	25,60	2,20	2,5
103	354	cullet	1425	90,00	45,000		18,20	27,80	3,30	1,9
103	354	cullet	1425	72,00	126,000		21,00	26,60	5,50	3,5
105	354	cullet	1425	88,00	44,000		17,20	27,20	5,70	3,6
105	354	cullet	1425	74,00	125,000		17,40	23,80	4,70	3,4
139	354	cullet	1425	22,50	11,250		14,60	59,00		
139	354	cullet	1425	24,00	34,500		16,00	30,40		
139	354	cullet	1425	24,00	58,500		10,00	27,60		
187	lithium	powder	1350	93,03	46,515	34,34	-3,06	15,56	6,20	9,3
187	lithium	powder	1350	70,39	128,224	30,16	3,44	13,10	8,26	13,0
180	lithium	powder	1425	90,75	45,375	57,86	1,72	18,84	11,93	18,6
180	lithium	powder	1425	70,42	125,959	45,36	10,02	19,14	10,67	15,4
200	lithium	powder	1500	88,83	44,417	85,76	13,16	21,88	19,15	32,0
200	lithium	powder	1500	71,58	124,625	68,36	22,20	21,50	18,84	23,9

Annex 4

Bubbles analysis.

In chapter 5 already is explained that the bubbles are analyzed by breaking a bubble in a high vacuum chamber and analyze the chemical gas composition of the bubble with a Balzers QMG 420 quadrupole mass spectrometer. The diameter of the analyzed bubbles is calculated using the volume of the bubbles. The volume of the bubble is calculated using the increase in the summation of the partial pressures of the known volume of the high vacuum chamber. The diameter of the prepared bubbles are measured by a microscope. The results of the measurements are given in the table of this annex.

Explanation of the table.

Exper. no.	: number of the test.
Time hrs.	: test duration in hours.
Temp. degree C	: temperature in ° C.
Glass	: used glass (cullet).
Bubbles no.	: counted number of bubbles in the sample.
Volume cm ³	: sample volume in which the bubbles are counted.
Bubbles N/cm ³	: counted number of bubbles per cm ³ .
Range mm	: the arithmetical average diameter in mm of the five largest bubbles found in the sample.
Number prep.	: number of bubbles prepared for analysis.
Diameter mm	: arithmetical average diameter in mm of the prepared bubbles.
Number anal.	: number of bubbles successfully analyzed.
Diameter mm	: arithmetical average diameter in mm of the analyzed bubbles.
O ₂ , N ₂ , CO ₂ and Ar	: the arithmetical average gas composition of the analyzed bubbles.

Exper. no.	Time hrs.	Temp. degree C	Glass	Bubbles no.	Volume cm3	Bubbles N/cm3	Range mm	Number prep.	Diameter mm	Number anal.	Diameter mm	O2	N2	CO2	Ar
16	100	1350	354	161	7,42	21,70	0,332	5	0,184	2	0,180	0,0	82,6	17,4	
21	100	1425	354	338	15,52	21,78	0,445	36	0,238	7	0,229	71,6	28,1	0,0	0,3
26	100	1500	354	309	11,97	25,81	0,403	54	0,203	24	0,215	93,5	5,1	1,5	0,0
43	100	1325-1375	354	32	5,91	5,41	0,229	30	0,121	2	0,160	0,0	89,5	10,0	0,6
28	100	1400-1450	354	212	6,32	33,54	0,383	41	0,186	13	0,217	46,2	7,1	46,6	0,1
32	100	1475-1525	354	78	13,09	5,96	0,621	31	0,221	9	0,267	99,0	1,0	0,0	0,0
78	100	1350	354	48	6,72	7,14	0,331	31	0,113	12	0,120	0,0	81,5	17,7	0,8
71	100	1425	354	118	7,40	15,95	0,396	38	0,128	14	0,169	50,1	47,4	2,1	0,5
69	100	1500		332	9,61	34,55	0,611	37	0,273	27	0,289	78,6	20,3	1,0	0,1
81	100	1350	395	30	10,41	2,88	0,232	42	0,122	8	0,120	0,3	78,0	20,9	0,8
79	100	1425	395	85	9,99	8,51	0,381	33	0,116	10	0,099	10,1	53,6	35,7	0,5
80	100	1500	395	389	9,73	39,98	0,497	34	0,196	18	0,204	65,7	30,1	4,0	0,3
93	100	1350	354 ZnO	43	11,52	3,73	0,322	32	0,113	18	0,109	0,0	90,1	9,2	0,7
89	100	1425	354 ZnO	157	10,95	14,34	0,540	40	0,145	19	0,179	31,2	60,9	7,5	0,5
94	100	1500	354 ZnO	568	9,68	58,68	0,602	32		22	0,217	80,5	18,6	0,8	0,1
90	260	1425	354	320	11,39	28,09	0,380	32	0,195	17	0,220	75,4	17,2	7,2	0,2
106	260	1425	354	513	12,52	40,97	0,432	38	0,179	17	0,213	70,0	27,3	2,3	0,3
92	260	1425	395	165	10,24	16,11	0,430	32	0,232	10	0,306	79,4	18,7	1,8	0,1
102	260	1425	354 395	483	10,35	46,67	0,465	36	0,134	18	0,163	24,2	65,7	9,5	0,6
104	260	1425	354 395Na/K	345	11,36	30,37	0,409	30	0,193	12	0,235	58,9	39,2	1,6	0,4
128	260	1425	354 395Ti	321	12,24	26,23	0,420	31	0,193	16	0,217	62,6	35,4	1,7	0,4
117	260	1425	354 395Zr	231	13,00	17,77	0,442	41	0,127	24	0,150	40,2	53,8	5,5	0,6
112	260	1425	354 395mu	322	11,08	29,06	0,427	35	0,214	21	0,233	67,6	30,1	2,1	0,2
125	260	1425	354 354Zn	230	10,77	21,36	0,503	32	0,187	15	0,158	59,4	39,1	0,9	0,4
108	260	1425	354 TA3779	414	11,92	34,73	0,434	37	0,174	15	0,188	58,8	36,6	4,2	0,4
142	260	1350	354	425	25,11	16,93	0,343	27		15	0,188	4,3	21,7	73,4	0,2
150	260	1350	395	130		11,06	0,251	24	0,083	6	0,097	0,0	31,6	68,0	0,3
153	260	1500	395	423	13,23	31,97	0,467	36	0,271	30	0,239	88,8	10,4	0,7	0,1
187	260	1350	Lithium	290	14,27	20,32	0,507	32	0,233	26	0,242	66,7	30,6	2,4	0,3
180	260	1425	Lithium	58	28,22	2,06	0,601	28	0,261	23	0,274	76,8	22,6	0,4	0,2
200	260	1500	Lithium	27	20,59	1,31	0,657	21	0,401	16	0,413	91,0	8,5	0,4	0,1
133	600	1425	354	221	11,01	20,07	0,450	29	0,182	17	0,206	92,4	6,6	0,6	0,0
161	600	1350	395	261	11,30	23,10	0,221	30	0,140	15	0,148	0,1	59,9	42,5	0,4
186	600	1350	395	75	13,70	5,47	0,189	18	0,114	9	0,140	24,8	43,0	31,8	0,4
148	600	1425	395	379	14,58	25,99	0,376	24	0,163	6	0,187	79,0	18,7	2,1	0,2
149	100	1350	426	393	12,08	32,53	0,382	32	0,176	21	0,199	49,3	38,6	11,7	0,4
147	100	1425	426	696	11,71	59,44	0,461	32	0,219	24	0,216	88,1	9,8	2,0	0,1
146	100	1500	426	622	12,50	49,76	0,566	32	0,263	21	0,227	93,5	6,1	0,4	0,1
214	100	1350	433	113	9,52	11,87	0,181	32	0,103	14	0,112	0,0	86,5	12,7	0,8
213	100	1425	433	439	8,95	49,05	0,432	32	0,140	23	0,141	56,5	42,3	0,8	0,4
212	100	1500	433	612	9,33	65,59	0,463	37		30	0,210	86,8	12,7	0,4	0,1

Glass composition and properties.
For definitions see annex 1.

composition	Glass							
	395Na/K	395Ti	395Zr	395mu	354Zn	TA3779	426	433
SiO ₂	61,78	62,77	64,55	58,75	63,45	59,27	63,80	59,60 weight%
Al ₂ O ₃	0,76	0,75	0,88	4,58	3,36	3,36	3,30	3,20 weight%
Li ₂ O							0,20	weight%
Na ₂ O	9,34	6,75	6,81	6,81	9,44	9,23	7,30	7,80 weight%
K ₂ O	7,03	9,19	9,07	8,87	6,18	6,54	7,30	7,70 weight%
MgO	0,28	0,29	0,25	0,30	0,98		0,25	0,40 weight%
CaO	0,41	0,40	0,40	0,38	1,40	1,51	0,35	0,60 weight%
SrO	9,38	0,94	9,23	9,29	2,95	8,91	7,00	8,60 weight%
BaO	7,84	7,78	7,78	7,87	10,51	8,38	8,90	9,60 weight%
ZrO ₂	2,09	2,06		2,07		2,07		2,50 weight%
TiO ₂	0,42		0,42	0,43				weight%
Sb ₂ O ₃	0,38	0,37	0,38	0,37	0,37	0,38	0,40	0,40 weight%
properties	*	*						
Density	2752	2,731	2,709	2,764		2,782	2,70	2,77 kg/m ³
Viscosity:								
strain point	487	482	474	499		501	465	495 C
annealing point	521	517	504	533		532	505	530 C
softening point	704	706	675	717		703	685	715 C
working point	1009	1026	1002	1045		1012	1025	1040 C
melting point	1416	1447	1430	1470		1418	1485	1460 C
Constants								
Fulcher equation:								
A			-1,874	-2,036		-2,021		
B			4874,471	5142,712		4917,760		
C			172,248	196,079		195,142		

* Calculated density and viscosity

Annex 6

Student or t-test.

For testing the difference of two means of small samples, the Student or t-test may be used.

The theory of Student's t distribution requires one to assume that the basic variables x_1 and x_2 possess independent normal distributions with equal standard deviations. If these assumptions are reasonably satisfied then one may treat the variable t as a Student t variable with $n_1 + n_2 - 2$ degrees of freedom.

In the case of the evaluation of the bubble analysis of the crucible experiments the means of the different groups of bubble analysis are tested assuming that there is no difference in the means. In all the tests a significance level of 0.05 has been chosen.

The used calculation method is describe below.

$$t = |X_1 - X_2| * S^{-1} * \{(N_1 * N_2) / (N_1 + N_2)\}^{0.5} \Rightarrow t_{(N_1 + N_2 - 2)}$$

$$S = [\{(N_1 - 1) * S_1^2 + (N_2 - 1) * S_2^2\} / (N_1 + N_2 - 2)]^{0.5}$$

in which

X_1 = mean of distribution 1.

X_2 = mean of distribution 2.

S_1 = standard deviation of distribution 1.

S_2 = standard deviation of distribution 2.

N_1 = number of values of distribution 1.

N_2 = number of values of distribution 2.

Literature reference: P.G. Hoel, Elementary statistics,
Fourth edition 1962,
J. Wiley & Sons, New York.

Samenvatting

De interactie van het gesmolten glas met het vuurvast materiaal van de industriële glassmeltwannen heeft een grote invloed op de kwaliteit van het geproduceerde glas. Het vuurvast materiaal dat het meest gebruikt wordt in de glasindustrie, in direct contact met gesmolten glas, is het smeltgegoten AZS (Aluminiumoxyde Zirconiumoxyde Silicaat). Als gevolg van de interactie van het gesmolten glas met het smeltgegoten AZS kunnen verschillende soorten inhomogeniteiten zoals stenen, knobbels en bellen in het glas gevormd worden.

Het doel van deze studie is het vinden, voor het geval van smeltgegoten AZS in contact met gesmolten glas, van het mechanisme van knobbel- en bel-vorming en de parameters die dit mechanisme beïnvloeden.

Het uiteindelijke doel is de ontwikkeling van een (semi) kwantitatief model dat de hoeveelheid glasfouten voorspelt ten gevolge van het contact van het gesmolten glas met het smeltgegoten AZS, zodat men in staat is de omstandigheden te kiezen met de laagste vormingssnelheden van deze glasfouten. De meeste bellen die ontstaan bij temperaturen boven 1400 °C zijn oorspronkelijk zuurstof bellen, veroorzaakt door een electrochemisch mechanisme in het vuurvast materiaal. Wanneer gesmolten glas in contact gebracht wordt met smeltgegoten AZS, transporteert de diffusie van kationen van de glassmelt in het AZS positieve lading in het inwendig van het AZS. De diffusie van de kationen wordt veroorzaakt door de lagere partiële Gibbs energie van de glassmelt kationen in het hoog Al_2O_3 houdende glasfase van het AZS vuurvast. De positieve lading ten gevolge van de kation diffusie wordt in balans gehouden door elektronen die van de glassmelt/AZS overgang naar het inwendige van het AZS bewegen om electroneutraliteit te handhaven. De elektronen afkomstig van de zuurstofionen in de glassmelt reduceren de polyvalente ion onzuiverheden (voornamelijk ijzer) van de smeltgegoten AZS. De snelheid van zuurstofgas vorming bij de vuurvast/glassmelt overgang, als een resultaat van de

redoxreactie (elektronen donor), wordt bepaald door de diffusie snelheid van de kationen van het gesmolten glas in de glasfase (de bindende fase) van het smeltgegoten AZS.

De zuurstofbellen ontstaan in de overgangslaag tussen smeltgegoten AZS en de glassmelt. De overgang bestaat uit een glasachtige laag van produkten, die resulteren uit de reacties tussen smeltgegoten AZS en de glassmelt, met nodulair ZrO_2 aan de vuurvast zijde. Een bel ontstaan in deze overgangslaag drukt zich door deze laag in de glassmelt, daarbij wordt soms ook een gedeelte van de Al_2O_3 rijke laag in de bulk van de glassmelt gedrukt.

Het hoge Al_2O_3 gehalte van de glasachtige gedeelte van de overgangslaag geeft deze "deeltjes" een zo hoge oppervlakte-spanning dat ze bolvormige glasachtige knobbels in de glassmelt vormen.

Dit betekent dat een enkele mechanisme verantwoordelijk is voor de vorming van zowel bellen als knobbels aan de overgang van glassmelt en smeltgegoten AZS.

Het snelheid bepalende element van dit proces, de kation diffusie, is gemeten voor de belangrijkste oxyden van een hedendaags TV-scherm glas (Li_2O , Na_2O , K_2O , BaO , SrO , CaO en MgO).

Het effect van Li_2O op de zuurstofbel vorming is erg groot, niet alleen zijn eigen bijdrage, maar ook veroorzaakt Li_2O dat ander oxyden een groter bijdrage hebben dan dat deze oxyden zouden hebben in een glas zonder Li_2O . Veruit de grootste bijdrage van de andere oxyden, behalve Li_2O , heeft K_2O vooral in het temperatuur gebied rond $1350\text{ }^\circ\text{C}$ (dit is ongeveer de bodemtemperatuur van de smeltwan). De vormingssnelheid van zuurstofbellen per mol procent van de oxyden die onderzocht zijn, in afnemende volgorde is: Li_2O , K_2O , Na_2O , BaO/SrO , CaO en MgO . De diffusiesnelheden van de kationen van deze oxyden in het AZS en, daaruit volgend, het belvormingspotentieel inclusief de invloed van de glassamenstelling en de temperatuur, zijn gebruikt in een eenvoudig model van een industriële smeltwan met realistische glassmelt/smeltgegoten AZS contacttemperaturen, zodat de belvormingspotentieel ten gevolge van de interactie van

smeltgegoten AZS en glassmelt berekend kan worden.

De verschillen in glasfoutpotentieel van de interactie tussen smeltgegoten AZS en verschillende glassmelten berekend met deze methode, komen overeen met de verschillen in de hoeveelheid bellen en knobbels gevonden in verschillende industrieel geproduceerde TV glazen.

De laboratorium experimenten tonen een stijging in aantal, in zuurstofgehalte en in diameter van de gevormde bellen, bij stijgende temperaturen (van 1350 naar 1500 °C).

De chemische samenstelling van de kern van de knobbels, afkomstig van de overgangslaag tussen glassmelt en smeltgegoten AZS blijft onveranderd gedurende het oplossen in de bulk van de glassmelt tot net voordat de knobbel helemaal opgelost is. Deze onveranderde chemische samenstelling maakt het mogelijk om de ontstaanstemperatuur van de knobbels te bepalen, doordat de chemische samenstelling van de overgangslaag voornamelijk bepaald wordt door de chemische samenstelling en de temperatuur van de glassmelt tijdens de interactie.

Dankwoord

Het onderzoek is verricht in het laboratorium van de Basic Technology Glass (BTG) van Philips.

De leiding van de BTG dank ik voor de gegeven mogelijkheid tot promotie op dit onderwerp.

Veel dank ben ik verschuldigd aan Ruud Beerkens die als co-promotor het schrijven van dit proefschrift op stimulerende wijze intensief heeft begeleid.

Prof. de Waal en Prof. van Loo dank ik voor hun begeleiding.

Het tot stand komen van dit proefschrift is mede mogelijk gemaakt door medewerkers van de BTG. Mijn hartelijke dank gaat met name uit naar: Ad Verbeek en Ivo Lemmens voor hun assistentie bij de experimenten en het analyseren van de bellen, Corrie Jaarsma, Hans Krüsemann en Brigitte van Dijk voor de SEM/EDX analyses en Martien Hendriks en Leen Jongeling voor hun ondersteuning op lichtmicroscopisch en materiaalkundig gebied en het identificeren van de knobbels.

Mijn vrouw ben ik erkentelijk voor haar geduld en steun tijdens het schrijven van het proefschrift.

Curriculum Vitae

Frans van Dijk werd in Leende geboren op 27 mei 1956. Vanaf 1968 tot 1972 volgde hij de MAVO opleiding, gevolgd door de studie chemie aan de H.T.S. te Eindhoven. Vanaf 1977 studeerde hij Scheikundige Technologie aan de Technische Universiteit te Eindhoven. In 1982 slaagde hij cum laude voor het ingenieurs-examen bij de vakgroep voor fysische technologie bij Prof. Rietema.

Vanaf 1982 is hij werkzaam bij Philips glas, met als zwaartepunt smelttechnologie. In deze periode heeft hij diverse functies uitgeoefend o.a. modelontwikkelaar, fabriekstechnoloog smelten, projectleider glasfouten onderzoeken en smelttechnoloog Basic Technology Glass.

STELLINGEN

behorende bij het proefschrift van F.A.G. van Dijk

- 1 De redox van het glas wordt in de literatuur verschillend gedefinieerd bijvoorbeeld als de verhouding Fe^{3+}/Fe^{2+} of de zuurstofdruk van de glassmelt. Deze definities zijn echter niet volledig. Een meer volledige definitie van de redox van het glas waarin behalve de beide genoemde, de concentratie van de polyvalente ionen is opgenomen, zou meer duidelijkheid scheppen.

Chopinet M.H. et.al., Glastech. Ber. **56K** (1983), p596.
Beerkens R., Glastech. Ber. **63K** (1990), p223.

- 2 De bij kamertemperatuur bepaalde C.O.D. waarde ter karakterisering van de redoxtoestand van het grondstoffen gemeng is niet zonder meer bruikbaar voor de bepaling van de redoxtoestand van de uit dit gemeng vervaardigde glassmelt, vanwege mogelijke redoxreacties die alleen bij hoge temperatuur plaatsvinden en de uitwisseling van zuurstof met de ovenatmosfeer.

- 3 De oude glassmelters vuistregel "hoe heter hoe beter" gaat niet in alle gevallen op vanwege de temperatuur afhankelijkheid van de vorming van bellen ten gevolge van de glassmelt/vuurvast interactie.

Nemec L. and Mühlbauer M., Glastech. Ber. **54** (1981), p99.
Dit proefschrift: Hoofdstuk 4.

- 4 De eenvoudigste manier om produktie uitval ten gevolge van glasfouten te voorkomen is gevonden door de firma RAYWARE uit de UK. "This piece of fine glass is totally handmade in the old world tradition. Seeds and bubbles sometimes occur in this process. These are not flaws, but illustrate the beauty of a totally handmade article."

- 5 De hypothese van Auerbach, dat zuurstofbellen die ontstaan bij de interactie tussen de glassmelt en het smeltgegoten AZS, het gevolg zijn van selectief transport in het AZS van moleculair zuurstof is onjuist.

Auerbach A., Symposium sur l'Elaboration du Verre, p295, Madrid 1973.

- 6 De beschikbare middelen voor research en ontwikkeling kunnen efficiënter ingezet worden indien vooraf de economische haalbaarheid van het gestelde doel onderzocht wordt.

- 7 Voor glasovens waarin een glas met een hoog kalium gehalte gesmolten wordt kan beter een smeltgegoten AZS gebruikt worden waarbij het bewust toegevoegde natrium vervangen is door kalium. Het aantal glasfouten tengevolge van de interactie tussen de glassmelt en het smeltgegoten AZS materiaal wordt hierdoor geringer voor deze glazen.

Dit proefschrift

- 8 De steeds strengere milieu eisen vormen in de glasindustrie een belangrijke impuls voor de introductie van nieuwe technologieën die in de toekomst ook het smeltproces kunnen verbeteren.

Technologisch Meerjarenplan Glasproducerende Industrie
1990-2010.

- 9 Een kenmerk voor een industrie op zijn retour is een toename van het aantal managers en een afname van het aantal technici.